Structure-function studies of the Kir6.2 channel and of its coupling with natural and artificial partners

Maria Antonietta Principalli

UNIVERSITÉ GRENOBLE ALPES

THÈSE

Pour obtenir le grade de

DOCTEUR DE L'UNIVERSITÉ GRENOBLE ALPES

Spécialité : **Biologie Structurale et Nanobiologie**

Arrêté ministériel : 7 août 2006

Présentée par

Maria Antonietta PRINCIPALLI

Thèse dirigée par **Dr. Michel VIVAUDOU** et
codirigée par **Jean REVILLOUD**

préparée au sein de l'**Institut de Biologie Structurale**
dans **l'École Doctorale Chimie et Sciences du Vivant**

Étude structure-fonction du canal Kir6.2 et de son couplage avec des partenaires naturels et artificiels

Thèse soutenue publiquement le **9 Octobre 2015**
devant le jury composé de :

Dr. Pierre-Jean CORRINGER
Président
Prof. Anna MORONI
Rapporteur
Prof. Bruno ALLARD
Rapporteur
Dr. Patrice CATTY
Membre
Dr Michel VIVAUDOU
Directeur de thèse
Jean REVILLOUD
Co-directeur de thèse

Université de Grenoble
École Doctorale Chimie et Science du Vivant

Thèse pour obtenir le grade de

DOCTEUR ès SCIENCES DE L'UNIVERSITÉ DE GRENOBLE

Specialité: Biologie Structurale et Nanobiologie

Presented and defended in public by

Maria Antonietta PRINCIPALLI

On October 9th 2015

Structure-function studies of the Kir6.2 channel and of its coupling with natural and artificial partners

---

Thesis directors:

Dr. Michel VIVAUDOU
Jean REVILLOUD

Jury:

President: Dr. Patrice CATTY
Reviewer: Prof. Anna MORONI
Reviewer: Prof. Bruno ALLARD
Examiner: Dr. Pierre-Jean CORRINGER

Acknowledgements

I would like to thank in the first place Prof. Anna Moroni and Prof. Bruno Allard for dedicating their time to the evaluation of this work. I would like to express my gratitude as well to Dr. Patrice Catty, Dr. Pierre-Jean Corringer and Dr. Hugues Nury for being part of my annual evaluation committee, for their precious advices and their optimistic vision of problematic projects.

A special thanks to Michel Vivaudou, my thesis director, for his advices and his sense of humour and for giving me the chance to experience an adventure like no other, scientifically and personally. Thanks to Jean Revilloud, my supervisor in the lab, for his patience, for saving my life during my first (and last) day on a pair of skies, and for teaching me the art of patch-clamping. Many thanks to Christophe Moreau, the most patient person I have ever known, for encouraging me to believe in my theories and for helping me exploring my ideas even though they looked crazy or useless to others. Special thanks to Kasia, my personal English teacher, who helped me in moving the first steps in the lab. Big thanks to Catalina, whose friendship and Latin spirit helped me reach the end of this adventure. Thanks to Laura for being an intelligent and fun co-worker, and to Karla for her calm in panic situations.

A particular thanks to Yann, Sonja, Ola, Hubert, Lionel, Céline, Michel T. and Isabelle for their priceless advices and their help.

Un grazie tutto particolare alla banda degli italiani a Grenoble: il Mollica, 'mamma tuttofare', DdS e mamma Rocha (italiana adottiva), per avermi salvato dai guai in più di un'occasione. Al piccolo Gabriel per avermi insegnato che non ci si veste mai per bene quando si deve fare da baby-sitter, a Filippo per il suo accento toscano e le sue email memorabili, a Sciaken per saper trasmettere la sua calma e il suo approccio positivo alla vita. Grazie a tutti voi ragazzi!

Un grazie speciale a Mizar, con cui ho intrapreso questa e molte altre avventure, amica sincera e cuoca personale, all'occorrenza pronta a darmi una strigliata affettuosa.

Grazie a mamma e papà per avermi supportata e per aver creduto in me, sempre.

Grazie ad Alex, per essere rimasto fino alla fine.

"There is nothing like looking, if you want to find something. You certainly usually find something, if you look, but it is not always quite the something you were after."

J.R.R. Tolkien

LIST OF ABBREVIATIONS

ABC
ATP binding cassette; 15
ACh
Acetylcholine; 61
ADP
Adenosine diphosphate; 15
AOX
Alcohol oxidase promoter; 78
ATP
Adenosine triphosphate; 15
cAMP
Cyclic adenosine monophosphate; 59
CFTR
Cystic fibrosis transmembrane conductance regulator; 17
COPI
Coat protein complex I; 34
CTD
Cytoplasmic domain; 33
$D2_L$
Long Dopaminergic receptor 2; 51
DAG
Diacylglycerol; 57
DDM
N-dodecyl β-D-maltopyranoside; 81
DEND
Developmental delay, epilepsy, and neonatal diabetes; 44
DEPC
Diethyl pyrocarbonate; 72
DNA
Deoxyribonucleic acid; 71
ECF
Energy-coupling factor; 21
ECL
Extracellular loop; 52
eGFP
Enhanced green fluorescent protein; 79
EGTA
Ethylene glycol tetra-acetic acid; 87
ER
Endoplasmic reticulum; 16
GDP
Guanosine triphosphate; 40
GIRK
G-protein activated inward rectifying potassium channel; 32
GPCR

G protein-coupled receptor; 40
GRAFS
Glutamate, rhodopsin, adhesion, frizzled/taste2, secretin receptor classes; 53
HA
Human influenza hemagglutinin; 75
hOR
Human olfactory receptor; 51
ICCRs
Ion channel-coupled receptor; 50
ICL
Intracellular loop; 52
IP3
Inositol trisphosphate; 57
IPTG
Isopropyl β-D-1-thiogalactopyranoside; 75
K-ATP
ATP-sensitive potassium channel; 15
KCO
Potassium channel opener; 48
Kir
Inwardly rectifying potassium channel; 15
LB
Luria-Bertani; 71
LC-CoA
long chain Co-enzyme A esters; 43
M2
Muscarinic receptor 2; 51
MAC
Metal affinity chromatography; 81
MNG-3
Maltose-neopentyl glycol; 81
mRNA
Messenger ribonucleic acid; 73
MRP
Multidrug resistance protein; 17
MSP
Membrane scaffold protein; 80
NBD
Nucleotide binding domain; 17
PBS
Phosphate-buffer saline; 82
PCR
Polymerase chain reaction; 78
P-gp
P-glycoprotein; 24
PHHI
Persistent hyperinsulinemic hypoglycaemia of infancy; 35
PIP_2
Phosphatidylinositol 4,5-bisphosphate; 42

POPC
1-palmitoyl-2-oleoyl-sn-glycero-3-phosphocholine; 80
SDS
Sodium dodecylsulfate; 71
SDS-PAGE
Sodium dodecyl sulphate - polyAcrylamide gel electrophoresis; 74
SEC
Size-exclusion chromatography; 82
SUR
Sulfonylurea receptor; 15
TBS
Tris-buffer saline; 75
TEVC
Two-electrode voltage-clamp technique; 90
TMD
Transmembrane domain; 17
TRIS
Tris(hydroxymethyl)aminomethane; 75
tRNA
Transfer ribonucleic acid; 83
UTR
Untranslated region; 72
VFTM
Venus flytrap mechanism; 56
YPD
Yeast extract peptone dextrose medium; 78

ELECTROPHYSIOLOGY GLOSSARY

Action potential: is a self-sustained electrical signal consisting of a transient increase of the membrane potential across the plasma membrane of excitable cells such as neurons, muscle cells and endocrine cells. In neurons, for example, the membrane potential of the cell at rest is around -70 mV. This value increases to about +50 mV during an action potential and, subsequently, returns to the resting level again. The action potential event is triggered by a depolarization and produced by the activation of voltage-gated ion channels.

Conductance: indicates the capacity of an ion channel to let ions move through its pore. It is measured in Siemens (S).

Gating: the phenomenon or mechanism by which an ion channel opens or closes its pore. Depending on the specific ion channel, this process is regulated by voltage, metabolic state of the cell (ATP/ADP concentration), intracellular ligands and/or second messengers (calcium, cAMP, etc.), or extracellular ligands (neurotransmitters).

Membrane potential: The voltage difference across the plasma membrane of cells. It is negative under resting conditions and becomes positive during an action potential. Its value depends on different factors: the concentration of ions at both sides of the membrane, the permeability of the membrane to these ions, the activity of electrogenic pumps that maintain the ions concentration outside and inside the cells.

Open probability (P_o): describes the fraction of time spent by an ion channel in its open conformation.

TABLE OF CONTENTS

PREAMBLE

The ATP-sensitive potassium channel is a large membrane protein resulting from the unusual association of a protein belonging to a family of transporters, the sulfonylurea receptor (SUR), and an inwardly rectifying potassium channel, Kir6. Immediately after its discover in 1983 by Akinori Noma, it obtained significant notoriety because of its implication in the insulin secretion process. Over the past years, huge progresses have been made regarding the understanding of its function, yet many questions remain to be answered. Among these, this thesis tried to help elucidate two main aspects of the K-ATP channel, its structure and the mechanism used by the two partners to communicate with each other in what is called 'functional coupling'.

To achieve this, the work was divided in three main projects. First, we attempted to heterologously express and purify the protein to obtain samples suitable for structural studies. Although the precise mechanism is not fully understood, it is known that binding of nucleotides or drugs to the SUR subunit activates the Kir6 channel. Thus, the second project focused on the role of SUR in activation of the channel. The third project is related to the second as it aims to better understand Kir6 regulation by SUR; but this time from the side of the pore-forming subunit. This last objective cannot be easily achieved with classical approaches as the region thought to be involved in Kir6 activation is in tight physical association with SUR and mutations at this level would compromise the general folding of the channel. Ion Channel-Coupled Receptor (ICCRs) technology, developed in our laboratory, provides a unique system to study Kir6.2 mechanistic.

In ICCRs, Kir6 is directly fused at its N-terminus to the C-terminus of a G protein-coupled receptor (GPCR) that tunes its gating depending on ligand binding. Using ICCRs we discovered a cluster of arginines in the Kir6 N-terminus responsible for channel gating modulation. These arginines were subsequently studied in the K-ATP channel to understand their involvement in the regulation of Kir6 gating by its natural partner SUR. The three projects embrace three large families of proteins such as ABC transporters, Kir channels and GPCRs. ABC transporters and Kir channels will be described in detail in the introduction of this manuscript. GPCRs, although a very important family of proteins, will not be described in detail because they are not directly the subject of this work. They are used only as a tool to understand SUR-Kir6 coupling.

INTRODUCTION

1. The ATP-sensitive potassium channel constituent subunits

1.1 K-ATP channel overview

ATP-sensitive potassium channels result from the unique partnership of two distinct proteins: the Sulfonylurea Receptor (SUR), which belongs to the ATP binding cassette (ABC) transporter family, and the inwardly rectifying potassium channel (Kir6). These particular channels are physiologically up-regulated by MgADP and down-regulated by ATP. This regulation allow the channel to 'sense' cell metabolism and, depending on the energy level of the cell, to change the potassium permeability of the membrane, which might result in a variation of the membrane potential. Variations in the membrane potential trigger a certain cellular response depending on the K-ATP localization. Examples of processes regulated by these channels are insulin secretion and regulation of the duration of the action potential in cardiac cells.

K-ATP channel subunits SUR and Kir6 exist in different isoforms depending on the cell type where these are expressed. The SUR protein (~ 170 kDa) exists as three isoforms: SUR1 mostly located in the pancreas and in the brain, SUR2A expressed in cardiac and skeletal muscles and SUR2B in smooth muscle blood vessels. The Kir6 channel (~ 45 kDa) is present in two isoforms: Kir6.1 in smooth muscle and Kir6.2 in pancreas, brain, cardiac and skeletal muscles.

In the vertebrate genome, we can find two Kir6 genes (*KCNJ8*, *KIR6.1* and *KCNJ11*, *KIR6.2*) and two SUR genes (*ABCC8*, *SUR1* and *ABCC9*, *SUR2*). Isoforms SUR2A and SUR2B derive from alternate splicing of the same gene. Interestingly, the genes for Kir6.2 and SUR1 are located next to each other on human chromosome 11p15.1 while the genes for Kir6.1 and SUR2 are also consecutive on chromosome 12p12.1, suggesting that an elegant gene expression regulation happens already at the transcription level (Nichols, Singh, and Grange 2013).

It takes four SUR and four Kir6 subunits to build a full-length K-ATP channel (Figure 1). The resultant hetero-octamer has a predicted mass of about 950 kDa. Kir6 is in charge of creating the pore, necessary to ensure K^+ flow, while the SUR protein finely plays on channel gating. The octameric arrangement has been confirmed by both electrophysiological and

biochemical studies (Inagaki, Gonoi, and Seino 1997; Clement IV et al. 1997) and a low resolution structure of the full-length complex (Mikhailov et al. 2005).

The presence of retention signals (RXR) on both subunits ensures that only properly assembled channels reach the plasma membrane. In particular, during K-ATP assembling, these motifs are masked so that the resultant complex is released from the ER (Zerangue et al. 1999). Physical association between SUR and Kir6 has been confirmed conducting co-immunoprecipitation experiments (Lorenz and Terzic 1999). Moreover, deletion of the last 36 amino acids in the Kir6.2 channel allows the formation of functional channels in absence of the SUR subunit (Tucker et al. 1997).

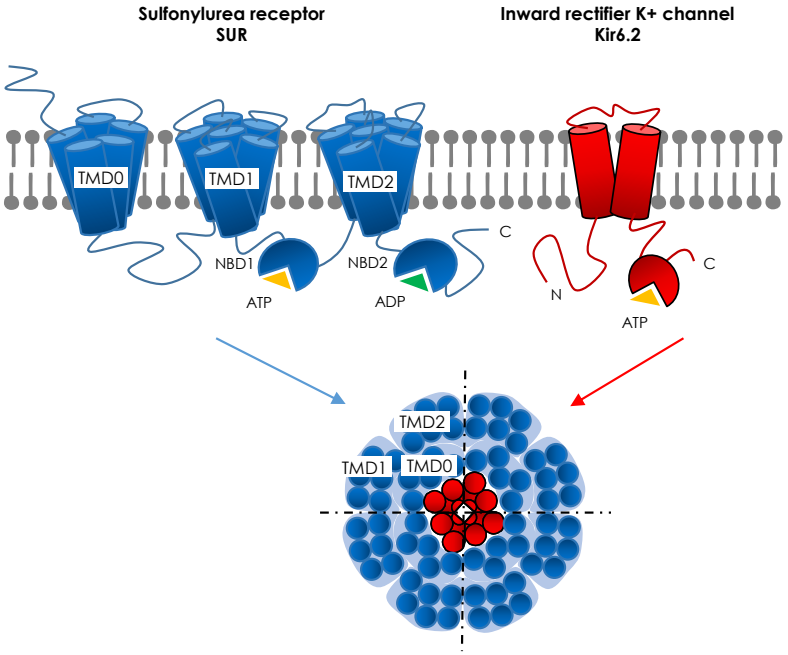

Figure 1. Cartoon of the K-ATP channel predicted folding. Kir6 and SUR are the constitutive subunits of the channel. Four subunits of the inwardly rectifying K^+ channel Kir6 associate with four ATP-binding cassette proteins, SUR, to form a functional K-ATP channel octamer. Kir6 has two transmembrane helices and a large cytoplasmic domain harboring an inhibitory binding site for ATP. SUR possesses three transmembrane domains (TMD0, 1&2), and 2 cytoplasmic nucleotide binding domains (NBD1&2).

1.2 The Sulfonylurea Receptor: an atypical transporter of the ABC family

The Sulfonylurea Receptor SUR belongs to the ATP-binding cassette family (ABC). In particular, SUR is located in the ABCC subfamily, together with MRP1 (multidrug resistance protein) and CFTR (cystic fibrosis transmembrane conductance regulator).

Despite their phylogenic correlation, these proteins share very little in terms of function. MRP1 is a multidrug exporter of glutathione conjugates which, taking advantage of ATP hydrolysis, transports substrates (Cole 2014). CFTR, known for its implication in cystic fibrosis, is an ion channel gated by ATP hydrolysis (Vergani et al. 2005). SUR modulates the gating of a K^+ channel using its NBDs domains to 'sense' ATP and ADP levels inside cells.

High-resolution structures of several bacterial ABC proteins suggest a mechanism by which ATP hydrolysis at the nucleotide-binding domains (NBDs) of ABC proteins is coupled to conformational changes that drive substrate transport (Locher 2009).

So far, the atomic structure of the SUR is not known. Nevertheless, alignments with other members of the ABC family, whose structure have been resolved, show the presence of common features. SUR N-terminus faces the extracellular side of the membrane while its C-terminus is intracellular (Mikhailov et al. 2005). The hydrophobic plot of the SUR sequence shows the presence of three transmembrane domains named TMD0, TMD1 and TMD2. These are interconnected by a long loop (L0) and two hydrophilic domains, the nucleotide binding domains NBD1 and NBD2.

TMD1 and TMD2 are common among ABC proteins and they typically present six spanning α helices. The TMD0 deserves a particular place among TMDs as it is found only in few members of the ABC family such as MRP1–3, MRP6–7 and YCF1 (yeast cadmium factor) and is connected to TMD1 through the long cytoplasmic loop (L0). It is considered an 'additional domain' of such members and its function it is not fully understood. Moreover, TMD0s from different ABC proteins show different amino acid sequences, which suggest a variability in their function. The TMD0 in MRP1 seems to be dispensable as its deletion does not affect the transport function or the cellular targeting of MRP1 (Bakos et al. 1998) or the

dimerization (Yang et al. 2007). The TMD0 of MRP2 is required for correct cellular targeting but is not necessary for transport function (Fernández et al. 2002).

In the case of the SUR protein, the TMD0 domain is essential for proper addressing of the K-ATP channel at the plasma membrane and has a critical role in Kir6.2 gating modulation (Chan, Zhang, and Logothetis 2003; Fang, Csanády, and Chan 2006). In particular, TMD0 cannot abolish the retention of full-length Kir6 channels (containing the RKR retention signal at the C-terminal) but it sensitively burst the expression of Kir6 channels deleted of the RKR motif. When Kir6.2 tetramers are forced to the cell surface by deleting the retention signal, they show a low maximal open probability in ligand-free solutions ($P_{o(max)}$). TMD0 alone is able to sensibly stabilized the burst and conducting states of Kir6.2 tetramers raising its $P_{o(max)}$ of 4-fold, suggesting that interactions of transmembrane helices are able to force channel opening (Andrey P. Babenko and Bryan 2003).

NBDs domains are cytoplasmic and present consensus sequences as the 'ABC signature' as well as the Walker A (GXXGXGK(S/T)) and Walker B (XXXXDE, where X is a hydrophobic amino acid) motifs. These signatures allow ABC proteins identification. NBDs function consists in sensing the intracellular ATP/ADP ratio, allowing the SUR subunit to modify Kir6 sensitivity to nucleotides.

Among all ABC proteins, SUR shares the highest level of similarity with the MRP1 protein. Despite a 48% of sequence similarity (Moreau, Prost, et al. 2005) (Figure 2), that suggests a common folding and so a common function, SUR and MRP1 show very different functions. Over the past years, scientists have taken advantage of such predicted structural similarities to create SUR-MRP chimeras to study SUR2A-Kir6.2 interactions (Rainbow et al. 2004; Dupuis et al. 2008; Lodwick et al. 2014). In particular, this same strategy has been used in the present study to pinpoint SUR1 determinants for functional interaction between SUR1 and Kir6.2.

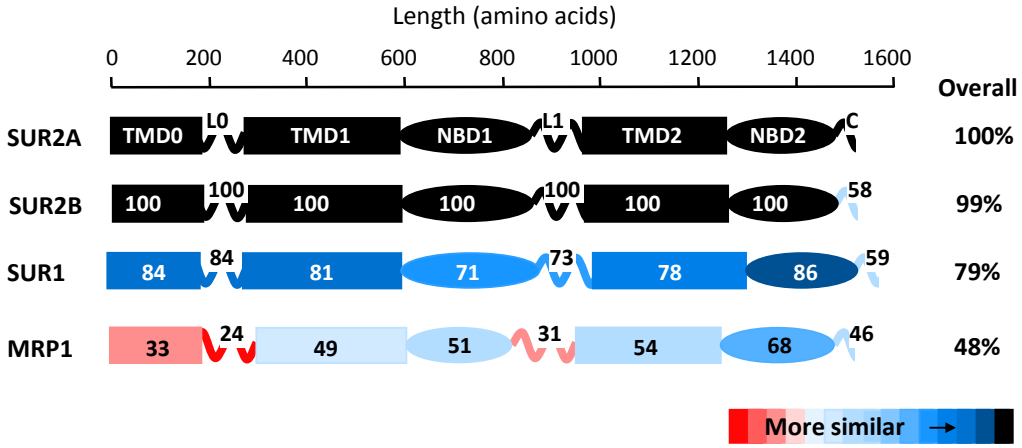

Figure 2. The human cardiac SUR2A isoform displays a high degree of sequence homology with MRP1 protein with the most convergence in domains NBD2 and TMD1 - TMD2 and the most divergence in domains TMD0 and connecting loops L0 and L1. Sequences were aligned individually with SUR2A using ClustalX. Similarity within each domain is specified in percent (Moreau, Prost et al., 2005).

The absence of structural data of proteins containing the TMD0 prevents the creation of full-length SUR models. Nevertheless, Bessadok and colleagues proposed, in 2011, a model of SUR1 in the outward-facing conformation, lacking the TMD0, based on the structures of other ABC transporters, MsbA and Sav1866 (Bessadok et al. 2011). This model is based on ~20% sequence identity and is supposed to be the physiologically relevant enzymatic state because it is the nucleotide-bound form (Figure 3).

Because full-length models of SUR are not yet feasible, a model of the full K-ATP channel complex remains utopic. The complexity of building such a model is further increased by the absence of solid data describing the interacting regions at SUR-Kir6 interface.

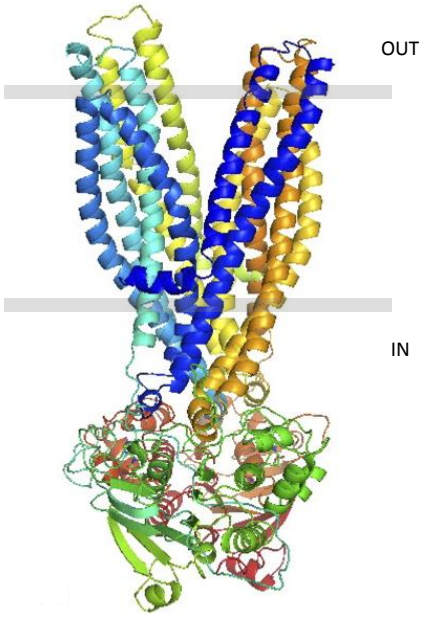

Figure 3. Outward-facing conformation model of SUR1 from Bessadok et al., 2011. SUR1 is shown with two transmembrane domains only (TMD1, in shades of blue & TMD2, in shades of yellow), and the two cytoplasmic nucleotide binding domains (NBD1, in shades of green and NBD2, in shades of brown).

1.2.1 The ABC family

The transport of organic and inorganic molecules across cell membrane is essential for living organisms. These molecules often need to be moved against their gradient. Transport against a chemical gradient can be driven by, for example, the free energy change associated with ATP hydrolysis (primary transport), or facilitated by the potential energy of the chemical gradient of another molecule (secondary transport). Primary transporters include a large family of integral membrane proteins referred as "ABC" (ATP-binding cassette) transporters.

These transporters represents the largest protein family identified to date. There are 48 ABC transporters in humans and, depending on their function for human health, many have been correlated to severe disease such as cystic fibrosis, Tangier disease (characterized by a severe reduction in the amount of high density lipoprotein), neonatal diabetes, macular dystrophy. Moreover, some ABC transporters are involved in the drug resistance of bacteria and cancer cells (Wilkens 2015).

The existence of methods that allow to closely look at protein structure sensibly improved the understanding of protein functions. On the other hand, obtainment of the atomic structure of proteins, and in particular of membrane proteins, it is a very complex and challenging process. To date, 14 ABC transporters have been structurally characterized:

- BtuCD, Vitamin B_{12} transporter (*E. coli*), (Locher, Lee, and Rees 2002);
- Sav1886, multidrug transporter (*S. aureus*), (Dawson and Locher 2006);
- ModB2C2, Molybdate transporter (*A. fulgidus*), (Hollenstein, Frei, and Locher 2007);
- HI1470/1, Metal-Chelate-type transporter, (*H. influenzae*), (Pinkett et al. 2007);
- MsbA, lipid 'flippase', (*S. typhimurium*) (Ward et al. 2007);
- MalFGK2, Maltose uptake transporter complex (*E. coli*), (Oldham et al. 2007);
- P-Glycoprotein, (*M. musculus*), (Aller et al. 2009);
- MetNI, Methionine uptake transporter complex (*E. coli*), (Kadaba et al. 2008);
- TM287-TM288, (*T. maritime*), (Hohl et al. 2012);
- HmuUV, heme transporter (*Y. pestis*), (Woo et al. 2012);
- ABCB10, Mitochondrial ABC transporter,(*H. sapiens*), (Shintre et al. 2013);
- Atm1-type, ABC exporter,(*N. aromaticivorans*), (Lee et al. 2014);
- Atm1, mitochondrial ABC transporter (*S. cerevisiae*), (Srinivasan, Pierik, and Lill 2014);
- McjD, antimicrobial peptide transporter (*E. coli*), (Choudhury et al. 2014);

These currently available structures have sensibly advanced our knowledge on the transport mechanism and revealed a sensible structural divergence (Beek, Guskov, and Slotboom 2014).

ABC transporters discovered so far are classified into two main groups: exporters and importers. The importers are further divided into class I and class II and a third group, the energy-coupling factor (ECF) family which is structurally and functionally more distinct (Figure 4). Bacteria use both importers and exporters while eukaryotes, with few exceptions, only employ exporters.

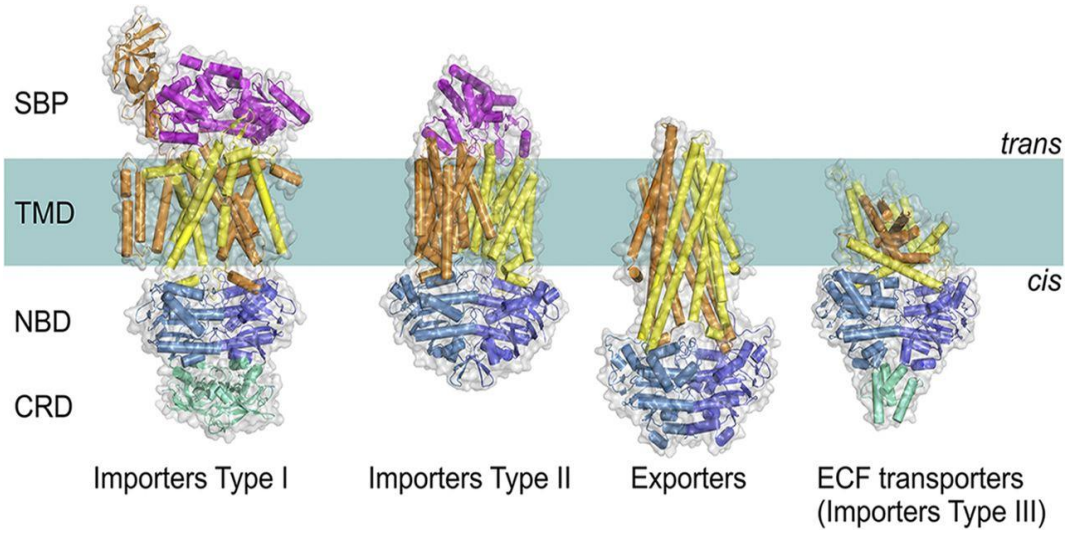

Josy ter Beek et al. J Gen Physiol 2014

Figure 4. ABC transporters folds. All share a similar general architecture: two NBDs (blue and sky blue) are attached to two TMDs (orange and yellow). In some transporters, additional domains are present (green), which often have a regulatory function. In Type I and II importers, the transported compounds are delivered to TMDs by SBPs (substrate-binding proteins, magenta) located in periplasm (Gram-negative bacteria) or external space (Gram-positive bacteria and Archaea).

A canonical ABC transporter is organized in four domains: two TMDs and two NBDs. While the NBDs are highly conserved among all ABC proteins, TMDs show a variable folding.

NBDs

Each NBD consists of two subdomains: the RecA-like domain and the α-helical domain. Alignment of NBDs sequences show highly conserved futures (Figure 5):

- The A-loop, which contains a conserved aromatic residue responsible for the correct binding of the ATP;
- The Walker A motif, a phosphate binding loop with a conserved K;
- The Walker B motif, which helps the coordination of Mg^{2+}, and possesses a conserved E that works as base to polarize water;
- The D-loop, important to maintain the geometry of the ATP hydrolysis site;
- The H-loop, which assists the positioning of the water molecule, Mg^{2+}, and the general base;

- The Q-loop, which has a conserved Q responsible for allowing the formation of an active site during ATP hydrolysis and is also in contact with the TMDs;
- The ABC signature motif (LSGGQ), ABC proteins hallmark.

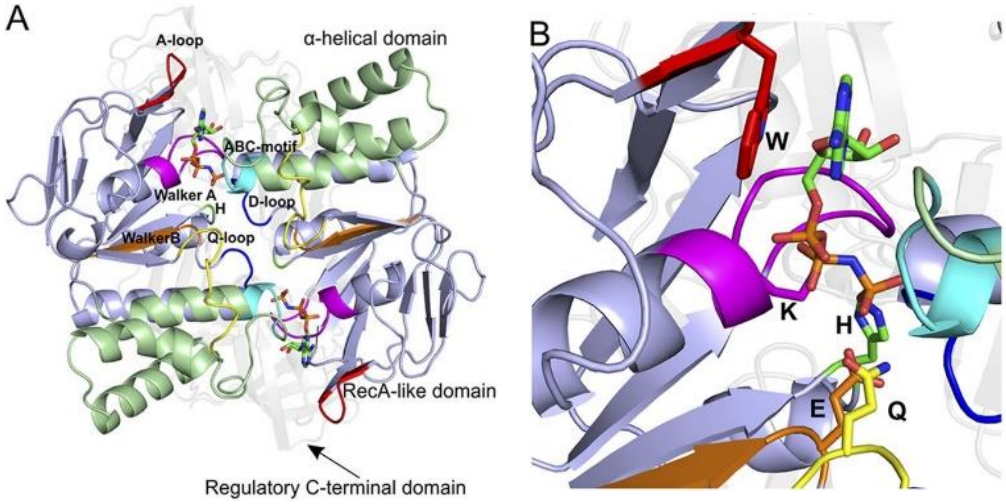

Figure 5. NBD structure (MalK dimer of the maltose transporter MalEFGK$_2$). (A) View along an axis perpendicular to the membrane plane from the trans-side onto the NBDs (The TMDs and SBP have been removed for clarity). Domains and highly conserved sequence motifs are color-coded: green, a-helical domain; light blue, RecA-like domain; faded gray, regulatory C-terminal domain; red, A-loop; magenta, Walker A; orange, Walker B; blue, D-loop; green, H-loop; cyan, ABC motif; yellow, Q-loop. The ATP analogue AMP-PNP is shown in sticks. (B) A closer look onto the nucleotide-binding site. The key amino acids are indicated (see NBDs for details) (Josy ter Beek et al., J Gen Physiol 2014).

TMDs

Depending on the transporter class, TM domains have 6 to 10 transmembrane α helices that are arranged in such a way that they form a pore necessary to allow substrate passage.

In general, the TMDs do not share sequence similarities but fold similarities, reflecting the need to transport a wide range of molecules.

Transport mechanism

The essential catalytic cycle of ABC transporters consists in a series of steps (Wilkens 2015):

- Binding of substrate;

- Binding of 2 Mg-ATP molecules to the NBDs;
- NBDs dimerization;
- Conformational changes into the TMDs to allow the passage of substrates;
- ATP hydrolysis;
- Release of phosphate, ADP and substrates;
- NBDs dissociation with subsequent return to the basal state.

This general cycle can be adapted to most ABC proteins but there is still a lot to clarify about number of ATP molecules used, mechanism of NBDs action and motion changes in the TMDs (Linton 2007) (Figure 6).

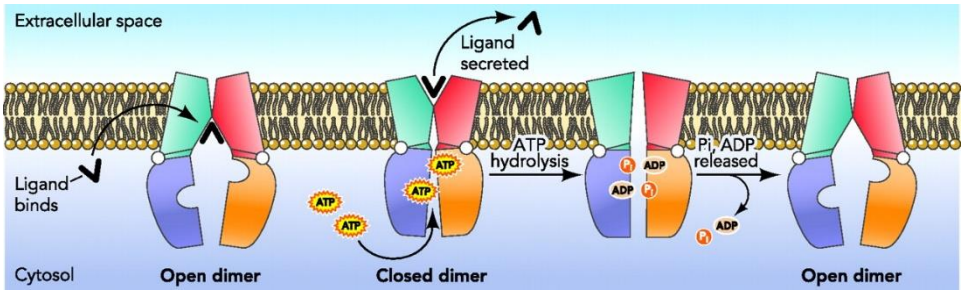

Figure 6. ABC transporters schematic mechanism of action.

To illustrate the progresses in deciphering the conformational changes at the TMDs level, it is useful to consider the recent results obtained with the P- glycoprotein (P-gp). The P-gp transporter is an ATP-dependent efflux pump with a wide substrate specificity. It has a great clinical and pharmacological significance as it is implicated in the transport of many drugs. Large amounts of this protein are found in cancer cells conferring them multi-drug resistance.

P-gp consists of two pseudosymmetric halves encoded into a single polypeptide. Each half is formed by six transmembrane helices (TMs) and one cytosolic nucleotide-binding domain (NBD) along with interconnecting loops and short helices. The TMs surround a central pocket, which contains multiple binding sites for ligands. Crystal structure studies employing a broad spectrum of ligands show that the binding of certain ligands produces a large conformational change in the fourth transmembrane helix (TM4) (Figure 7), which is postulated to be positioned to potentially transmit a signal to the NBDs (Szewczyk et al.

2015). This helix may possess a high degree of flexibility which is consistent with a role in substrate binding. Mutations in this region, which favour a well ordered, straight-helical conformation, disrupt substrate transport (Kodan et al. 2014), reinforcing the predicted role for TM4 in facilitating substrate entry and/or binding. The ligand binding-induced kinking of TM4 begins at Pro219.

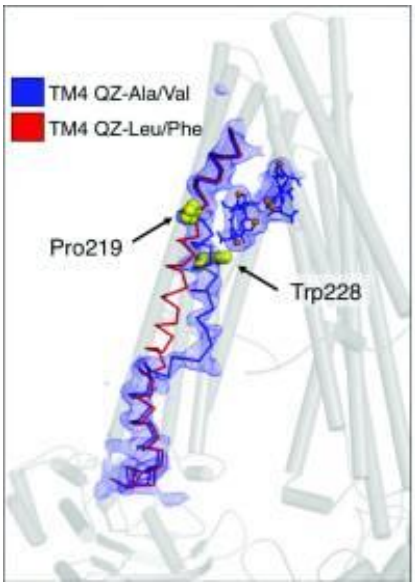

Figure 7. Overview of two different conformational changes in the TM4 mediated by 2 different classes of substrates. The kinking of TM4 in response to ligand QZ-Ala/Val (in stick-and-balls format) is shown (blue ribbon) in comparison to its 'straight' topology of the ligand QZ-Leu/Phe co-crystal structures (red ribbon). Essential residues Pro219 and Trp228 are shown as yellow spheres.

Such detailed knowledge of the mechanism of ABC transporters remains restricted mainly to P-gp, the most studied ABC protein. Studies of other ABC proteins, such as SUR, are needed to understand their specific function and pharmacology.

1.3 Kir6 channels

Kir6 channels belong to the inwardly rectifying potassium channels family (Kir channels). Both members of this subfamily, Kir6.1 and Kir6.2, show a common predicted folding. Each subunit folds into a short cytoplasmic N-terminus, two transmembrane α-helices (TM1 and TM2) connected by a loop (H5 loop) and a short helix (pore helix) containing the Kir channels signature (TVGYG for K^+ channels, TVGFG for Kir6 channels) and a large cytoplasmic C-terminal (Antcliff et al. 2005). Full-length Kir6 channels result from the assembly of four subunits that arrange to build a central pore that allows potassium flow. Tetrameric Kir6 channels can result from the assembly of Kir6.1 or Kir6.2 channels only (homotetramer) or from the association of Kir6.1 and Kir6.2 channels (heterotetramers) (Teramoto et al. 2009).

Kir6 channels are widely expressed in mammals. Kir6.1 is mostly expressed in smooth muscle (Inagaki, Inazawa, and Seino 1995) while Kir6.2 is highly expressed in pancreatic cells (Suzuki et al. 1997).

1.3.1 Inwardly rectifying potassium channels (Kir)

Inwardly rectifying potassium channels comprise a large family of voltage-independent potassium channels. The inward rectification is caused by cytoplasmic ion such as polyamines and Mg^{2+}, which block the outward passage of ions in favour of an inward current when the cell is at rest. Because of their peculiar characteristics, Kir channels stabilize the resting membrane potential close to the K^+ equilibrium potential by mediating transport of potassium across the membrane (Nichols and Lopatin 1997).

Depending on their degree of rectification, they are classified into 'strong', for channels that are more sensitive to Mg^{2+} and polyamines block, or 'weak' rectifier for channels that are less sensitive to these molecules.

So far, 15 Kir channels have been characterized. They are divided into seven subfamilies, depending on their characteristics such as degree of rectification, conductance, and sensitivity to diverse mediators. These subfamilies can be divided into four groups: Classical Kir channels (Kir2.x), G protein-gated Kir channels (Kir3.x), ATP-sensitive K^+ channels (Kir6.x) and K^+ - transport channels (Kir1.x, Kir4.x, Kir7.x), (Hibino et al. 2010) (Figure 8).

Kir1 subfamily includes weak rectifiers expressed mostly in the kidney and in the brain involved in transepithelial transport (C. G. Nichols and Lopatin 1997). Kir2 channels are strong rectifiers with high conductance variability. They are involved in the control of the excitability of cardiac and cerebral tissues (Reimann and Ashcroft 1999). Kir3 family is represented by G protein–activated strongly rectifying K^+ channels expressed in cardiac, neuronal and neurosecretory cells. Kir4 channels can exist as homo- or heteromers with Kir5 channels and they are expressed in glia cells, cochlea and kidney. In kidney, heteromers help the activity of Na^{2+}- K^+ ATPase by supplying potassium to the extracellular side of the plasma membrane (Hibino et al. 2010). Kir7.x channels function is still unknown. These channels are expressed in the epithelial tissue.

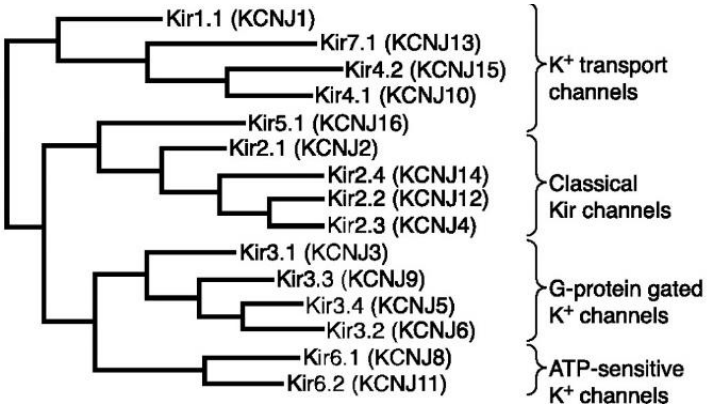

Figure 8. Kir channels phylogenetic tree (Hibino 2010).

1.3.2 Inward rectification

In physiological conditions, when the cell membrane is depolarized, Kir channels allow weak outward potassium current while the inward flow of potassium is stronger (Figure 9). This characteristic depends on the voltage-dependent block of outward current by cations (mostly Mg^{2+} and polyamines) that bind the cytoplasmic side of the pore and obstruct the outward flux of potassium ions (Bichet, Haass, and Jan 2003).

According to the presence of binding sites for positively charged molecules and ions, we can discriminate between strong rectifiers and weak rectifiers. It has been found that two residues located into the transmembrane helix 1 and in the channel C-terminal respectively are responsible for the binding of Mg^{2+} and polyamines. In particular, aminoacid at position 171

(N171) in Kir1.1 (weak rectifier) is uncharged, while in strong rectifier, such as Kir2.2, it is replaced by an aspartate (Yang, Jan, and Jan 1995; Lu and MacKinnon 1994). By mutating the uncharged asparagine in Kir1.1 into aspartate, it is possible to convert this weak rectifier into a strong rectifier channel.

A proposed mechanism to explain how Kir channels are clogged suggests that polyamines bind deep into the channel pore, at the transmembrane level, whereas the cytoplasmic region is a transient binding site that increases the local concentration of polyamines (Kubo and Murata 2001).

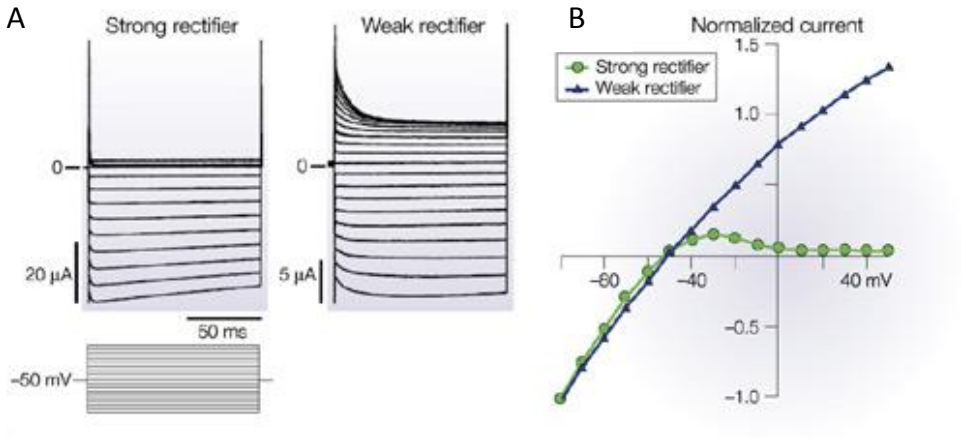

Figure 9. Inward rectification. A, TEVC recordings from Xenopus oocytes expressing strong and weak Kir channels. B, associated current-voltage relations. The protocol of stimulation shown below the current traces consists of voltage steps of 10 mV increments from -140 mV to +50 mV from a holding potential of -50 mV. Oocytes were bathed in a physiological extracellular solution (Bichet, Haass, and Jan 2003).

1.3.3 Kir channel structures

The ion channel field has been revolutionized by the resolution of the atomic structure of the KcsA channel from *S. lividans* in 1998 by Roderick MacKinnon and colleagues (Doyle et al. 1998). The high-resolution structure of this channel provided for the first time the structural basis for the K^+ selectivity and conduction that was only hypothesized at the time from electrophysiological studies. A characteristic hallmark of potassium channels is the combination of high selectivity (at least 10,000 times more permeant to K^+ than Na^+) and rapid throughput (up to 10^8 ions per second). These features allow K^+ to pass at such high rates that the protein seems to represent no limitation at all, while simultaneously acting as a concrete barrier to the smaller Na^+ ion.

The amino acid sequence of the KcsA channel core is similar to that of other K^+ channels, including vertebrate and invertebrate voltage-dependent K^+ channels, vertebrate inward rectifier and Ca^{2+}-activated K^+ channels, K^+ channels from plants and bacteria, and cyclic nucleotide-gated cation channels (Doyle et al. 1998).

The structure showed that KcsA is a homotetramer of four subunits that arrange to create an inverted cone. Each subunit participate to the formation of the tetramer with two transmembrane α-helices connected by a string of about 30 residues that constitute the pore. This region includes the turret, the pore helix, and the selectivity filter with its characteristic sequence highly conserved among potassium channels, TVGYG. The selectivity filter is structured to create a pile of oxygen rings organized with such a precision that they match the dimensions for coordinating a dehydrated K^+ ion (Figure 10).

The first structure at 3.2 Å resolution was followed by a refinement at 2 Å. This new highly detailed view of the channel provided a deeper understanding of the potassium conduction thanks to the removal of the hydration shell (Figure 11).

The new data provided by the refinement let the viewer see K^+ ions actually traversing the pore, as the pictures catch the ions at several stages of movement (Zhou et al. 2001).

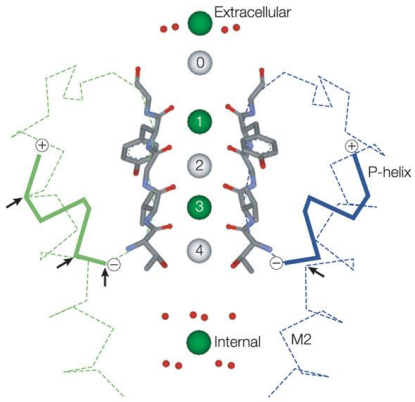

Figure 10. KcsA selectivity filter showing the linear array of K^+ binding sites. The TVGYG signature is shown in ball-and-stick representation. At the extracellular and internal ends of the filter, water molecules surround K^+ ions. As ions enter the filter, their hydration shell is progressively replaced by interactions with the backbone carbonyls of the selectivity filter (positions 0 to 4). The filter contains two ions simultaneously, either at positions 1 and 3 (green spheres), or at 2 and 4 (white spheres) (Bichet et al., 2003).

The inner and outer ion configurations are precisely balanced in terms of free energy, so that potassium ions travel very rapidly along the filter (Miller 2001). These refined X-ray results also provide for the first time the complete inner hydration shell of the ion inside the channel aqueous cavity that occurs at the intracellular side of the selectivity filter, halfway across the membrane. Eight molecules of water are individually visible, with their oxygens packed against the K^+ ion. This geometry matches the arrangement of the K^+-coordinating oxygens in the selectivity filter (Figure 11).

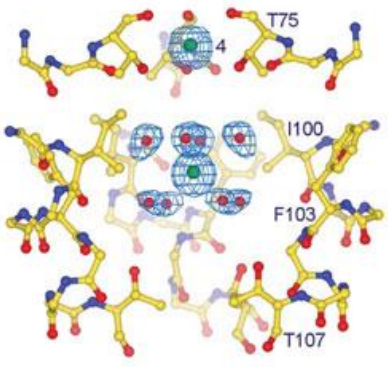

Figure 11. Eight water molecules (red spheres) surround a single K+ ion (green sphere) in the cavity. Residues forming the cavity are shown in ball-and-stick representation. For clarity, only backbone atoms and the side chains facing the cavity (Thr 75, Ile 100, Phe 103, Gly 104 and Thr 107) are shown. The subunit closest to the viewer has been removed for clarity (Zhou et al. 2001).

The structure of the eukaryotic Kir2.2 channel, a strong rectifier, was solved later, in 2009, and provided the structural basis of the rectification mechanism (Tao et al. 2009). As predicted earlier, the selectivity filter resembles other potassium channel filters (Kuo et al. 2003) with some important changes. First, the filter sequence TXGYGFR in Kir2.2 and other eukaryotic Kir channels, differs from the canonical signature TXGYGDX (where X represent an aliphatic residue). Moreover, eukaryotic Kir channels contain a conserved pair of cysteine residues flanking the pore region that serve to create a covalent linkage between the segment before the pore region and the segment after the selectivity filter. The resultant disulphide bridge is essential for both channel folding and function (Figure 12).

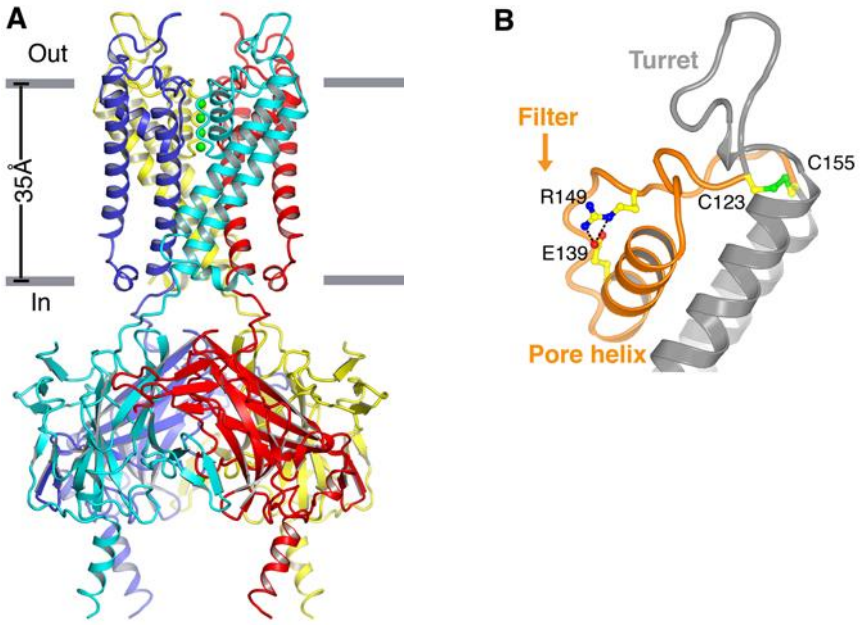

Figure 12. Structure of Kir2.2. A, ribbon representation of the Kir2.2 tetramer side view. B, close-up view of the pore-region of a single subunit (in ribbon representation). Side chains of residues E139, R149 and a pair of disulfide-bonded cysteines (C123 and C155) are shown as sticks and coloured according to atom type: carbon, yellow; nitrogen, blue; oxygen, red; and sulfur, green. The region flanked by the two disulfide-bonded cysteines is coloured in orange (Tao et al., 2009).

The pore lining on the intracellular side of the selectivity filter is mainly hydrophobic in most K^+ channels but eukaryotic Kir channels constitute an exception as their central region of the pore (central cavity) contains a polar residue. In Kir2.2 and other strong rectifiers, this

polar amino acid is an aspartate (D173), whereas in weak rectifiers such as Kir1.1 and Kir6.1 it is asparagine, which confers a reduced ability to bind polyvalent cations.

Another representative channel of the Kir family, the G-protein activated Kir3.2 channel (GIRK2) was crystallized in 2011. Its structure resembles the structure of the Kir2.2 channel with two main distinct characteristics. The first concerns the extracellular pore vestibule. In Kir3.2 channel, the turrets are arranged to create a larger vestibule for ions entry. This structural difference may provide an explanation for observed pharmacological differences between classical inward rectifiers and GIRK channels. Some pore-blocking toxins such as tertiapin inhibit many GIRK channels, including GIRK2, whereas classical inward rectifier channels are not affected. The larger vestibule in GIRK2 would allow tertiapin to fit in, whereas the more restrictive turrets in classical inward rectifiers appear to prevent toxin binding by physically restricting their binding site. The second difference occurs at the interface between the TMDs (transmembrane domains) and CTDs (cytoplasmic domains). In Kir2.2, the CTDs and the TMDs are far from each other compared to the corresponding domains in GIRK2. Here the CTDs and TMDs are tightly packed next to each other (Whorton and MacKinnon 2011) (Figure 13).

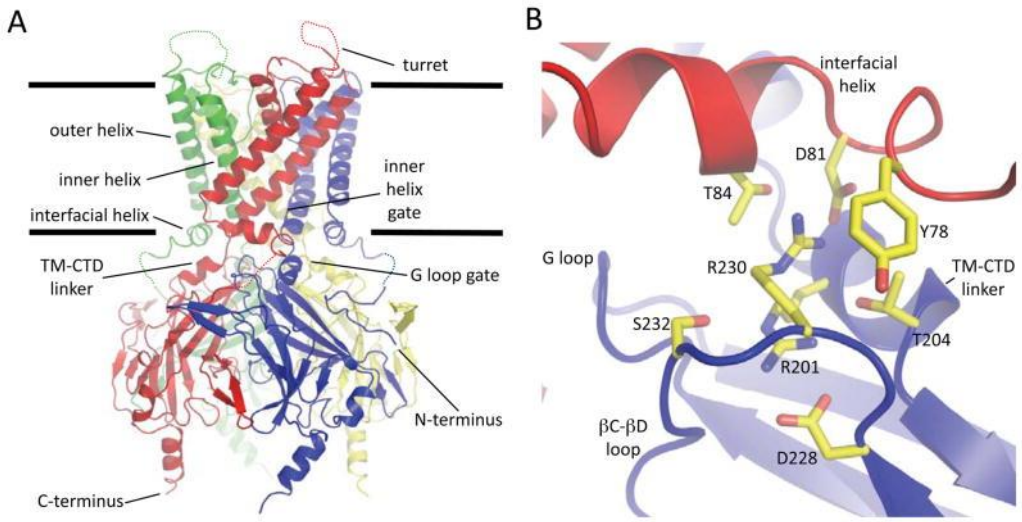

Figure 13. (A) Cartoon diagram of the GIRK2 structure. Each subunit of the tetramer is a different color. Unmodeled segments of the turret and N-terminal linker are drawn with dashed lines. (B) A cartoon diagram of key residues that mediate the contacts at the interface between the cytoplasmic and transmembrane domains (Whorton and MacKinnon 2011).

Concerning the gates, the structures of the eukaryotic Kir3.2 and Kir2.2 reveal the presence of two constrictions along the ion conduction pathway that have been proposed to act as gates. The first constriction, the inner helix gate, is located at the end of the inner transmembrane region of the channel. The second gate is represented by the G loop gate, located at the top of the cytoplasmic region of the tetramer (Whorton and MacKinnon 2011) (Figure 14).

The inner helix gate results from the inner helices of the TMDs, which stand above the cytoplasmic region. In Kir2.2 channel, two residues of the TM2, I177 and M181, form two hydrophobic seals, which shrink the pore at the interface between cytoplasm and membrane (Tao et al. 2009). The G loop gate is formed by the G-loop at the top of the CTD, immediately outside the membrane. In the PIP_2-free structure of Kir2.2 channel, where CTD is positioned far away from the TMD, the gates are as well positioned far away from each other. In the structure of Kir2.2 in complex with an analogue of the PIP_2, as well as in the structure of Kir3.2 channel (GIRK2), both gates are closely associated suggesting their possible cooperation (Niescierowicz 2013).

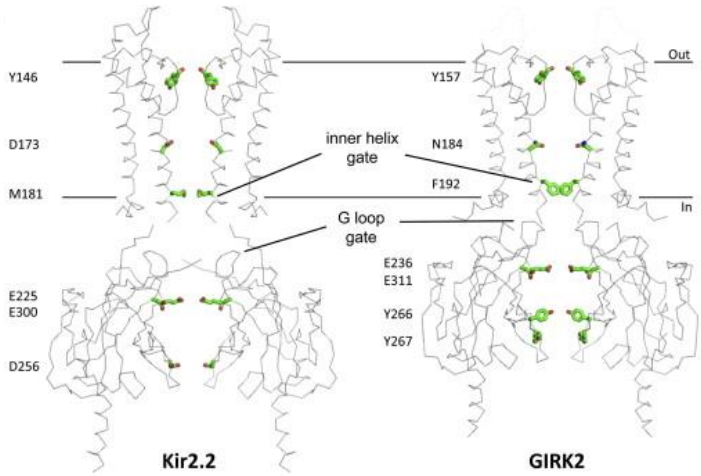

Figure 14.Comparison of the Kir2.2 and GIRK2 Structures. Key gating and rectification residues are highlighted in stick format (Whorton and MacKinnon, 2010).

2. SUR-Kir6 assembly and functional coupling

2.1 SUR-Kir6 association

The atypical association between SUR and Kir6 is unique among protein complexes. To communicate properly, both partners need to physically associate first. The association is poorly understood at the molecular level as a high-resolution structure of the K-ATP is still missing. SUR and Kir6 are separately expressed and retained in the ER until their association grants their release. In particular, the RKR sequence present in both proteins (between the helix 11 and the NBD1 in SUR1, and in the C-terminal tail of Kir6.2) is recognized by the protein COPI (coat protein complex I), preventing trafficking to the cell surface when the two partners are separated. Subsequently, when SUR and Kir6 start to associate, the RKR motif on Kir6.2 is masked by the presence of SUR1, preventing COPI binding. At this stage only the RKR motif present on SUR1 is exposed. This motif is inactivated by direct binding of the 14-3-3 protein to this region of the SUR1 or could be indirectly inactivated by 14-3-3 recruitment to a binding site near the distal tail of Kir6.2. (Heusser et al. 2006) (Figure 15).

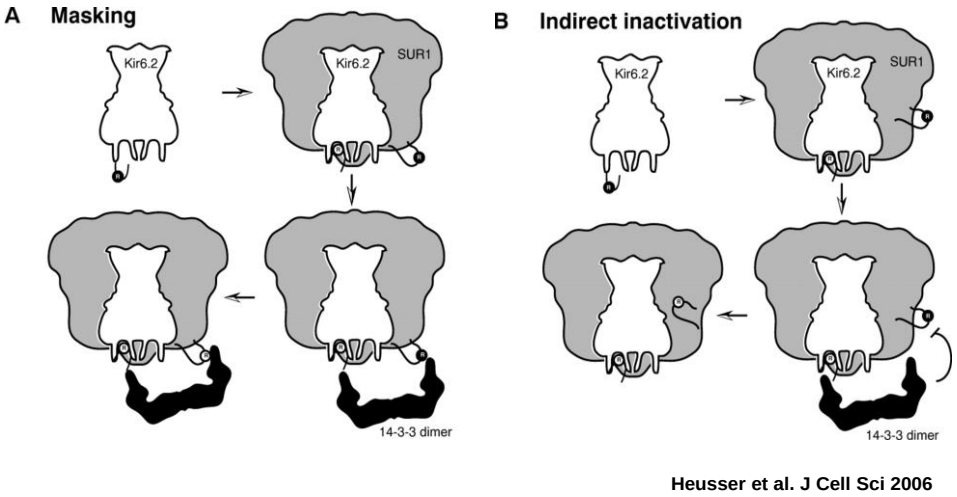

Figure 15. Retention signals inactivation models. As 14-3-3-binding sites other than the one provided by the distal tail of Kir6.2 remain unknown, the position of the 14-3-3 dimer is hypothetical. Filled circles with white Rs represent active RKR signals, open circles symbolize inactivation of the signal. (A) The signal of SUR1 could be inactivated by direct binding of 14-3-3 to this region of the protein (masking) or (B) be indirectly inactivated by 14-3-3 recruitment to a binding site in the vicinity of the distal tail of Kir6.2 (Heusser et al., 2006).

However, Kir6.2 deleted of its last 36 or 26 amino acids (in which the RKR signal is contained) is capable to traffick to the plasma membrane forming functional tetrameric channels in absence of the SUR subunit (Tucker et al. 1997).

Physical contacts between SUR and Kir6 occur at several levels inside the complex in order to favour K-ATP assembly. Despite the lack of a reliable map of these interactions, several regions have been proposed as essential for the association. SUR TMD0 has been proven to strongly associate with Kir6.2 and control its gating. K-ATP channels lacking this domain are not able to traffick to the plasma membrane (Fang, Csanády, and Chan 2006). Mutations in this domain have been correlated with severe diseases such as PHHI (persistent hyperinsulinemic hypoglycaemia of infancy) (Aguilar-Bryan and Bryan 1999), and Cantù Syndrome (van Bon et al. 2012). While for the Cantù Syndrome the molecular mechanism involved in the development of the disease is not known, PHHI onset seems to be directly correlated with the disruption of SUR-Kir6 association due to mutations A116P or V187D in the TMD0.

Moreover, TMD0 has been shown to enhance the expression of Kir6.2 deleted in its last 26 residues. On the other hands, TMD0 alone is incapable of rescuing the expression of non-truncated Kir6.2, suggesting that other regions of the SUR are necessary to mask the Kir6.2 retention signal in the C-terminus. This indicates that other regions of SUR are physically interacting with Kir6.2 (Chan, Zhang, and Logothetis 2003).

In order to understand whether TMD0 affects the gating of Kir6.2, single channel recordings of SUR1+Kir6.2ΔC26, TMD0+Kir6.2ΔC26 and Kir6.2ΔC26 in nucleotide-free solutions have been analysed.

As can be seen in Figure 16, single channel recordings of SUR1+Kir6.2ΔC26 and TMD0+Kir6.2ΔC26 are very similar and differ from the behaviour of the Kir6.2ΔC26 channel. In particular, both SUR1 and TMD0 are able to increase the burst duration and P_o of the channel. The values of P_o of these two channels are ~ 0.6, which is 4 times the value of P_o of Kir6.2ΔC26 channels. This can be explained with the lower frequency of openings and the lower open time of the truncated Kir6.2 (0.76 ms for Kir6.2ΔC26 and 1.8 ms of SUR1+Kir6.2ΔC26 and TMD0+Kir6.2ΔC26).

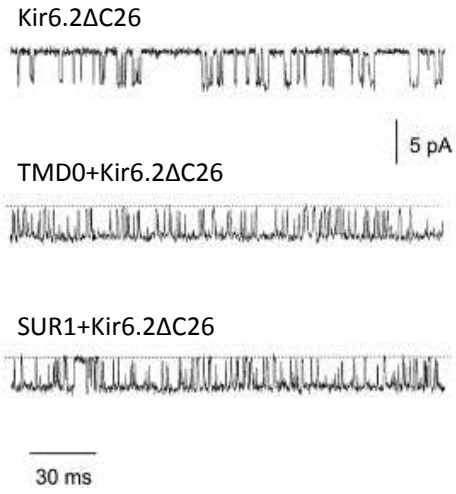

Figure 16. Single channel recordings in ligand-free solution. Single channels were recorded at -80 mV from inside-out patches with 96 mM K^+ on both sides of the patches (Chan, Zhang, and Logothetis 2003).

The association between SUR and Kir6 also modifies the ATP sensitivity of Kir6 (Figure 17) (Chan, Zhang, and Logothetis 2003).

SUR1 and TMD0 confer different sensitivities to ATP to Kir6.2ΔC26. The IC_{50} value for ATP inhibition of Kir6.2ΔC26 is ~ 100 μM. This value increases when truncated Kir6.2 channels are expressed with TMD0 (IC_{50}= ~ 300 μM) and decreases for SUR1+Kir6.2ΔC26 (IC_{50}= ~ 15 μM), (Chan, Zhang, and Logothetis 2003). It has been shown that ATP is more likely to bind to the channel when this is in the closed conformation (Enkvetchakul et al. 2000). The lower sensitivity for ATP of TMD0+Kir6.2ΔC26 channels compared to Kir6.2ΔC26 could be explained by the higher (P_o) given by the TMD0 domain. In fact, for high values of P_o the IC_{50} is also high. This observation is in agreement with Kir6.2ΔC26 channels having a low P_o and a low IC_{50} compared to TMD0+Kir6.2ΔC26 channels (higher P_o and a higher IC_{50}). On the other hands, this model does not fit with SUR1+Kir6.2ΔC26 channels, which have higher P_o but a low IC_{50}. This means that TMD0 alone is not sufficient to confer to Kir6.2ΔC26 all the characteristics of the K-ATP channel. This differential behaviour of the full SUR and the TMD0 is related to the presence of the NBDs in SUR.

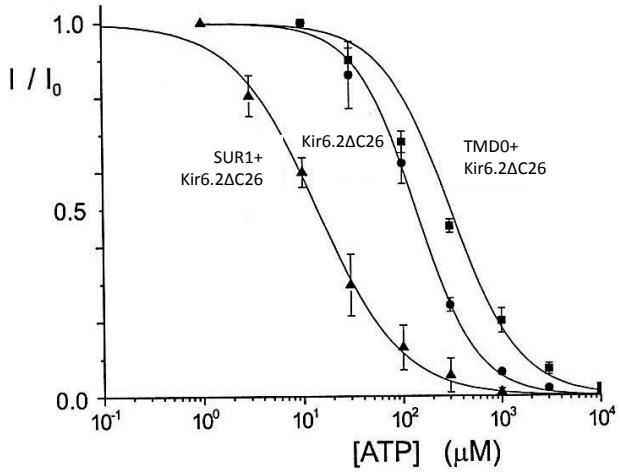

Figure 17. Dose-response curves for ATP inhibition (Chan, Zhang, and Logothetis 2003). Patches included in the measurements were recorded at -80 mV from inside-out patches with 96 mM K^+ on both sides of the membrane.

Another region of SUR (SUR2A specifically) involved in the physical association with Kir6.2 is the segment linking TMD2 with NBD2. This fragment (between residues 1295 and 1358) co-precipitates with Kir6.2 and competes with the full-length SUR for binding to Kir6.2 (Rainbow et al. 2004). The specificity of this interaction was also investigated in experiments performed using chimeric Kir6.2-Kir2.1 channels, as Kir2.1 does not associate with SURs to form functional channels.

Another proposed region of interaction involves residues 196-288 in SUR1 and Kir6.2 residues 28-32. Co-immunoprecipitation studies in *Xenopus* oocytes expressing Kir6.2 wild type or mutated in the N-terminal (deletion Δ28-32) and residues 196-288 of SUR1 reveal that the interaction between SUR1(196-288) and Kir6.2-Δ2832 is significantly reduced. This supports the idea that residues 196-288 of SUR1 form an essential part of the binding site between SUR1 and the N terminus of Kir6.2 and that this interaction is disrupted by deletion of residues 28-32 in Kir6.2 (Craig et al. 2009).

Other regions of the Kir6 channel participate to the physical association with SUR. Both N- and C-terminal plus the transmembrane helix 1, have been found to physically interact with SUR (Schwappach et al. 2000; Tammaro and Ashcroft 2007; Lodwick et al. 2014). Taken together, these observations are in line with the postulated architecture of the full-length K-ATP channel in which the helix 2 of Kir6, predicted to participate in the formation of the

selectivity filter, is buried in the center of the complex and protected from the interaction with SUR.

2.2 SUR-Kir6 functional coupling

Beside the physical association, the most suggestive feature of the K-ATP channel is the functional coupling occurring between SUR and Kir6.

With the expression 'functional coupling', we refer to the ability of ligands that bind to SUR to trigger Kir6 gating modifications. The SUR domains involved in this process are still largely unknown. To date, only few regions have been linked to ligand-induced functional coupling between SUR and Kir6. One of these is a domain reach in aspartate and glutamate (ED) (Karger et al. 2008). This domain has been proposed to act as an allosteric transducer enabling functional communications between the SUR2A and Kir6.2. The ED consists of a string of 15 aspartate and glutamate residues and it is located in the cytoplasmic loop 6 (CL6) between TMD1 and TMD2. It is positioned far from the postulated binding sites of openers and blockers of the K-ATP. Its main function would be to contribute to the cooperative interaction between the NBDs that is critical for conformational arrangements of MgADP-induced K-ATP channel activation. The ED it is not known to interact physically with Kir6.2 but is an essential part of the allosteric machinery that controls NBDs action and signal transduction to Kir6.2.

Another region of the SUR2A involved in the communication between K-ATP subunits is a region in the proximal C-terminus. Importantly, three residues at this level (E1350, I1310 and L1313) are essential for transmitting activation messages from the SUR2A to the pore-forming subunit. Mutation of these residues resulted in drastic reduction of channel activation by both MgADP and pharmacological openers mediated by SUR2A (Dupuis et al. 2008). The second project of this thesis work examines the role in the activation pathway at this proximal C-terminal region in the SUR1 subunit.

Interestingly, in contrast with what has been observed for the ED, mutation of the three residues do not affect the inhibitory pathway but only the activation network. These results support the theory that multiple transduction pathways between SUR and Kir6 might exist.

3. K-ATP channel mechanism and regulation

3.1 Physiological regulation of the K-ATP channel mediated by SUR

Transmembrane ABC proteins display transport activity with few exceptions such as SUR. Binding of MgATP at the SUR nucleotide binding domains (NBDs) results in NBD dimerization and hydrolysis of MgATP at the NBDs that leads to channel opening. Although it has a limited capacity to hydrolyse MgATP, (Bienengraeber et al. 2000), SUR is not a transporter. To date, SUR only known function is the gating regulation of Kir6 channels.

SUR brings to the K-ATP channel the capability to be activated by nucleotides when these are in complex with magnesium, as this class of molecules naturally inhibits Kir6. Moreover, SUR is target of drugs that can regulate either opening or blocking of the pore.

K-ATP channels are physiologically regulated by molecules that can target SUR or Kir6 or both. The resultant regulation is very complex and despite a large amount of functional data a lot remain to be clarified.

Regulation by MgADP and other nucleotides associated to Mg^{2+}

K-ATP channel activation mediated by ADP is one of the most important characteristics of the SUR protein. The activation requires the presence of Mg^{2+} and that both NBDs are intact (Gribble, Tucker, and Ashcroft 1997). Moreover, studies conducted on SUR1 show that the NBD1 strongly binds ATP rather than ADP, even in absence of Mg^{2+} and that MgADP, through binding at NBD2, antagonizes the Mg2+-independent high affinity ATP binding at NBD1. Furthermore, MgADP is more likely to bind to NBD2 than to NBD1 (Ueda, Inagaki, and Seino 1997). MgADP stimulates K-ATP channels with different affinities depending on the SUR isoform present. In particular, SUR1 and SUR2B are more stimulated that SUR2A. Experiments using chimera and mutant SURs suggest that the 42 amino acids at the C-terminal end of SURs (C42) play critical roles in the ADP-mediated activation of K-ATP channels and that the C42 of SUR2A may reduce ADP-mediated channel activation at NBD2 (Matsuoka et al. 2000).

The mechanism by which Mg-ADP binding to SUR is translated into channel opening remains unclear. It is now generally accepted that cooperative interaction between NBDs is essential for Kir6 gating, yet pathways of allosteric inter-subunit communication remain uncertain. Disruption of 15 negatively charged aspartate/glutamate amino acid residues

(948–962) of the SUR2A isoform blocks cooperative NBDs interaction and interrupts the regulation of K-ATP channel by MgADP. Moreover, three residues in the SUR2A (E1305, I1310, L1313) are implicated in the transmission of the activation message from SUR to Kir6.2. When these residues are mutated, SUR can no longer activate the channel (Dupuis et al. 2008). Taken together, these data suggest a substantial rearrangement of the SUR general folding and especially at SUR2A/Kir6.2 interface, just after MgADP binding, which triggers conformational changes in Kir6.2 that responds by opening the gate.

Other nucleotides are able to trigger K-ATP channel opening through binding to SUR such as MgATP, MgGDP and MgGTP (Trapp, Tucker, and Ashcroft 1997).

Regulation by Zinc

Applied at either the extracellular or the intracellular side of the membrane, zinc is a potent, reversible activator of K-ATP channels. In particular, zinc performs its action through binding at the extracellular side of SUR1-based K-ATP channels at the level of two histidines (H326 and H332) (Bancila et al. 2005). Moreover, in both SUR1- and SUR2A-based channels, zinc shows an activator intracellular effect (Prost et al. 2004).

Regulation by G proteins

G_{α} and $G_{\beta\gamma}$ proteins, released after GPCRs activation, have a role in activating K-ATP channels. In particular, the $G_{\alpha i1}$ subunit stimulates SUR1-based K-ATP channels while the $G_{\beta\gamma 2}$ subunits have been correlated to both SUR1 and SUR2A-based channels activation (Wada et al. 2000).

3.2 Physiological regulation of the K-ATP channel mediated by Kir6 channels

Nucleotides

Kir6 channels are strongly inhibited by ATP. ATP binding site in Kir6 does not resemble any of the classical nucleotide binding sites, such as the NBDs of SUR. In particular, ATP cannot be hydrolysed by Kir6. As the structure of Kir6 is still missing, we can only rely on functional data to locate the ATP-binding site. To date, most data agree that this site is formed by both N- and C-terminal domains (Tucker et al. 1998; Proks et al. 1999). With improvements of protein modelling, a putative ATP-binding site in Kir6.2 has been identified (Antcliff et al. 2005). The model, reinforced by experimental tests, locates the binding site for ATP near the top of the intracellular domain (IC). Each of the four binding pockets lies at the interphase between N- and C-terminal domains of the same subunit with a little contribution by the neighbour C-terminal of the subsequent chain (Figure 18).

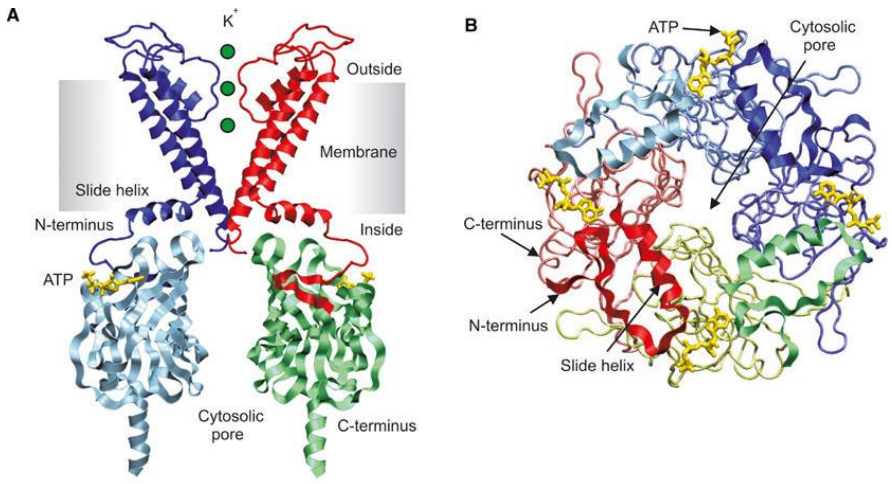

Figure 18. The ATP-binding site. A, side view of the ATP-binding site. For clarity, the TMs of only two subunits and the IC domains of two separate subunits are illustrated. ATP (yellow) is docked into its binding sites. B, Kir6.2 tetramer, top view, with the TMs removed (residues 64–177). The N-terminal domain is shown in ribbon format and the C-terminal domain in backbone format. Different colours represent individual subunits (Antcliff et al., 2005).

Once ATP binds, its phosphate tail interacts with R201 and K185 in the C-terminal of one chain and with R50 in the N-terminal of the next chain. The binding of a single ATP

molecule appears to be sufficient to trigger the conformational changes necessary for channel closure (Markworth, Schwanstecher, and Schwanstecher 2000).

Moreover, other nucleotides can bind in this pocket but with a lower affinity (Dabrowski, Tarasov, and Ashcroft 2004). If phosphates are removed, the binding affinity diminish by several orders of magnitude (Tucker et al. 1998).

Lipids

Like other channels, also Kir6 activity has been shown to be dependent on phosphatidylinositol 4,5-bisphosphate (PIP_2). In particular, PIP_2 increases channel open probability in absence of ATP and reduces the inhibitory effect of the ATP by decreasing the channel apparent affinity for this molecule (Hilgemann and Ball 1996; Fan and Makielski 1997). The binding of PIP_2 to Kir6.2 has not been precisely located. Nevertheless, mutagenic experiments have shown that PIP_2 effect is carried out through electrostatic interactions of the polar head with positively charged residues present in the N-terminal (K39, R54), transmembrane (K67) and C-terminal (R176, R177, R301) regions. The aliphatic chain would be anchored at the membrane. The structure of the Kir2.2 channel in complex with a PIP_2 analogue suggests an explanation of the effect mediated by this lipid. PIP_2 binds at the interphase between TMD and CTD producing a conformational change in Kir2.2 that would stabilize the channel in an open conformation.

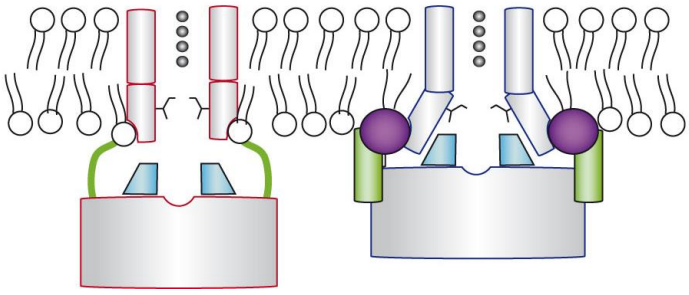

Figure 19. Proposed mechanism of Kir2.2 activation by PIP_2. PIP_2 (purple sphere) binds at an interface between the TMD (grey cylinder) and the CTD (grey rectangle) and induces a large conformational change. The flexible linker (green line) contracts (green cylinder), the CTD moves towards and becomes tethered to the TMD, the G-loop (cyan wedge) inserts into the TMD and the inner helix activation gate opens (Hansen et al. 2011).

Other lipids of physiological relevance such as the long chain Co-enzyme A esters (LC-CoA) also activate Kir6 channels by decreasing the affinity of these channels to ATP (Gribble et al. 1998). The cholesterol has also been proposed as possible regulator of Kir6 channels but its action remains controversial as some studies suggest an activator effect and others an inhibitory action.

3.3 K-ATP channel physiology and physiopathology

The K-ATP channel ability to sense the ATP/ADP ratio inside cells gives it a primary role as metabolic sensor, able to modulate membrane excitability depending on the metabolic state of the cell. At rest, K-ATP activation is translated into membrane hyperpolarization while its inhibition triggers membrane depolarization. Depending on the localization, variations in the membrane potential will provoke different cellular responses.

K-ATP channels in pancreas

K-ATP channel function has been best characterized in pancreatic β cells where its activity is linked to insulin secretion (Figure 20) (Ashcroft, Harrison, and Ashcroft 1984). When the level of glucose in the blood is low, K-ATP channels are partly active at rest and their activity helps to maintain the membrane hyperpolarized. In contrast, when the level of glucose in the blood increases, this is shuttled into the pancreatic β cell where it is be metabolized to produce ATP. ATP level rises, triggering K-ATP channel closure. As the K-ATP channel is highly expressed at the plasma membrane of these cells, channel closure provokes membrane depolarization that in turn activates voltage-dependent Ca^{2+} channels. These channels allow influx of Ca^{2+} that triggers insulin secretion. Thus, K-ATP channel activity in the pancreas is crucial.

Malfunctions due to K-ATP channel mutations have been correlated with severe pathologies: PHHI characterized by high levels of insulin, type II diabetes involving low levels of insulin secretion despite high levels of glucose in the blood (Gloyn, Siddiqui, and Ellard 2006). Most PHHI mutation are classified as 'loss of function' mutations in the gene encoding for SUR1 (Ashcroft 2005). These mutations can be divided in two groups: mutations causing reduced expression of channels (class I) and mutations that reduce channel open probability (class II). SUR1 'gain of function' mutations, resulting in overactive channels, are linked to a rare disease, neonatal diabetes. Depending on the mutations, the severity of the associated

pathologies varies from transient neonatal diabetes to neurological disorders (DEND syndrome).

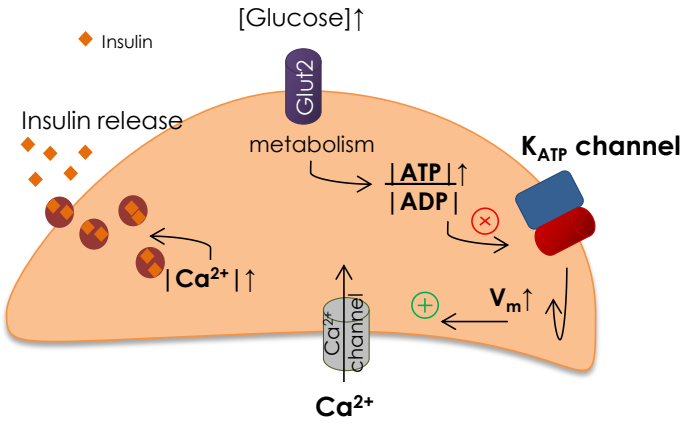

Figure 20. K-ATP role in insulin secretion. Glucose is be metabolized in pancreatic β cells to produce ATP. When ATP level rises, K-ATP channels are inhibited. Channels closure triggers membrane depolarization that in turn activates voltage-dependent Ca^{2+} channels. Influx of Ca^{2+} facilitates insulin secretion.

K-ATP channels in cardiomyocytes

K-ATP channels are as well expressed in cardiomyocytes where they appear to be involved in a mechanism of protection against ischemia. During ischemic stress, the concentration of ATP in the cells decreases, triggering K-ATP channel opening and increasing resting K^+ permeability of the membrane. The K-ATP channel action favours hyperpolarization and reduces excitability. This change in the membrane potential reduces Ca^{2+} influx, shortens the action potential duration and decreases the contraction. This protective effect has been observed in mice knock-out for the Kir6.2 gene (Gumina et al. 2007). Mutations of these K-ATP channels (at the NBD2 of SUR2A) are correlated with cardiomyopathy, ventricular arrhythmia and atrial fibrillation.

K-ATP channels in the central nervous system

K-ATP channels can be found as well in brain tissues. GABAergic neurons preferentially express SUR1 in complex with Kir6.2 while the dopaminergic neurons express both SUR1-

Kir6.2 and SUR2B-Kir6.2 complexes (Liss, Bruns, and Roeper 1999). In the hypothalamus K-ATP channels are mostly composed of SUR1-Kir6.2 heteromers.

The role of these channels in the brain has been studied comparing the effects of hypoxia in wild type and knock-out mice. In event of hypoxia (caused by deprivation of oxygen), neuronal activity slows down in wild type mice, while in mice knock-out for the Kir6.2 gene, the activity increases (Yamada et al. 2001). As result, these mice are more susceptible to generalized seizure after hypoxia. For the wild type mice has been suggested that the K-ATP channels might have a protective role against ischemia when under metabolic stress these channels start to be more active because of the reduced concentration of ATP. Transgenic mice overexpressing SUR1 in both cortex and hippocampus are more resistant to ischemic attacks after exposition to kainic acid. This molecule is a potent neuroexcitatory amino acid that acts by activating receptors for glutamate. It is used to study the effects of neurons ablation in animal models because it produces neuronal death if injected in large amounts. These data suggest a protective effect mediated by the SUR1 subunit (Hernández-Sánchez et al. 2001).

3.4 K-ATP channel pharmacology

K-ATP channel is targeted by many drugs that can be divided in two main categories: potassium channels blockers, which inhibit K-ATP activity, and potassium channels openers (KCO), which trigger activation of the K-ATP.

3.4.1 K-ATP channel inhibitors

This class of molecules can be subdivided in two groups: those targeting SUR (sulfonylureas and benzamido derivatives) (Ashcroft and Gribble 1999) and those interacting with Kir6.2 (imidazolines) (Mukai et al. 1998). Sulfonylureas have been shown to interact with Kir6 as well but with much lower affinity (Gribble et al. 1997).

All compounds trigger conformational rearrangements that result into channel closure and possible subsequent membrane depolarization. Some of these inhibitors stimulate insulin secretion and they are therefore used in the treatment of type II diabetes (sulfonylureas). The stimulatory effect on insulin secretion of some sulfonylureas has been discovered long before

the identification of the blocking effect on K-ATP channels (Sturgess et al. 1985). Sulfonylureas were used to clone the SUR1 gene (Aguilar-Bryan et al. 1995).

It has been suggested that two different binding sites for blockers might exist on SURs. In particular, SUR1 would possesses both sites while SUR2A just one of these. This would explain the differential affinities for sulfonylureas of SUR1 and SUR2A-based channels (Table 1).

Table 1. IC_{50} of K-ATP channels blockers (adapted from Vivaudou, Moreau and Terzic, 2009).

	Tolbutamide	Glibenclamide	Meglitinide
Kir6.2	1.7 mM	40 μM	> 1 mM
SUR1-Kir6.2	5 μM	8 nM	0.7 μM
SUR2A-Kir6.2	1 mM	0.04 μM	0.3 μM

These differential affinities are used to target specific K-ATP channels. As examples, tolbutamide targets SUR1-based channels while glibenclamide and meglitinide block both SUR1- and SUR2A-based channels (Proks et al. 2002).

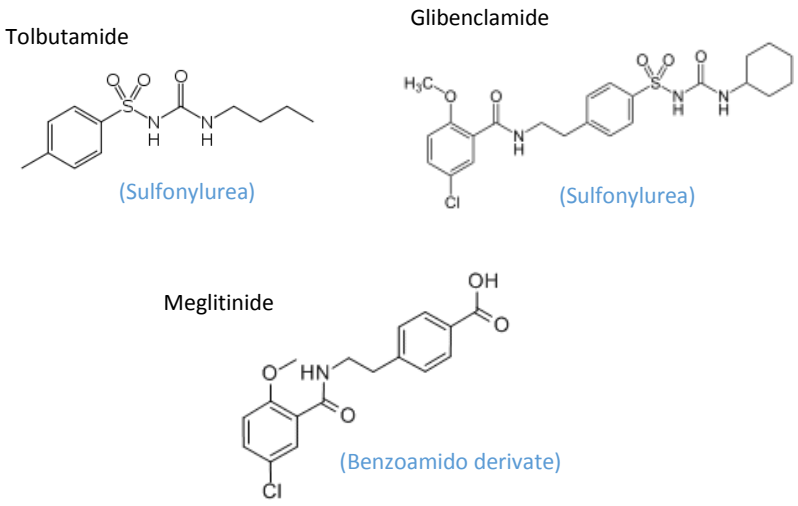

Figure 21. Chemical structures of K-ATP channel inhibitors.

It appears that a first binding site for blockers in the SURs involves the cytoplasmic loop linking helix 15 to helix 16. In particular, residue S1237 of SUR1 favours tolbutamide blocking while, in SUR2, this amino acid is substituted by a tyrosine that interferes with the tolbutamide-mediated effect (Ashfield et al. 1999).

A second binding site would involve loop L0 that connects TMD0 to TMD1 (Mikhailov, Mikhailova, and Ashcroft 2001) and probably the Kir6.2 N-terminal region. This second binding site is conserved in both SUR1 and SUR2 and is possibly involved in the binding of the benzoamido group of glibenclamide. In contrast, the first site, absent in SUR2, recognizes the sulfonylurea group. As a consequence, glibenclamide, which possesses both the sulfonylurea group and the benzoamido group, would not properly bind to SUR2, inducing a lower effect compared to the effect mediated by SUR1.

A later synthetized sulfonylurea, HMR1833, is able to bind with higher affinity to the SUR2 isoform than to the SUR1. This makes it suitable to specifically target cardiac K-ATP channels (Russ et al. 2001).

A particular K-ATP channel blocker has been developed in order to discriminate between Kir6 isoforms. This molecule is the guanidine U-37883A (imidazoline class). Although its action actually depends on the SUR isoform present in K-ATP channels, it inhibits selectively Kir6.1-based channels like the vascular SUR2B-Kir6.1 channels (Teramoto 2006).

3.4.2 K-ATP channel openers (KCO)

This group of compounds contains a wide variety of molecules that induce opening of K-ATP channels, which might result into membrane hyperpolarization. This class of compounds are classified into chemical families according to their molecular structure. Among these, the most common used in laboratories include benzothiadiazines (diazoxide), benzopyrans (cromakalim), cyanoguanidines (pinacidil), nicotinamides (nicoradil).

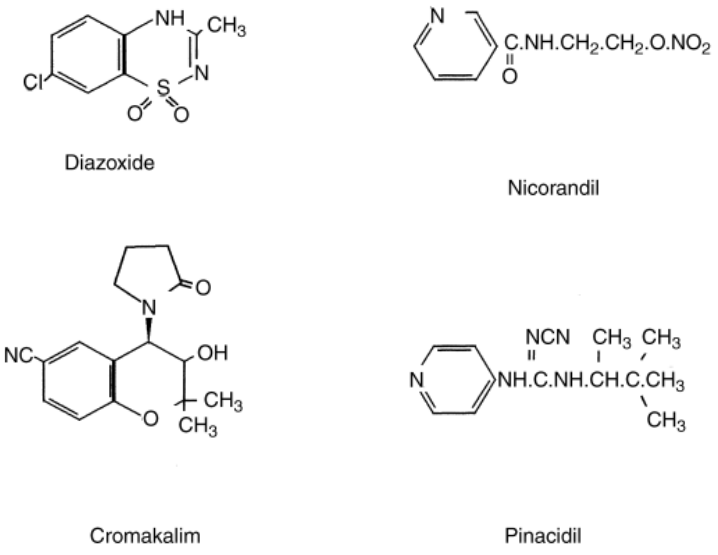

Figure 22. Structures of representative K-ATP channel openers.

KCOs acts though the SUR subunit, exhibiting different affinities for K-ATP channels depending on the SUR subunit present. Most openers preferentially target SUR2A and SUR2B subunits, with the exception of the diazoxide that has a higher effect on SUR1 activity (Moreau, Gally, et al. 2005).

Two residues in helix 17 of SUR2 (L1249 and T1253 in SUR2A) are involved in the binding of non-diazoxide openers. When these residues are mutated, SUR2A loses the ability to be regulated by openers (Moreau, Prost, et al. 2005). Other studies also highlight the importance of the loop region connecting helix 13 to 14 (Uhde et al. 1999). Taken together both studies report the essential role of the TMD2 domain in the binding of SUR2-selective KCOs.

The Diazoxide binding site has not been precisely located yet and the existing data are contradictory. Nevertheless, it appears that the TMD1 domain has a primary role in diazoxide binding (Babenko, Gonzalez, and Bryan 2000).

The activity of openers is correlated with the presence of MgATP and MgADP. For example, diazoxide, which acts specifically on SUR1, can bind to SUR2 in presence of MgADP

(D'hahan et al. 1999). Furthermore, it has been demonstrated that KCO binding is positively modulated by MgATP through NBDs (Schwanstecher et al. 1998).

Table 2. Concentrations of K-ATP channels openers causing half-maximal activation. Values recorded in presence of MgATP + ADP are reported in parenthesis (adapted from Vivaudou, Moreau and Terzic, 2009).

	diazoxide	**nicoradil**	**pinacidil**	**cromakalim**
SUR1-Kir6.2	30 μM	unknown	1 mM	> 1 mM
SUR2A-Kir6.2	> 1 mM (100 μM)	1 mM (100 μM)	10 μM	10 μM

In this thesis work, the SUR2A opener used is an analogue of the pinacidil called P1075.

4. Ion Channel-Coupled Receptors (ICCRs)

4.1 Principle of the ICCR concept

The ICCR concept was inspired by the organization of the K-ATP channel in which a receptor (SUR) co-assembles with a potassium channel (Kir6.2). Thus, in principle, the SUR can be replaced with any receptor capable of communicating conformational changes to the pore-forming subunit after the binding of a specific ligand. Such channel would respond to the message transferred by the receptor by modifying its gating. Gating modifications can be easily detected by classical electrophysiology techniques (Figure 23). The amplitude of the current, generated by the potassium flow through Kir6.2, would depend on ligand concentration, enabling the estimation of apparent affinities by dose-response measurements.

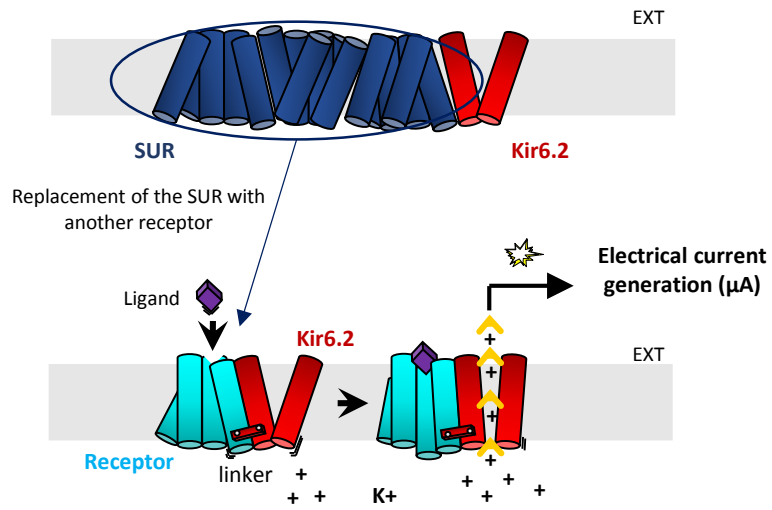

Figure 23. ICCR design strategy. The SUR receptor of the natural K-ATP channel is replaced by another receptor that is fused to the Kir6.2 in order to grant physical association. Receptor and Kir6.2 are linked in such a way that the binding of a ligand upon the receptor triggers conformational changes that are transmitted to Kir6.2. Kir6.2 responds to these changes by modifying its gating. The current generated by the flow of K^+ ions though Kir6.2 is detected by electrophysiological techniques.

The class of receptors chosen for ICCR creation is the G protein-coupled receptors (GPCR), as these proteins represent the biggest family of receptors and have a huge relevance as target of drugs (for a GPCR overview see section 4.4).

4.2 ICCR engineering

ICCRs are created by the fusion of the C-terminus of a G Protein-Coupled Receptor (GPCR) to the N-terminus of the Kir6.2 channel (pore-forming subunit of the K-ATP channel). The fusion ensures a necessary physical link between these two proteins and a functional role in the transmission of the ligand binding events upon the receptor to the Kir6.2 gates (Moreau et al. 2008).

Kir6.2 homotetramerizes to form a potassium selective pore. This organization guides the assembly of the full ICCR complex with four GPCR-Kir6.2 monomers per channel.

In ICCRs, the channel acts as a direct reporter of the conformational changes occurring at the GPCR level, detecting agonist- and antagonist-bound states of the receptor (Moreau et al. 2008). The fusion between receptor and channel does not guarantee a functional communication between the partners. The linker domain must be adjusted by precise deletion of the channel N-terminus. Obtaining of the functional coupling represents the challenging event in the engineering of ICCRs.

To date, the ICCR concept has been successfully validated in our laboratory on several GPCRs including the human M2 muscarinic, the $D2_L$ dopaminergic, the β2 adrenergic and the bovine rhodopsin receptors (Moreau et al. 2008; Caro et al. 2011; Caro et al. 2012). Moreover, the success of the ICCR technology developed in the 'Channels' group, inspired the creation of another ICCR containing the human olfactory receptor hOR by Oh and colleagues (Oh et al. 2015).

4.3 Applications of the ICCR technology

The initial objective of the ICCR was the design of electrical biosensors to insert in micro-electronic systems for *in vitro* diagnostic or drug screening miniaturized devices. ICCRs combine in one protein the ability of GPCRs to specifically recognize their ligands and the capability of the channels to generate detectable signals. The signal amplitude generated by Kir6.2 is correlated with the ligand concentration, allowing label-free assays with high signal-to-noise ratio and fast real time measurements (Moreau et al. 2008). Since the signal is independent of downstream intracellular pathways, including the heterotrimeric G proteins, ICCRs have been proved to be a unique tool for functional characterization of altered GPCRs optimized for crystallographic studies (Niescierowicz et al. 2014), not anymore able

to interact with G proteins. Moreover, ICCRs have been used recently by another laboratory to develop a platform for high-throughput screening of the activity of olfactory receptor-based ICCRs (Lim et al. 2015).

4.4 G protein-coupled receptors (GPCRs) at a glance

4.4.1 GPCRs general informations

GPCRs constitute the largest family of membrane proteins in the human genome, encoded by more than 800 genes. GPCRs share a common architecture with seven transmembrane helices containing several GPCRs signatures, an extracellular N-terminal domain and an intracellular C-terminal tail. Transmembrane helices are interconnected by loops: three extracellular loops (ECL1, ECL2, ECL3) and three intracellular loops (ICL1, ICL2, ICL3). In the Rhodopsin-like class, the intracellular part usually includes a short amphipathic helix (helix VIII) followed by a tail carrying signalling sites (palmitoylation and phosphorylation), (Katritch, Cherezov, and Stevens 2012). Despite this common architecture, GPCRs share low sequence identity that can be explained by their ability to recognize a wide range of ligands.

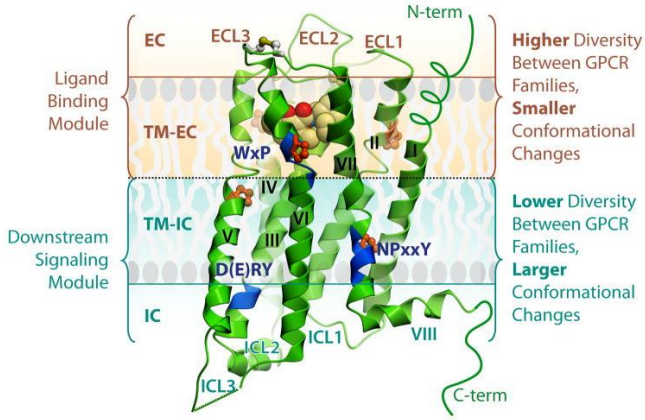

Figure 24. General architecture of GPCRs. Major regions and structural features are shown on example of the D3R crystal structure. The 7TM helical bundle contains a number of proline-dependent kinks (prolines shown in orange), that approximately divide the receptor into two modules. The EC module (EC and TM-EC regions) is responsible for binding diverse ligands and has much higher structural diversity. In contrast, the IC module (IC and IC-TM regions), involved in binding downstream effectors is more conserved between GPCRs, but undergoes larger conformational changes upon receptor activation. Blue ribbon patches highlight highly conserved, functionally relevant motifs in the TM helices of Class A GPCRs. The C-terminus in most GPCRs includes helix VIII (Katritch, Cherezov and Stevens, 2012).

GPCRs populate cell membrane of all tissues in human body. Their role consists in recognition of a large spectrum of ligands and subsequent transmission of the related messages to downstream effectors inside the cell. Among the very broad physiological functions of GPCRs, they are involved in smell, vision, inflammation, pain sensation and mood regulation. Because of their ability to induce cell responses and the easy access of their ligand binding site at the cell surface, GPCRs represent a major pharmaceutical target (Wise, Gearing, and Rees 2002).

4.4.2 The GPCR superfamily

To date, there are several systems to classify GPCRs but the most popular ones are based on ligand binding mode and/or structural similarities (A-F classification system, (Kolakowski 1994)) or on phylogenetic relationship (GRAFS) (Lagerström and Schiöth 2008).

The A-F classification system covers all GPCRs members in both vertebrates and invertebrates. However, the most used system is the GRAFS, which divides GPCRs into five

main families: Rhodopsin (R, 701 members), Secretin (S, 15 members), Glutamate (G, 15 members), Adhesion (A, 24 members), Frizzled/taste2 (F, 24 members), (Figure 25).

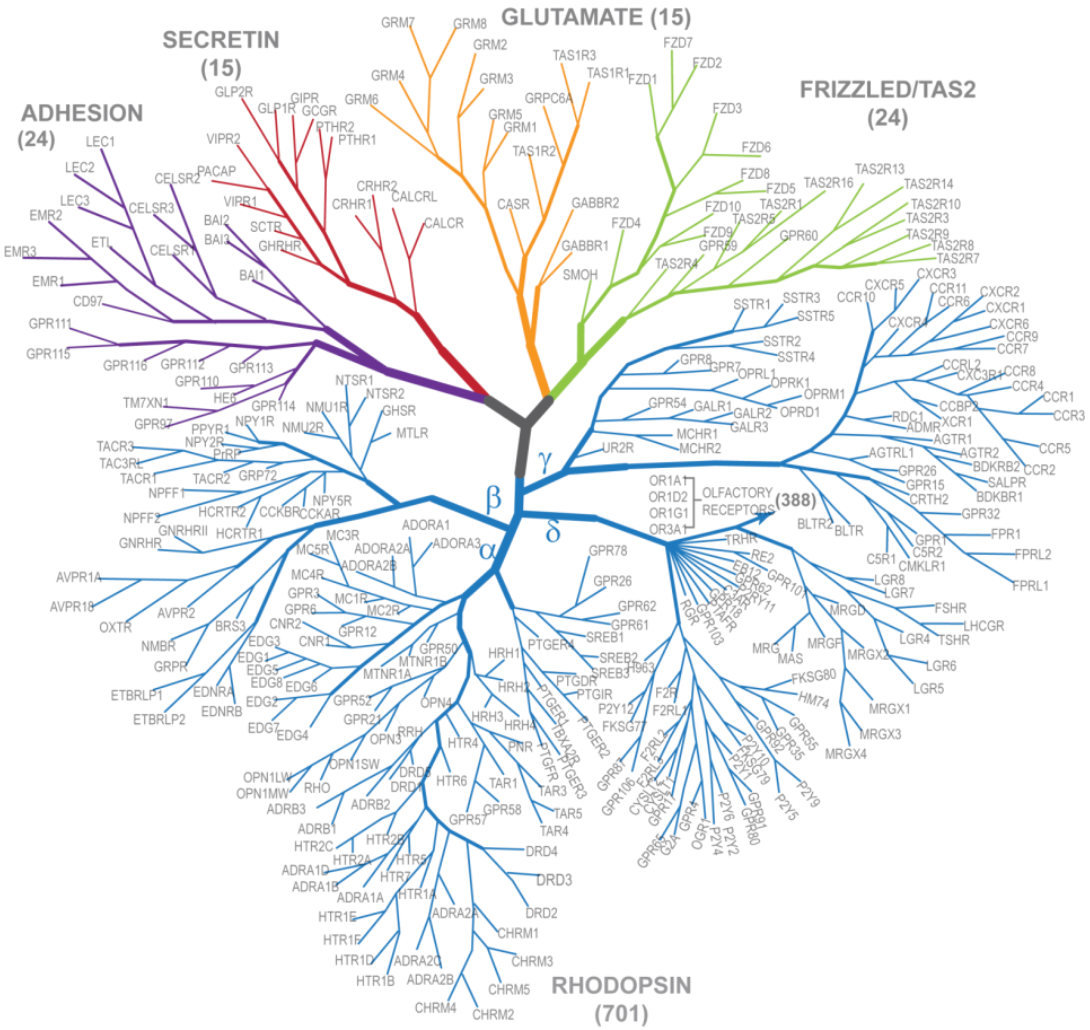

Figure 25. Phylogenetic tree of the GRAFS (Glutamate, Rhodopsin, Adhesion, Frizzled/Taste 2, Secretin receptors classes) classification (from Katritch, Cherezov and Stevens, 2012). Because the Rhodopsin family comprises the largest number of members, it is further divided into four groups (α, β, γ and δ).

- The rhodopsin family

Comprises the largest number of members and, because of this variety, was further divided into four groups (α, β, γ and δ). It includes the light-activated opsin receptor, the odorant molecules stimulated olfactory receptors, receptors activated either by small molecules (amines, prostaglandins), peptides (hormones), or proteins (chemokines, glycoproteins)

(Niescierowicz 2013). Nevertheless, common structural futures are recognizable such as the NSXXNPXXY motif in the helix VII or the DRY motif between helix III and the ICL2. Such motifs are involved in receptor stabilization in specific states (inactive, active, partially active) and coupling with G proteins. The ligand binding site is generally located in TM domains with some exceptions for glycoproteins binding receptors in which substrate binding site is at the N-terminus.

- The secretin receptor family

All members of this family possess an extracellular hormone-binding domain to bind peptide hormones. The 15 Secretin receptors share between 21 and 67% sequence identity and most of the variation is in the N-terminal regions (Fredriksson et al. 2003). They contain conserved cysteine residues in the ECL1 and ECL2. Moreover, almost all of these receptors contain conserved cysteine residues that form disulphide bridges in the N terminal domain.

- The glutamate receptor family

Most members of this group are characterized by long N- and C-terminal regions. Moreover, binding of endogenous ligand happens within the N-terminal region. The ligand-binding mechanism of the extracellular region has been compared to a Venus flytrap mechanism (VFTM), in which two lobes of the region form a cavity where glutamate binds to a conserved ligand binding site (Fredriksson et al. 2003) and activates the receptor.

- The adhesion receptor family

These receptors are rich in functional domains and most of the receptors have long and diverse N-termini, rich in cysteine and proline residues, which are thought to be highly glycosylated and form a rigid structure. The N-terminus of these receptors also contains a proteolytic domain that is removed at the level of the endoplasmic reticulum to allow proper addressing of the protein to the plasma membrane (Krasnoperov et al. 2002).

- The frizzled/taste 2 receptor family

In this group, we can actually distinguish two clusters of receptors, grouped together because of the presence of specific common motifs in the C-terminal region. Frizzled receptors present a long N-terminus of about 200 residues in contrast with the short N-terminus of the related taste 2 receptors group. Frizzled receptors are known to be implicated in cell proliferation and development while Taste 2 receptors function remains unclear. It has been

postulated that they may be involved in bitter taste sensation as they are expressed in the tongue and in the palate epithelium (Fredriksson et al. 2003).

4.4.3 GPCR ligands

GPCRs ligands and drugs are defined according to their action on the receptor activity. According to its biological activity, a ligands can be classified as:

- Agonist: molecule that triggers the activation of the receptor and stimulates a specific biological effect;
- Neutral antagonist: a ligand that neither activates the receptor nor inhibits its basal activity and blocks binding of endogenous agonists to the receptor (Tate 2012);
- Inverse agonist: ligand that inhibits the basal activity of the receptor by stabilizing it in inactive state.

4.4.4 GPCR-mediated signalling through G Proteins

G proteins, so called because of their ability to bind guanine nucleotides, are cytosolic proteins able to mediate numerous signal cascades in the cell. These proteins are heterotrimeric (Gα, β and γ) and interact directly with GPCRs. The first step in the G protein-mediated signalling is the binding of a ligand onto the GPCR. The induced conformational changes of the receptor stimulate the exchange of GDP in GTP on the Gα subunit leading to the dissociation of Gβγ dimer from Gα. Activated Gα and Gβγ proteins modulate downstream effectors (ion channels, adenylyl cyclases, and phospholipases) which in turn generate second messenger molecules (Ca^{2+}, IP3, DAG, cAMP).

This mechanism triggers the formation of a cascade of signals within the cell that influences a wide variety of metabolic functions (Dorsam and Gutkind 2007).

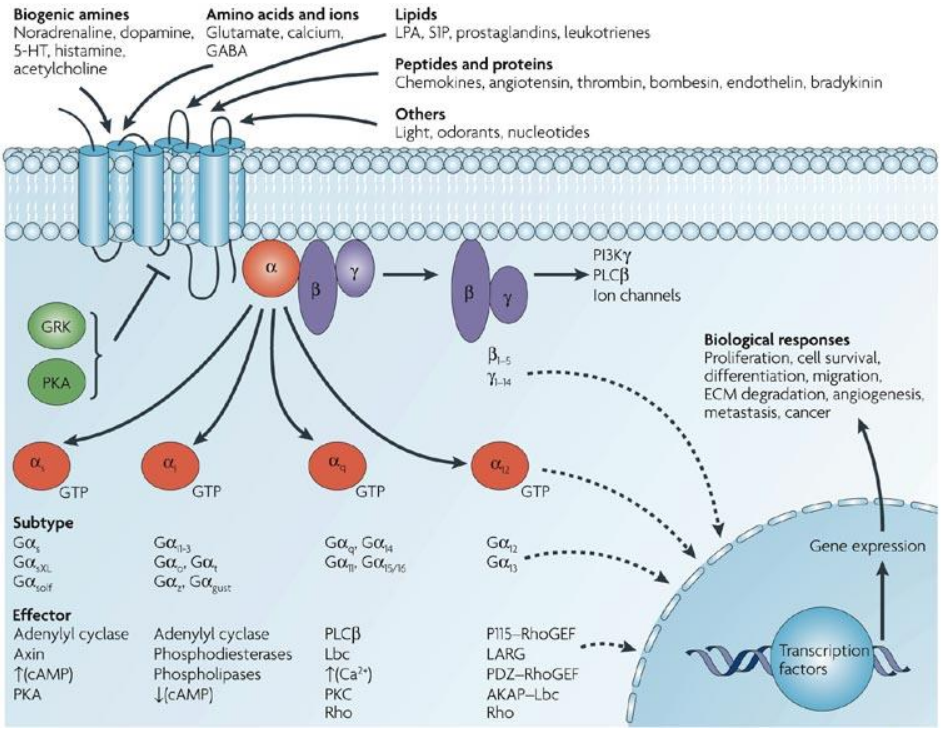

Figure 26. G protein-mediate signalling network (Dorsam and Gutkind, 2007).

Many ligands act through GPCRs to stimulate targets at the membrane, cytoplasmic and nuclear level. GPCRs interact with heterotrimeric G proteins that are bound to GDP at the resting state. Binding of agonist induces a conformational change in the receptor, which catalyses the dissociation of GDP from the α subunit. Subsequently the GTP binds to Gα triggering the dissociation of Gα from Gβγ subunits. G proteins α subunits are divided into four subfamilies: Gαs, Gαi, Gαq and Gα12. A single receptor can interact with one or more families of Gα proteins. G proteins activate several downstream effectors: Gαs stimulates adenylyl cyclase increasing the levels of cAMP; Gαi inhibits adenylyl cyclase and lowers cAMP levels; Gαq activates phospholipase C (PLC), which cleaves PIP_2 into diacylglycerol (DAG) and inositol triphosphate (IP3). Both Gβ subunits and Gγ subunits work as a dimer to activate phospholipases, ion channels and lipid kinases. Gβγ, Gα12 and Gαq subunits also control the activity of intracellular signal-transducing molecules. These include GTP-binding proteins belonging to the Ras and Rho families, members of the mitogen-activated protein kinase (MAPK) family, extracellular signal-regulated kinase (ERK), c-jun N-terminal kinase (JNK), p38 and ERK5, through a complex network of signalling that remains largely unclear.

The anomalous activity of G proteins and/or of their downstream effectors can contribute to cancer onset and diffusion (Figure 26) (Dorsam and Gutkind, 2007).

4.4.5 The M2 muscarinic acetylcholine receptor

In this thesis work, the ICCR used to carry out experiments is a M2 muscarinic-based ICCR. The M2 receptor belongs to the Rhodopsin family of GPCRs. Muscarinic receptors mediate the response to acetylcholine released from the parasympathetic system. In particular, the M2 muscarinic receptor is essential in the physiological regulation of the cardiovascular system through the activity of G proteins coupled to Kir channels. M2 signalling follows the general architecture described in the paragraph 4.4.4.

The M2 receptor plays an important role in the regulation of potassium conductivity via release of Gβγ subunits. These bind to hetero-tetrameric cardiac potassium channels Kir3.1/Kir3.4 to activate them. Moreover, the M2 receptor regulates the inhibition of adenylyl cyclase via G proteins, which result in lower intracellular levels of cAMP in the cell (Ockenga et al. 2013).

After ligand binding and stimulation, muscarinic receptors are desensitized in a process that is dependent on receptor phosphorylation at serine and threonine residues. Phosphorylation of the receptor allows β-arrestins to bind, which suppresses the G protein interactions and terminates the signal (Hosey et al. 1995).

In humans, M2 receptors are mostly expressed in the heart, where they slow down the heart rate by decreasing the speed of depolarization after a stimulus.

A recent structure of the human M2 receptor in complex with an agonist (iperoxo) and an allosteric modulator, provided insights into allosteric and orthosteric regulation (Kruse et al. 2013). As seen in Figure 27, binding of the orthosteric agonist triggers conformational rearrangements within the TM helices. In particular, helix 6 is displaced outward while helix 7 moves inward. These motions are responsible for the formation of the intracellular cavity necessary for G protein binding.

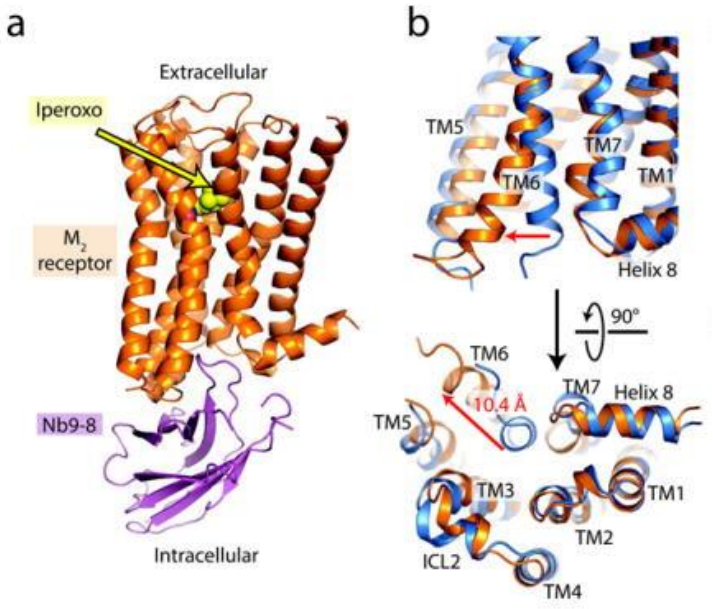

Figure 27. Intracellular changes on activation of the M2 receptor. A, overall structure of the active-state M2 receptor (orange) in complex with the orthosteric agonist iperoxo (yellow) and the active-state stabilizing nanobody (purple). B, compared to the inactive structure of the M2 receptor (blue), transmembrane helix 6 (TM6) is substantially displaced outward, and TM7 has moved inward (Kruse et al., 2013).

The structure of the inactive M2 receptor (Haga et al. 2012) confirmed the presence of a large extracellular vestibule, able to bind allosteric modulators. Located above the orthosteric site, this cavity shows a significant contraction upon activation of the M2 receptor, due to the rotation of TM6. This motion provides a structural link among three regions of the receptor: the extracellular vestibule, the orthosteric binding pocket, and the intracellular surface. The structural coupling of these three regions suggests that allosteric modulators can affect the affinity and efficacy of orthosteric ligands.

The structure of the M2 receptor in complex with both an agonist and an allosteric modulator is very similar to the structure of the receptor in complex with the agonist only, suggesting that the allosteric binding site is pre-formed in the presence of agonist (Kruse et al. 2013).

5. Engineering of the GPCR-Kir6.2 fusion to obtain functional coupling

For the creation of ICCRs, the muscarinic M2 C-terminus and the Kir6.2 N-terminus were initially linked through a sequence of six glycines. The resulting protein was well expressed but not functional as the electrical current generated by the channel was not affected by Acetylcholine (ACh). Controls showed that both proteins were individually active but, unfortunately, the GPCR was not able to control the activity of the fused ion channel. To explain this behaviour, it was postulated that physical contacts were needed for efficient transduction of the GPCR conformational changes to the ion channel gates. To validate this hypothesis, a set of M2-based ICCR constructs, with a progressively shorter linker length, was designed (Figure 28). In particular, these constructs were created by shortening of the Kir6.2 N-terminus in blocks of five residues at the time. From electrophysiological studies (TEVC), it appeared that progressive deletions in the channel N-terminal domain generated an ACh-induced activation of the channel and improved the amplitude of the current signal with an optimum at 25 residues deleted in the channel N-terminal domain (Moreau et al. 2008). A deletion longer than 25 residues (for example 30) abolished the ACh induced signal, revealing the level of precision of the deletions required to generate functional ICCRs.

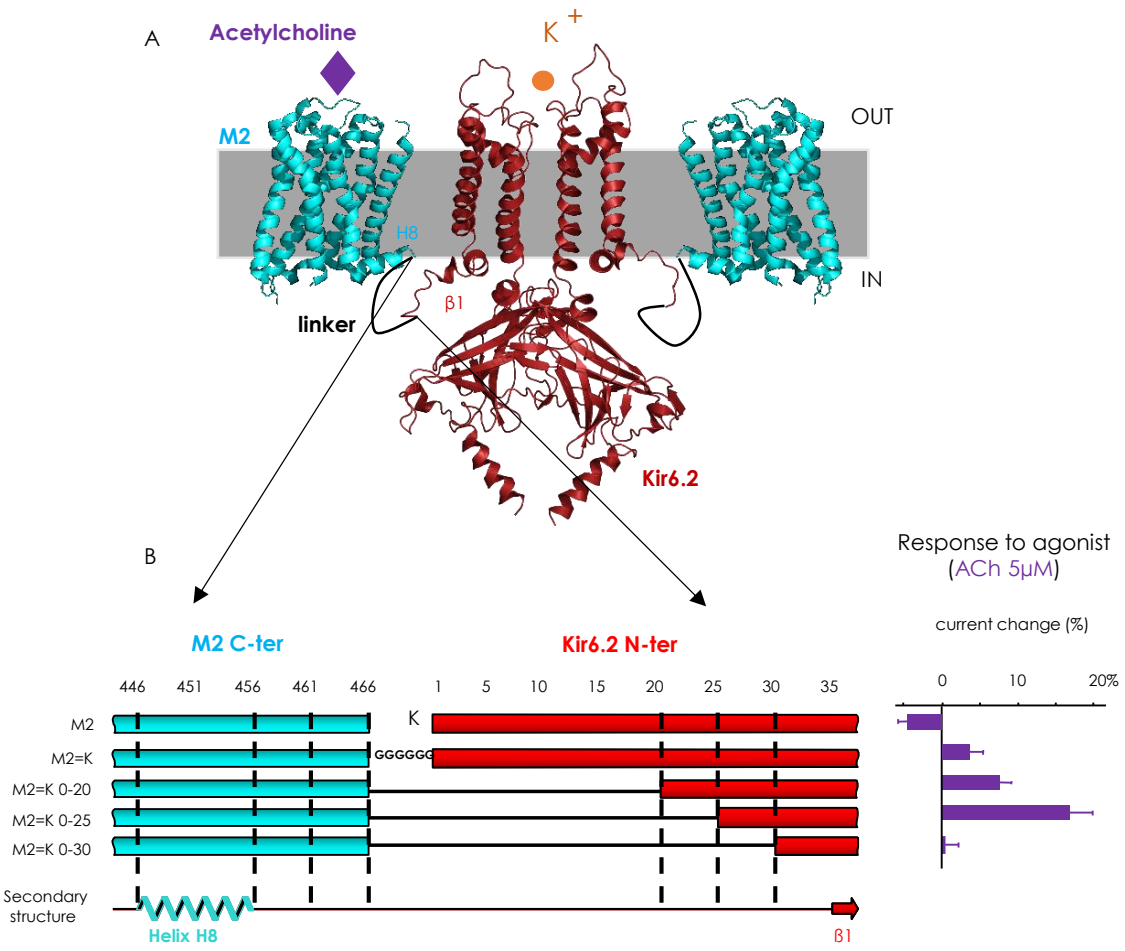

Figure 28. A, model of the M2=K ICCR as seen from the membrane plane. Front and back monomers have been removed for clarity. B, linker region engineering to obtain functional ICCRs and relative responses to Acetylcholine 5μM.

The power of the ICCR technology is based on the versatility of the fused receptor.

Functional M2-based ICCR stimulated the application of the same principle to other GPCRs. Subsequent trials were performed with the dopamine $D2_L$ receptor, starting directly with the optimal deletion of 25 residues at the Kir6.2 N-terminus. The resultant construct is called D2=K0-25. The nomenclature is easily explained: The D2 receptor (D2) is physically linked (=) to the Kir6.2 (K) by deleting zero (0) residues in the receptor C-terminus and 25 (-25) in the Kir6.2 N-terminus. This nomenclature is applied to all ICCR constructs cited in this work.

The construct D2=K0-25 was functional and, surprisingly, the application of the agonist Dopamine resulted in an opposite effect on the channel regulation, with an induced inhibition (~ 35 % inhibition).

The D2 receptor possesses a shorter C-terminus compared to the M2. In order to determine whether this opposite regulation of Ki6.2 was due to the different linker length, the GPCR C-terminus lengths were adjusted by shortening the M2 (to mimic the D2 C-terminus length) and by elongating the D2 (to mimic the M2 C-terminus length) respectively. Results are shown in Figure 29. Shortening of the M2 inverted the channel regulation (ACh induced inhibition of M2=K-9-25) and reciprocally, the extended D2 ICCR [D2=K(+9M2)-25] is now activated by dopamine. These results demonstrate the role of the GPCR C-terminus length on the sign of the current generated by the Kir6.2 channel (unpublished data).

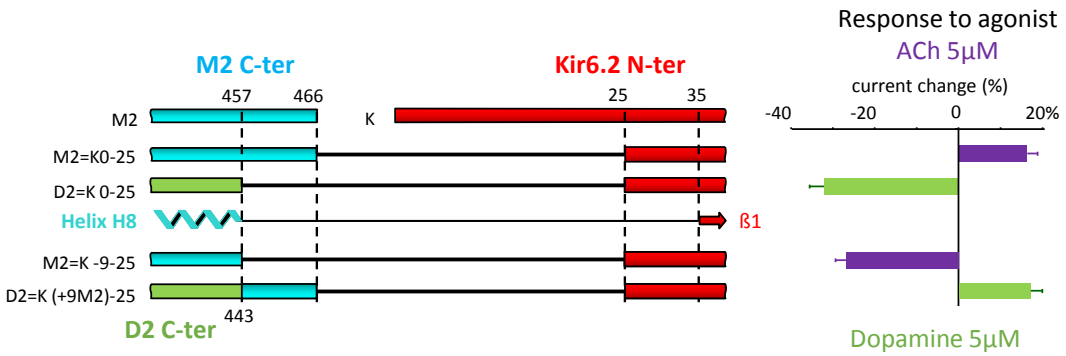

Figure 29. Linker engineering of M2- and D2-based ICCRs. The initially identified optimal deletion of 25 residues in the Kir6.2 N-terminus, was used to create a Dopaminergic-based ICCR (D2=K0-25). This construct shows an opposite response (inhibition) to the agonist compared to the M2=K0-25. As the D2 receptor possesses a shorter C-terminus compared to the M2, we tried to verify whether this opposite regulation of Ki6.2 was due to the linker length. The GPCR C-terminus lengths were adjusted by shortening M2 (to mimic the D2 C-terminus length) and by elongating the D2 (to mimic the M2 C-terminus length) respectively. Shortening of the M2 produces a receptor (M2=K-9-25) that is now inhibited by ACh, while the extended D2 ICCR [D2=K(+9M2)-25] is now activated by Dopamine.

The length of the linker is involved in the function of the ICCR; however, could also the sequence influence the channel regulation? To answer this question a control has been created from M2=K0-25 by deleting nine residues in the channel N-terminal domain

(M2=K0-34) instead of in the M2 C-terminal domain (M2=K-9-25). Both constructs (-9-25 and 0-34) have similar linker length but a different sequence (Figure 30).

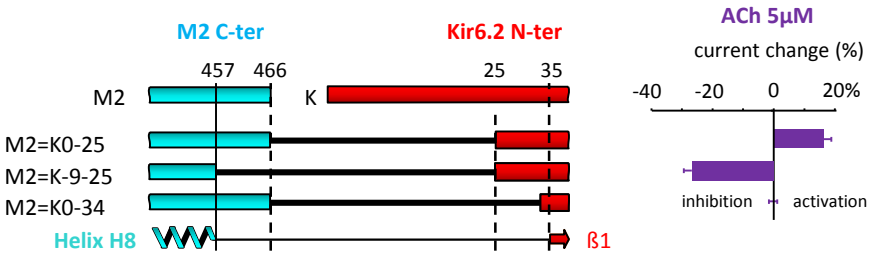

Figure 30. Linker engineering strategy of M2-based ICCRs. Deletion of nine additional residues in the channel N-terminal and re-integration of nine residues in the GPCR C-terminus originate the construct M2=K0-34. Constructs -9-25 and 0-34 have similar linker length but a different sequence. The first construct is inhibited by ACh while the new control 0-34 does not respond to the agonist.

The functional characterization of M2=K0-34 revealed a loss of channel regulation while the M2=K-9-25 is inhibited by ACh as previously shown. These results indicate that the sequence of the linker has also an impact on the GPCR-Kir6.2 functional coupling and therefore the linker length is not the only important parameter for the regulation of the fused ion channel (unpublished data). The only difference in the sequence between M2=K-9-25 and M2=K0-34 is the nine residues at the junction between the two proteins. The sequence alignment reveals the presence of a cluster of five arginines in the functional ICCR, that is missing in the ACh-insensitive M2=K0-34 (Figure 31). The last project of this thesis work aims at deciphering the possible role of this cluster of arginines in the regulation of Kir6.2.

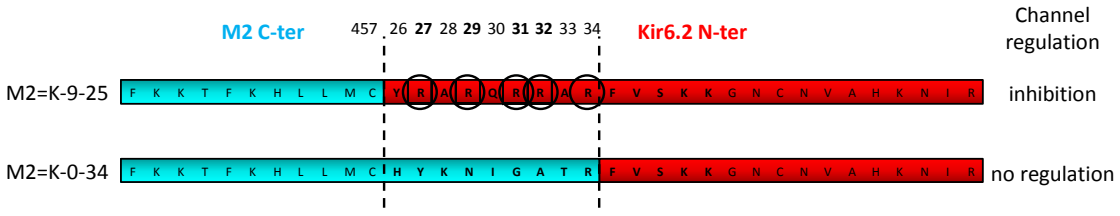

Figure 31. Linker alignment of M2=K-9-25 and M2=K0-34. The sequence alignment shows the presence of a cluster of five arginines in the inhibited M2=K-9-25 that are missing in the ACh-insensitive M2=K0-34.

Materials and Methods

A project that aims to characterize functionally and structurally an ion channel demands a wide range of techniques that fall in the fields of molecular biology, biochemistry and electrophysiology.

6. Molecular biology

The preliminary steps are required to build the DNA that will be successively used to obtain the protein subject of the study.

6.1 Genes and expression vectors

Genes (Table 3)

Table 3. List of genes.

Gene	Project	Origin	Source	Tag	Cleavage site
SUR2A-Kir6.2	1	Human	GenScript	HA 9-His	Factor Xa
SUR2A	1	Human	Realized per PCR	9-His	Factor Xa
TMD0-Kir6.2	1	Human	Realized per PCR	9-His	Factor Xa
Kir6.2	1	Human	Realized per PCR	9-His	-
TMD0-eGFP	1	Human	GenScript	HA 9-His	Factor Xa
SUR2A	2	Rat	Dr. S. Seino	-	-
SUR1	2	Hamster	Dr. J. Bryan	-	-
MRP1	2	Human	Dr. S. Cole	-	-
M2 (GPCR)	3	Human	Dr. D. Logothetis	-	-
Kir6.2	2 and 3	Mouse	Dr. S. Seino	-	-
M2=K-9-25 (ICCR)	3	Human (M2) Mouse (Kir6.2)	Realized per PCR	HA	-

Expression vectors (Table 4)

Depending on the expression system used, each gene has been subcloned in a proper vector (see table below).

Table 4. List of vectors.

Vector	*Expression system*	*Source*	*Promoter*	*Resistance*
pGH	*Xenopus laevis*	Dr. D. Logothetis	T7/SP6	Ampicillin
pET24a+	*Escherichia coli*	GenScript	T7	Kanamycin
pYES	*Saccaromyces cerevisiae*	Dr. P Catty	Gal1/T7	Ampicillin/Ura3
pPICZb	*Pichia pastoris*	Invitrogen	AOX1/EM7	Zeocin
pIVEX2.3	*In-vitro/ E.coli extract*	5PRIME	T7	Ampicillin

6.2 Mutagenesis

6.2.1 Site-directed mutagenesis

This technique has been used to insert mutations in the targeted gene in order to get mutated proteins.

For electrophysiology studies, these mutants are usually created to study the involvement of a certain aminoacid/region in a function. For structural studies, mutagenesis is also a way to insert/remove tags used during protein purification or to build chimeric proteins optimized for heterologous expression.

In our investigations, we used the QuickChange Lightning Site-Directed Mutagenesis Kit (Agilent Technologies). Its principle is illustrated in Figure 32. The method is based on the PCR technique in which *pfu*Ultra high fidelity DNA polymerase conducts mutagenic primers-directed replication of the plasmid strands.

Complementary primers (forward and reverse) hybridize with the specific region of the DNA strand in which we intend to introduce the mutation. Subsequently, primers are elongated by the polymerase to originate a new mutated plasmid.

The PCR product is then digested with *DpnI* endonuclease, in order to eliminate the parental (methylated) DNA and to allow selection of only newly produced plasmids. This DNA will be successively incorporated in *E.coli* during the transformation step.

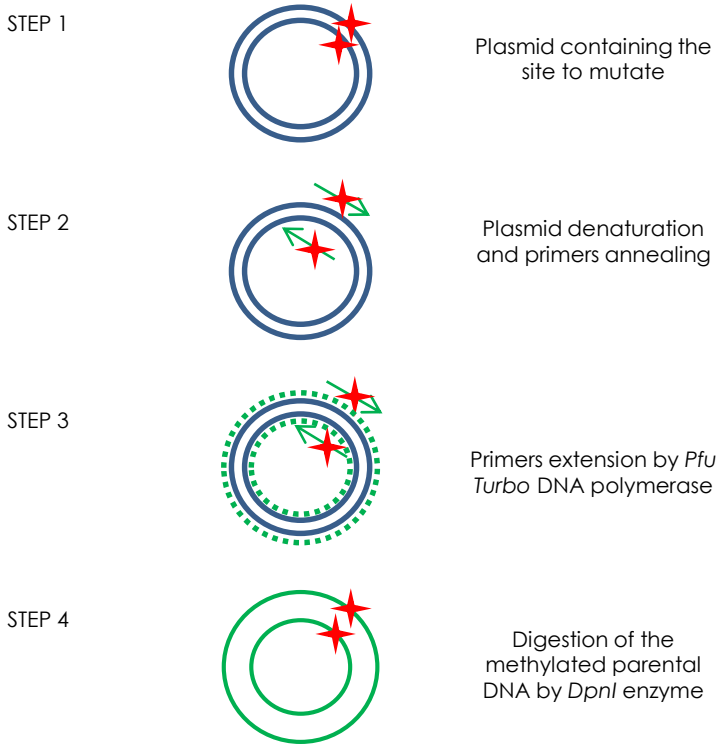

Figure 32. QuickChange Lightning Site-Directed Mutagenesis protocol. Complementary primers (forward and reverse) hybridize with the specific region of the DNA strand in which we intend to introduce the mutation. Primers are then elongated by the polymerase to originate a new mutated plasmid. The PCR product is digested with DpnI in order to eliminate the parental DNA and to allow selection of only newly produced plasmids.

6.2.2 Deletion of long fragments

The full-length K-ATP channel was not the only construct designed for expression in heterologous systems. In order to increase the chance of getting structural information on the complex, we decided to focus our studies also on specific domains of the K-ATP channel. Once the full-length K-ATP channel was subcloned in various vectors, depending on the expression system to test, we obtained specific domains, ready to be expressed, by deleting fragments by PCR.

For instance, to obtain Kir6.2 we used the full-length K-ATP as a template and we designed primers to excise the region encoding SUR2A. The principle is illustrated in Figure 33 (Raman and Martin 2014).

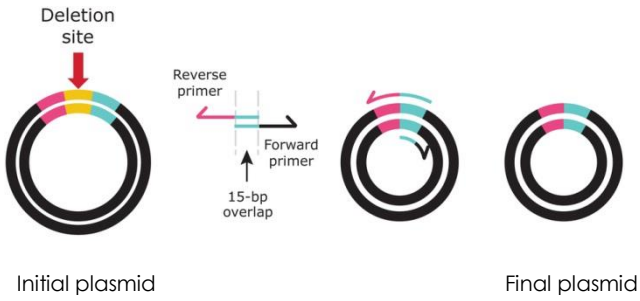

Figure 33. Deletion strategy. Forward primer 3' region is complementary to the beginning of the region encoding for Kir6.2 (light blue). Reverse primer possesses a 3' complementary to the 3' region of the Forward (light blue) and a 5' complementary to the vector (pink). Each primer has a length of ~30 bp and Forward and Reverse overlap for ~15 bp. During the elongation step of the PCR, the DNA polymerase will synthetize a new strand excluding the SUR2A (yellow) region.

Primers were designed as follows: Forward primer 3' region is complementary to the beginning of the region encoding for Kir6.2. Reverse primer possesses a 3' complementary to the 3' region of the Forward and a 5' complementary to the vector. Each primer has a length of ~30 bp and Forward and Reverse overlap for ~15 bp. Using this strategy, during the elongation step of the PCR, the DNA polymerase will synthetize a new strand excluding the SUR2A region.

6.3 Subcloning

The subcloning technique was used to transfer the K-ATP gene from one vector to another specifically developed for expression in other systems. In particular, the K-ATP was moved from pGH vector (for expression in *Xenopus* oocytes) to pYES vector (for expression in *S. cerevisiae*), to pPICZb vector (for expression in *P. pastoris*) and to pIVEX3.2 (for expression *in-vitro*). The principle of the method is illustrated in Figure 34. Taking advantage of restriction enzyme sites present at both 5' and 3' extremities of the K-ATP gene, the construct 'K-ATP_pGH' was digested in order to excise the gene from this vector. At the end of this reaction, the product is loaded in an agarose gel in order to separate the two bands corresponding to the gene and the pGH vector. The band corresponding to the K-ATP is

then cut out from the gel and the DNA is purified using the GeneClean kit (MP Biomedicals). Successively, the recipient plasmid (pYES, pPICZb, pIVEX3.2) is digested by the same restriction enzymes used during the excision of the K-ATP from the pGH. With this strategy, 5' and 3' extremities of the recipient plasmid will be compatible with the extremities of the excised gene. K-ATP and recipient plasmid are eventually ligated by a ligase (Rapid DNA Ligation Kit, Roche).

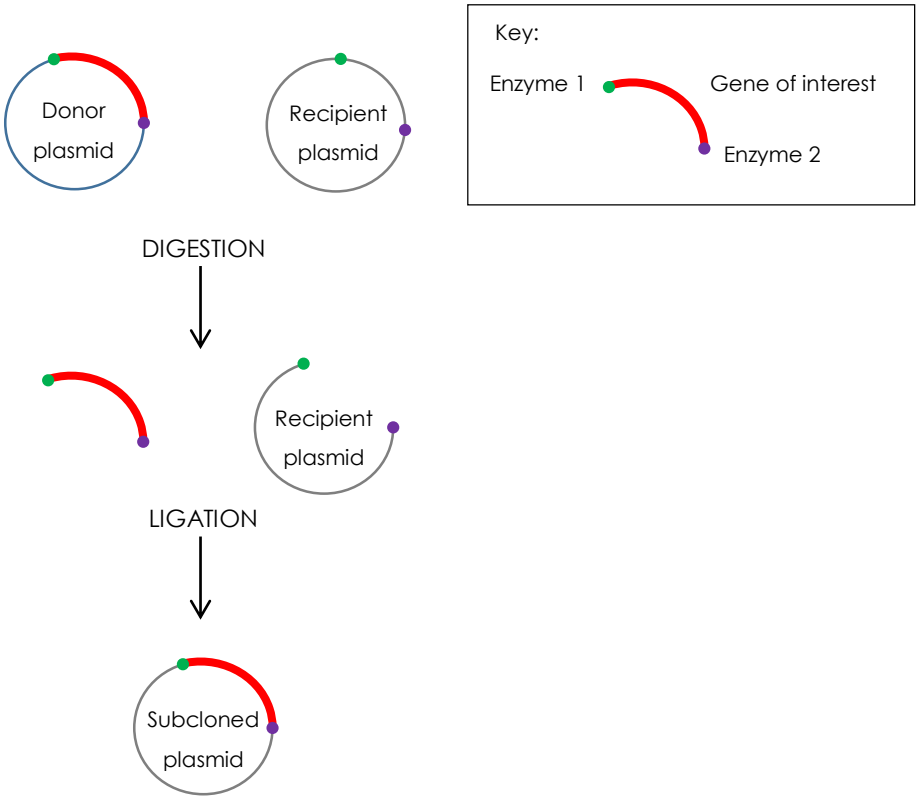

Figure 34. Subcloning strategy. Restriction enzyme sites present at both 5' and 3' extremities of the K-ATP gene were used to excise the gene from the vector. Product's reaction is loaded in an agarose gel to separate the two bands corresponding to the gene and the pGH vector. The K-ATP band is cut out from the gel and the DNA is purified. Successively, the recipient plasmid (pYES, pPICZb, pIVEX3.2) is digested using the same restriction enzymes of the excision of the K-ATP from the pGH. 5' and 3' extremities of the recipient plasmid will be compatible with the extremities of the excised gene. K-ATP and recipient plasmid are eventually ligated by a ligase.

6.4 Amplification of genetic material

6.4.1 Transformation of competent bacteria

In order to amplify the DNA of interest we use 'ultracompetent' bacteria (*Epicurian coli* XL-10 Gold) provided by the QuickChange Lightning Site-Directed Mutagenesis kit (Agilent Technologies). About 50µl of competent bacteria are incubated on ice for 30 minutes in presence of the DNA to amplify. By inducing a thermal shock at 42°C for 45 seconds, DNA crosses the bacterial wall and is 'captured' by the bacteria. Recombinant bacteria possess resistance to antibiotic, usually Ampicillin or Kanamycin, thus only bacteria carrying the plasmid of interest will be able to grow on LB (Luria-Bertani) agar culture medium containing the antibiotic.

6.4.2 Amplification and purification of the DNA plasmid

Plasmid extraction from bacteria is based on the alkaline lysis method using solutions containing detergent (Sodium Dodecylsulfate, SDS) and an alkali (Sodium Hydroxide, NaOH). SDS ensures cell lysis and protein denaturation while NaOH denatures genomic DNA, plasmid DNA and proteins. This method principle is based on the different physical-chemical characteristics of the linear genomic DNA and the supercoiled plasmid DNA. When the neutralizing solution of potassium acetate (pH 5.2) is added to the cellular lysate, only the plasmid DNA renatures while genomic DNA is irreversibly denatured. The precipitate containing membranes, proteins, RNA and genomic DNA is separated from plasmid DNA by centrifugation (14000 rpm at 4°C per 15 minutes) or with columns (MidiPrep Qiagen kit). The plasmid is recovered from the supernatant by precipitation with isopropanol (14000 rpm at 4°C for ≥ 30 minutes), and washed with 70% ethanol to remove contaminants. The DNA pellet is dissolved in distilled water once dry.

We use two methods of plasmid amplification and purification: 'Miniprep' method to screen a high number of clones and 'Midiprep' method to scale up DNA preparation of positive clones.

6.4.3 Miniprep and Midiprep methods

The Miniprep method is used to select positive clones of recombinant bacteria. Bacteria grown on agar plate are used to inoculate 5ml of LB medium containing antibiotic. After overnight growth, the cultures are treated with solutions provided by the Qiagen kit as

described above. The selection of positive clones is realized by digestion of the DNA with specific restriction enzymes and analysis of the restriction profile. Selected clones are then sequenced.

The Midiprep method is used to obtain high quantity of highly pure DNA. This DNA is subsequently used for *in-vitro* transcription or to overexpress the protein of interest into a heterologous system. The purity of the obtained DNA increases due to the filtration step enabling the elimination of all bacteria debris, and the anion-exchange column, which selectively binds the plasmid DNA. Bacteria grow in 50 ml of LB medium supplemented with antibiotic, which results in a larger quantity of genetic material compared to Miniprep. The Qiagen Plasmid Purification kit provides all solutions required. Purified DNA concentration is estimated using the NanoDrop 2000 (Thermoscientific) spectrophotometer by measuring the optical density at a wavelength of 260 nm (Niescierowicz 2013).

6.5 RNA preparation

RNA handling requires maintenance of 'RNase-free' conditions. In order to ensure that, we perform RNA preparation experiments using dedicated pipettes, tips and tubes. Moreover, water used during all the steps is treated with diethyl pyrocarbonate (DEPC) which deactivates RNases.

Plasmid DNA is linearized before *in-vitro* transcription using restriction enzymes which cut at sites, located downstream of the 3' UTR sequence. Twenty units of enzyme are used to digest 10 μg of DNA during overnight digestion at 37°C. The linearized DNA is extracted and purified using the phenol/chloroform/isoamyl alcohol method. Quantity and quality of the DNA is estimated on a 0.8% agarose gel.

The mMessage mMachine T7 kit (Ambion) which uses a RNA T7 polymerase provides all reagents used for transcription. The kit allows to get large amounts of RNA capped at the 5' with a methylated guanosine, crucial for the initiation of the transcription and for protection against RNA degradation. After 4 hours of transcription at 37°C, synthesized mRNA is

purified using the phenol/chloroform mixture. Quantity and quality of the RNA is estimated using both NanoDrop2000 analysis and agarose gel electrophoresis.

RNA is then diluted to the desired concentration and stored at –80°C (Table 5).

Table 5. RNA concentrations for injection in oocytes.

mRNA	*Concentration (μg/μl)*
SUR	0.12
Kir6.2	0.04
ICCR	0.08

7. Biochemistry: Production and purification of recombinant proteins

This section concerns a part of my thesis project focused on the attempt of expressing and purifying the K-ATP channel (or subunits of it). The final aim was to solve its structure. In order to do so, several expression systems were tested.

7.1 Basic techniques of biochemistry

7.1.1 Protein electrophoresis (SDS-PAGE)

SDS-PAGE(Sodium Dodecyl Sulphate - PolyAcrylamide Gel Electrophoresis) is used to separate proteins according to their electrophoretic mobility, which depends on mass, conformation and charge. During our experiments, we used this technique to check protein production.

The protein sample is mixed with Laemmli buffer 4x (β-Mercaptoethanol 4 %, Bromophenol blue 0.04 %, Glycerol 40 %, SDS 8 %, Tris-HCl 250 mM – pH 6.8-) in the ratio 2:1. Samples are then loaded on a polyacrylamide gel (Tris-HCl pH 8.8 300 mM, acrylamide/bisacrylamide 8-12 % w/v, SDS 0.1 % w/v, ammonium persulphate 0.1 % w/v, TEMED 0.001 % w/v) with a different concentration of polyacrylamide, depending on proteins predicted mass. Bio-Rad systems have been used for both gel preparation and migration. Electrophoresis uses a constant voltage of 150 mV in a buffer containing Tris 25 mM, glycine 250 mM, SDS 0.1 % w/v. In order to visualize proteins bands, the gel is stained after running with a solution containing Coomassie blue 1.5 g/l, acetic acid 10 % v/v, ethanol 30 % v/v. Colour excess is washed out by un-staining the gel in a mixture of acetic acid 10 % v/v and ethanol 30 % v/v.

7.1.2 Western blot technique (immunodetection)

The Western blot technique is used to reveal the presence of the produced protein of interest taking advantage of the presence of tags. After migration on polyacrylamide gel, proteins are transferred to a nitrocellulose blotting membrane (Amersham Hybond ECL) using electrophoresis. Transfer is realized overnight in cold a room at 100 mA using the buffer Tris 25 mM, glycine 190 mM, SDS 0.1 %. The membrane is incubated 30 minutes in a blocking buffer supplemented with milk. Milk is rich in proteins that bind to the nitrocellulose, preventing non-specific binding of the antibody. The buffer content varies

according to the antibody used. During my thesis work, I used antibodies for both histidine (His-tag) and human influenza hemagglutinin tags (HA-tag). After this first step, the membrane is incubated with the antibody at a concentration dependent on the supplier's recommendations. Antibody excess is washed out and revelations of antibody-protein binding is realized using Sigma Fast Diaminobenzidine Tablets. Alternatively, for a more sensitive analysis, revelation can be realised with SuperSignal West Pico Substrate Working Solution (Thermo Scientific) and subsequent revelation on films in the darkroom.

7.2 Expression in *Escherichia coli* and solubilisation of bacterial membranes

Escherichia coli is the most common expression system used. Its popularity is given by some important characteristics such as time of protein production, handiness and cost.

In order to find the optimal conditions for protein expression, several bacterial strains were tested during a small scale trial: BL21(DE3), C43(DE3), Rosetta(DE3). Bacteria were transformed with the plasmid containing the gene of interest and spread on a Petri-dish containing LB medium supplemented with Agar and antibiotic (Kanamycin). After overnight incubation at 37°C, cells were inoculated into a liquid medium (LB, 50 ml) supplemented with Kanamycin (0.1 g/l) and incubated at 37°C under shaking. After few hours, the culture turns cloudy, meaning that bacteria started to grow. Cloudiness is measured with a spectrophotometer (absorbance at 600 nm, OD_{600}) and gives an idea of bacterial concentration. When the OD_{600} reaches a value between 0.5 and 0.8 (exponential phase of bacterial growth) the culture is 'induced' by adding Isopropyl β-D-1-thiogalactopyranoside (IPTG) (1 mM). IPTG triggers protein expression by removing the Lac repressor bound to the T7 promoter. Once the repressor is removed, the RNA polymerase can recognize the promotor and initiate the transcription. Cultures are re-incubated at 37°C under shaking for 3 or 5 hours. 1 ml samples of cultures before and after 3 hours of induction are collected in order to verify protein expression levels. These samples are centrifuged at 4000 rpm for 15 minutes. Cells in the pellet are re-suspended in Laemmli 1x buffer and stored for later gel analysis. Remaining samples are used for membrane extraction, in order to localize the protein of interest.

20 ml of bacterial culture with an OD_{600} of 0.8 are centrifuged at 4000 rpm and cells are re-suspended in 20 ml of TBS buffer 1x (100 mM TRIS, 140 mM NaCl, HCl - pH 7.4)

supplemented with proteases inhibitors (Complete Protease Inhibitor Cocktail Tablets, Roche). Suspended cells are then lysed using a microfluidizer machine M-110P (Microfluidics). The extract is centrifuged at 11600 rpm for 20 minutes. Unbroken cells are pelleted while membranes remain in the supernatant. The supernatant fraction is ultra-centrifuged at 38800 rpm for 1 hour. The membrane fraction should now be in the pellet, which can be either re-suspended in Laemmli buffer for gel loading and protein expression detection, or used for a protein solubilisation trial.

Once the protein is produced, we need to extract it from the bacterial membrane using detergents that mimic the natural environment of the membrane protein. Extraction assay of the produced proteins from the membrane fraction is realized with several detergents (Table 6):

Table 6. List of detergents for protein solubilisation trials.

Detergent	**Critical micelle concentration (CMC)**	**Concentration used**
Dodecyl Maltoside (DDM)	0.0087 %	2 %
Anapoe-C12E9	0.003 %	2 %
LAPAO	0.052 %	2 %
Fos-Choline-12	0.047 %	2 %

In order to solubilize the protein, the detergent needs to organize in spherical structures called micelles. Micelles are formed by the aggregation of several molecules of detergent arranged to create an internal non-polar environment (suitable to arrange membrane proteins) and an external polar face that will adapt to aqueous buffers. To create micelles, a certain concentration of detergent molecules is needed and it depends on the specifics of the detergent itself. This concentration value is often referred as critical micelle concentration (CMC). This is defined as the concentration of detergents above which micelles are spontaneously formed. This value is very important because at concentrations above it the

detergents form complexes with lipophilic proteins but below this borderline, detergents cannot accommodate membrane proteins.

We used TBS buffer 1x supplemented with protease inhibitors and detergent for pellet re-suspension. Samples were incubated at 4°C for 6 hours and then centrifuged at 68000 rpm. Proteins in the supernatant correspond to the solubilized fraction.

7.3 Expression in the yeast *Saccharomyces cerevisiae*

S. cerevisiae is considered the *E. coli* of the eukaryotic world. Culturing yeast is in fact simple, economical and rapid.

Yeast strain BY 4741 (Genotype: MATa; his3D1; leu2D0, met15D0, ura3D0) was transformed, using a protocol with lithium acetate, with the pYES2 plasmid (Invitrogen), containing the gene of interest. The pYES2 plasmid contains the *URA3* gene for selection of yeast transformants in uracil-deficient medium. Colonies grown on plate are used to start 50 ml liquid cultures (Yeast Nitrogen Base medium supplemented with galactose to induce protein production). After overnight incubation under shaking at 30°C, yeast are pelleted by centrifugation at 4000 g for 3 minutes at 4°C. The pellet is re-suspended in TBS buffer supplemented with protease inhibitors. Cells are then mechanically lysed using glass beads and vortex. The lysate is centrifuged at 65000 rpm at 4°C for 1 hour. The pellet is re-suspended in TBS buffer + protease inhibitors and treated with chloroform/methanol for protein precipitation. We used the Western blot technique to verify protein expression.

7.4 Expression in the yeast *Pichia pastoris*

As a yeast, *Pichia pastoris* shares the advantages of *S. cerevisiae* with the added advantage of 10- to 100- fold higher heterologous protein expression levels. *P. pastoris* is a methylotrophic yeast, meaning that it is capable of metabolizing methanol as its only carbon source. The first reaction in methanol metabolism is the oxidation of methanol to formaldehyde by alcohol oxidase that is produced in large amount to compensate the low affinity of the enzyme for O_2. To take advantage of this enzyme overproduction, the alcohol oxidase promoter AOX1 is used to promote the expression of heterologous proteins too. Expression is induced with methanol.

The *Pichia pastoris* system (EasySelect Pichia Expression Kit, Invitrogen) has been used for the production assay of three constructs (full K-ATP, SUR2A and Kir6.2). The yeast is transformed with the linearized DNA of interest that is integrated in its genome by recombination. Cells grow in a YPD medium (Yeast Extract Peptone Dextrose Medium), 50 ml, at 30°C under shaking until the OD_{600} reaches a value of ~ 0.8. Cells are gently centrifuged and the pellet is washed with sterile water. Water is then decanted and cells are re-suspended in lithium chloride 100 mM. Cells are then pelleted and re-suspended in a mixture of 50% PEG, 1 M lithium chloride, DNA carrier (used to carry DNA of interest inside the cell) and the linearized DNA of interest. After 30 minutes incubation at 30°C in this solution, the heat shock at 42°C is performed. The supernatant is removed and cells are re-suspended into 1 ml of YPD medium and incubated at 30°C for 1 hour. Cells are spread on YPD plates containing the antibiotic Zeocin, for selection of transformants. The correct insertion of the DNA of interest in *P. pastoris* genome is checked by genomic extraction and subsequent PCR using 5' AOX and 3' AOX primers (which should flank the gene of interest if recombination occurred). Positive clones are selected for expression trials.

Pre-cultures of the positive clones are incubated over the weekend and then used to inoculate 10 ml of YPD medium supplemented with methanol. Production is carried out for 5 days adding methanol daily. Cells are then collected and lysed chemically. Total extract is loaded on polyacrylamide gels for Western blot analysis.

7.5 *In-vitro* synthesis

This method enables the production of recombinant proteins in solution using translation machinery extracted from cells. Because protein synthesis occurs in cell lysates rather than within cultured cells, the method is also called cell-free protein expression. Cell-free synthesis of membrane proteins emerged recently as a powerful tool to overcome problems such as misfolding, protein aggregation and toxicity, encountered in classical expression systems.

The Institut de Biologie Structurale (IBS) possesses a facility for cell-free production of membrane proteins that we decided to use in order to test the expression of some of our constructs. The main advantage, for membrane proteins production, is given by the possibility to supplement the reaction recipe with detergents that will help protein folding, as the natural environment of such proteins, the plasmatic membrane, is missing. Moreover, the production of membrane proteins already in complex with detergents, helps skipping the step of extraction of the protein from the plasmatic membrane envisaged using classical heterologous systems, which can cause protein misfolding.

Lionel Imbert, the engineer in charge of the platform, prepares the cell extract (*E. coli* S30 extract) and all components necessary for the reaction (Apponyi et al. 2008). The substrates used for the reaction, including our plasmid, amino acids, nucleotides, tRNA, RNA polymerase and cell extract, are mixed to create a unique solution in which both DNA transcription and subsequent mRNA translation occur. We performed an initial small-scale trial, necessary to test several conditions of reaction such as duration, temperature, detergents and additives. Each reaction has a final volume of 50 µl and uses a concentration of plasmid of 10 µg per ml of reaction. After incubation, samples are spun at 14000 rpm at 4°C for 20 minutes. Both supernatant and pellet are tested for protein expression by the Western blot technique. For production of the TMD0-eGFP protein the most successful detergent was the Brj35, while, for Kir6.2 production, we used Nanodiscs. These two proteins are produced using two different protocols.

For the production of TMD0-eGFP we used a protocol which involves the use of 1 ml dialysis tubes. Proteins are produced inside these tubes that are placed into 50 ml Falcon tubes containing what is called 'feeding solution'. This solution contains all the substrates necessary to feed the reaction of synthesis. The dialysis tube presents, indeed, a semi-

permeable membrane that enables the passage of substrates that will feed the reaction (**dialysis mode**).

Kir6.2 production does not require any particular kind of tubes. The reaction is carried out in Eppendorf tubes (**batch mode**).

Yann Huon de Kermadec, a PhD student working in the nanodiscs field, provided the nanodiscs for Kir6.2 production. Nanodiscs are nanoscaled fragments of a lipid bilayer stabilized in solution by membrane scaffold proteins (MSP) (Figure 35). Lipids present in these nanodiscs come from an *E.coli* extract (Avanti Superlipids), supplemented with fluorescent POPC (Avanti Superlipids). The lipidic composition was improved by inserting PIP_2, essential for Kir6.2 activity. Moreover, the MSP carries a His tag, used for metal affinity chromatography purification.

Once the optimal conditions were established, we were able to run large-scale reactions (2 ml final volume). In these conditions, plasmid concentration is increased to 16 µg per ml of reaction. Incubation time depends on the construct: for TMD0-eGFP the reaction runs overnight, for Kir6.2 the timing is reduced to 3 hours. Samples are then spun at 14000 rpm at 4°C for 20 minutes. The supernatant can then be purified.

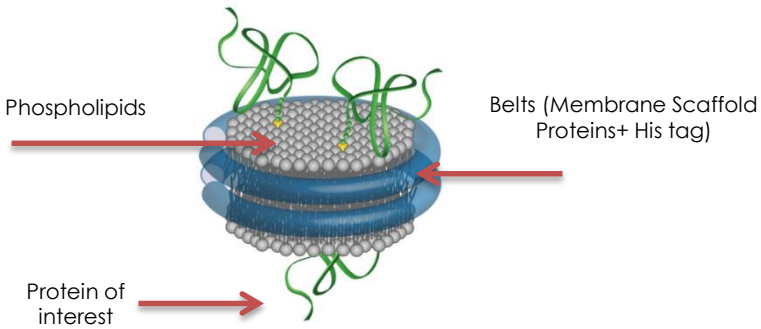

Figure 35. Nanodisc architecture. Membrane scaffold proteins (MSP) surround a patch of a lipid bilayer to form a disc-like particle.

7.6 Protein purification

After production, proteins undergo a purification process that can require several steps, depending on the amount and kind of impurities in the sample. During this work, proteins were generally fist purified using metal affinity chromatography and a subsequent size-exclusion chromatography. Only for proteins produced using the cell-free technique we have been able to reach the purification step. In these conditions, proteins are already in a soluble state as the detergent, Brij 35 or nanodiscs, is present in the cell-free recipe. Brij 35 is an ionic detergent, not compatible with crystallographic studies. For this reason, we performed detergent exchange during metal affinity chromatography. To screen a large number of detergents compatible with TMD0-eGFP, we used the RoBioMol platform at IBS. DDM, together with MNG-3 and Cymal-6, were found to be the best detergents.

7.6.1 Metal affinity chromatography (MAC)

This technique takes advantage of a matrix of beads functionalized with nichel-nitriloacetic acid (Ni^{2+}-NTA). The matrix coordinates nickel ions through four coordination sites, leaving two of the metal coordination sites exposed to interact with histidine residues of the protein tag.

The supernatant coming from cell-free production is diluted in buffer TBS 1x for TMD0-eGFP, or buffer phosphate PBS (10 mM NaPi, 150 mM KCl, pH 7.4) for Kir6.2 in nanodiscs. TBS buffer is supplemented with DDM (or MNG-3 or Cymal-6) and 2 ml of slurry (diluted resin, His60 Ni Superflow Resin, Clontech). TMD0-eGFP in TBS buffer is incubated for 2 hours at 4°C under gentle shaking. After incubation, the sample is poured into a gravity-flow column and the liquid fraction (flow-through) is discarded. The resin is washed twice with a washing buffer (TBS 1x supplemented with detergent and imidazole 15 mM). Because Imidazole competes with the polyhistidine tag for binding to the resin, the low concentration of imidazole in this last buffer will help to elute proteins and components that aspecifically bind to the resin. Proteins are eventually eluted using TBS buffer supplemented with DDM (or MNG-3 or Cymal-6) and imidazole 150 mM and subsequently analysed on SDS-PAGE.

For purification of Kir6.2 produced in nanodiscs, we used a HisTrap column (GE Helthcare) that we connected to an NGC chromatography System (Bio-Rad). The software ChromLab (Bio-Rad) is used to control the machine. The supernatant coming from the cell-free production is injected into the column through a 3.5 ml loop. Once the sample has passed

through the resin, this is washed with a washing buffer (PBS 1x, imidazole 20 mM). Proteins are then eluted using the elution buffer (PBS 1x, imidazole 300 mM) and analysed on SDS-PAGE.

7.6.2 Size-exclusion chromatography (SEC)

SEC separates biomolecules according to their hydrodynamic volume (radius of gyration). The resin consists of spherical porous particles with a controlled pore size, through which proteins diffuse depending on their shape. Small molecules enter the pores easily and therefore spend longer time to pass through the entire column while larger molecules spend little or any time at all in the pores and are eluted quickly. During our experiments, we have been using a Superdex 200 10/300 GL (GE Helthcare) column. Proteins previously purified using MAC are concentrated using Vivaspin 6 concentrators (Sartorius stedim biotech) with a 50 kDa membrane cut-off, to a final volume of 500 µl. Sample is then centrifuged for 10 minutes at 14000 rpm to remove most aggregates and subsequently injected in the column through a 500 µl loop. Column is connected to the NGC system. Protein elution, is detected using a UV-multi-wavelength detector that measures the absorbance of the proteins at 280 nm as they elute through the column. The absorbance is plotted as a function of the elution volume and produces a curve (chromatogram) that can be followed on a screen. Fractions corresponding to peaks are successively analysed on SDS-PAGE.

8. Heterologous expression in *Xenopus* oocytes

8.1 *Xenopus laevis* oocytes

Xenopus laevis oocyte is a cell model widely used in electrophysiology for functional characterization of ion channels, transporters and receptors (Miledi, Parker, and Sumikawa 1983).

A *Xenopus laevis* oocyte at stage VI of development is a spherical cell (diameter between 1 and 1.3 mm) which is particularly easy to handle. Its cytoplasm is rich in proteins, ribosomes, tRNA and enzymes essentials for protein expression and function. This kind of cells can be handled at room temperature in non-sterile conditions and without the help of any complex support. Moreover, they are characterized by a little background activity, allowing registration of heterologous ion channels activity with high signal-to-noise ratio. From a morphological point of view, *Xenopus* oocytes are characterized by the presence of two main regions: a brown hemisphere called the 'animal pole', which contains the nucleus and a yellow 'vegetal pole', containing the yolk platelets. A 'Vitelline layer', made of glycoprotein matrix, which protects the cell against pressure shocks, surrounds *Xenopus* oocytes. An extra layer of follicle cells protects the oocytes.

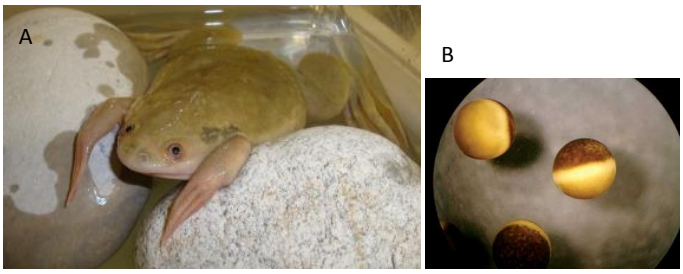

Figure 36. A, a fully developed Xenopus laevis. B, Xenopus oocytes at stage VI of development.

Oocytes are localized in the abdomen of the *Xenopus laevis* inside ovaries. Each ovary is subdivided in multiple lobes and each lobe contains hundreds of cells at different stages of development, blood vessels and connective tissue.

8.2 Extraction and preparation of oocytes

The Xenopus Express Company (Vernassal) provides the *Xenopus laevis* used during our experiments. Animals are raised in water tanks in a room at 22°C with a 12h/12h night cycle. In order to perform surgery, animals are first anesthetized with a solution of acid aminobenzoic ethyl ester at a concentration of 1g/l. About 20 minutes after, the *Xenopus* is placed on ice. An incision of ~ 8mm is performed on the skin of the abdomen and an extra incision of the muscle is required to get access to the ovarian lobes. Oocytes are extracted and transferred to a Barth's isotonic solution (NaCl 88 mM, KCl 1 mM, $NaHCO_3$ 2.4 mM, Hepes 16 mM, $MgSO_4$ 0.82 mM, $Ca(NO_3)_2$ 0.3 mM, $CaCl_2$ 0.41 mM, pH 7.4). After oocytes extraction, both incisions are stitched with absorbable thread (5-0, tip 16 mm 3/8c, 75 cm VICRYL Ethicon). The animal is then rinsed and placed into a water tank to recover.

A two-hours enzymatic defolliculation allows the release of the oocytes from the lobes (Type 1A Collagenase, Sigma-Aldrich). Digestion is performed at 19°C under gentle shaking. Separated oocytes are then rinsed with Barth's solution. Cells in stages V-VI of development are selected individually by choosing those with the best shape and homogeneity of pigmentation. Selected oocytes are stored in Barth's solution supplemented with penicillin and streptomycin.

8.3 RNA microinjection

The day after surgical extraction, oocytes are manually injected with the RNA obtained after *in-vitro* transcription. The injection is performed using a Nanoject machine (Drummond) which is set to release a volume of 50 nl per each injection. Glass microcapillary (3.5" Drummond # 3-000-203-G/X), pulled horizontally (Micropipette puller P-97, Sutter Instruments Co.) and then broken to a final size of ~ 7 μm, are filled with incompressible mineral oil (Sigma-Aldrich) and placed on the Nanoject's piston. The glass pipette is then filled with RNA (see concentration used in Table 5).

Oocytes are placed on a net situated at the bottom of a Petri dish filled with Barth's isotonic solution and they are manually injected by moving the microcapillary from one cell to the next one. Injected oocytes are then transferred to a 96-well plate filled with Barth's solution supplemented with antibiotics. Plates are incubated at 19°C for 48/72 hours to allow RNA

translation. After incubation, cells are ready for functional characterization of the ion channels.

9. Functional characterization of ion channels by electrophysiology techniques

Once the oocyte expresses the injected mRNA in protein, we use the patch clamp technique and the two-electrode voltage clamp technique to characterize its function.

9.1 The patch clamp technique

The patch-clamp technique is a very powerful real-time method that enables the study of ion channels behaviour. The flow of ions through an ion channel triggers a change of current that can be experimentally measured using this technique. The patch-clamp technique is the result of the refinement of the voltage-clamp technique that allows the measurement of ion flow across membranes as an electrical current, while the membrane potential of the cell is held under constant control.

Invented in 1976 by Neher and Sakmann (Nobel prizes for Medicine and Physiology in 1992), the patch-clamp technique allows the study of single or multiple ion channels depending on its configuration (Hamill et al. 1981). A borosilicate micropipette is applied on the plasmatic membrane of the oocytes, prior removal of the transparent vitelline layer, in order to isolate a little piece of it ('patch') with the help of suction. The patch can be placed in front of different kinds of solutions to allow the study of the variation of activity of the ion channels. A certain potential is imposed to the membrane (-50 mV in our experiments) (voltage clamp) and we measure the current to constantly inject into the system in order to keep the value of the voltage constant. This value of injected current corresponds to the current of ions that crosses the membrane through ion channels.

Several factors can have an impact on the current value:

- Membrane equilibrium potential of the considered ion (K^+ in our case), E_K, which depends on the concentration of the ion at both sides of the membrane (given by the Nernst equation);
- Membrane potential (V_m);

- Conductance of the channels (G), which quantifies the ability of the channel to conduct ions.

These values are linked by the following equation:

$I = G\ (V_m - E_K)$

V_m is constant in voltage clamp mode; E_K is zero, as the concentration of potassium ions is equivalent at both sides of the membrane in our conditions. Thus, I is proportional to G, that is characteristic per each kind of channel (76 pS for the K-ATP channel (Miki, Nagashima, and Seino 1999)).

9.1.1 Patch clamp configuration

The patch clamp technique can be used in different configurations depending on the ion channel studied. For K-ATP channel characterization, we choose the 'excised inside-out' configuration.

In this configuration, a little piece of membrane, containing expressed channels, is excised from the oocyte's membrane, so that the intracellular face can be exposed to different solutions. This configuration is particularly suitable for K-ATP channel analysis since its regulation depends mostly on ATP and ADP molecules that bind at the intracellular side of the protein. The analysis requires different steps:

a) *Oocyte preparation*

   48 to 72 hours of incubation at 19°C after micro-injection, oocytes are placed in a hyperosmotic solution. After few minutes the oocyte shrinks, so that the vitelline layer can be removed with the help of tweezers. After vitelline layer removal, the cell is very fragile so it is immediately transferred to the patch clamp set-up.

b) *Microelectrodes and solutions*

   In order to record a current from a membrane it is necessary to make electrical contact between the membrane itself and the electronic recording device. This is realized using microelectrodes that in our conditions are made of borosilicate pipettes (~1 μ diameter) filled with isotonic solution containing a fixed concentration of potassium ions (150 mM). Potassium concentration is maintained equal on both sides of the membrane (patch) so that the reversal potential for potassium can be considered zero within the pipette. A filament made of silver, opportunely

chlorinated, represents the metallic conductor that allows conversion of ionic currents in electrons currents.

c) *Seal formation*

Gigaohm seal formation is considered the essence of patch clamping. In order to excise a piece of membrane from a cell it is essential to obtain first an intimate connection between the membrane and the pipette. Pipette is gently rested onto the oocyte membrane and once the contact is established a light pressure is applied by aspirating into a tube directly connected to the pipette. The aspiration ends when the connection between membrane and tip is so strong that the pipette resistance will be in the order of the gigaohm. The membrane patch can now be excised by quickly removing the pipette from the oocyte surface and then it is placed in front of an automated perfusion pipes system containing the testing solutions. In order to make sure to record potassium channels current only, a chelator (EGTA) is added to remove calcium ions that can activate endogenous calcium-activated chloride channels.

The current I_K of potassium ions passing through ion channels in the patch is equal to: $I_K = G_K (Vm - E_K)$, where Vm is held at -50 mV, E_K (reversal potential for potassium ions) is zero. Thus, I_K is proportional to G_K (membrane conductance to potassium ions).

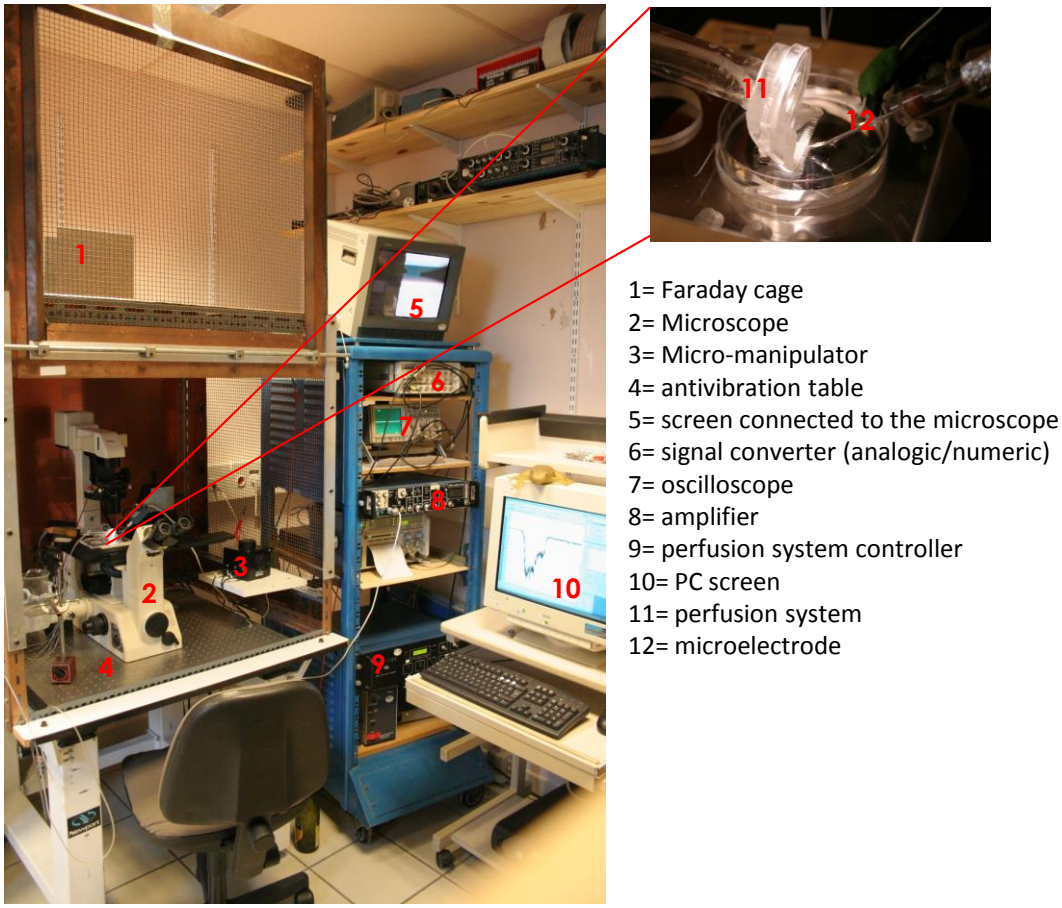

1= Faraday cage
2= Microscope
3= Micro-manipulator
4= antivibration table
5= screen connected to the microscope
6= signal converter (analogic/numeric)
7= oscilloscope
8= amplifier
9= perfusion system controller
10= PC screen
11= perfusion system
12= microelectrode

Figure 37. Patch clamp set-up at 'Channels' group. The Faraday cage protects the experiment from possible electromagnetic perturbation. The microscope is an Olympus ULWCD 0.30 with three lenses (X 4, X 10, X 40). The micromanipulator enables precise movement of the pipette in the three dimensions. The microelectrode in glass is filled with an electrolytic solution in which an electrode in silver is placed. Through this pipette we realize the patch excision. The electrode allows to impose a certain voltage (voltage clamp) on the patch but also to measure the current induced by the ionic flow through the ion channels present in the patch. The perfusion system controller RSC-100 (Rapid-Solution-Changer, Bio-Logic) enables a rapid and automatic exchange of solutions to test and is directly connected to the perfusion system. It is controlled with a software developed by Michel Vivaudou (Perf). The perfusion system is directly connected to the solutions to test. A screen connected to the microscope allows to follow the experiment. The signal converter (Digidata 1322) allows to convert the analogic signal generated into a numeric signal that is read by the computer. The oscilloscope (HM-407, Hameg) enables to visualize the recorded current in real-time. The patch clamp amplifier RK-300 (Bio-Logic) adapted for very small currents (picoAmpere), allows the current to voltage conversion and also to impose a certain voltage or current. The computer is used to manage and follow the experiment. The anti-vibration table allows to dampen possible mechanical vibrations that may damage the experiment.

9.1.2 Data processing and analysis

Signals recorded during the experiments are sampled at 1 KHz and subsequently filtered between 100 and 10 Hz, depending on current values. Traces are treated using a software developed by Michel Vivaudou called Erwin. Baseline fluctuations are removed by interactive fitting with a spline curve and subtraction of this fit from the signal. Non-linear curve fitting was performed with Dr.Fit software, developed by Michel Vivaudou. The following standard Hill equations were used for fitting.

For activation by openers:

$$f(|X|)=i_0 + i_{MAX}/ [1+(K½/|X|)^h]$$

where |X| is the concentration of activator, i_0 is the control normalized current in absence of activator, i_{MAX} is the maximal activator-induced current, K½ the concentration for half-maximal activation and h the Hill coefficient (Figure 38).

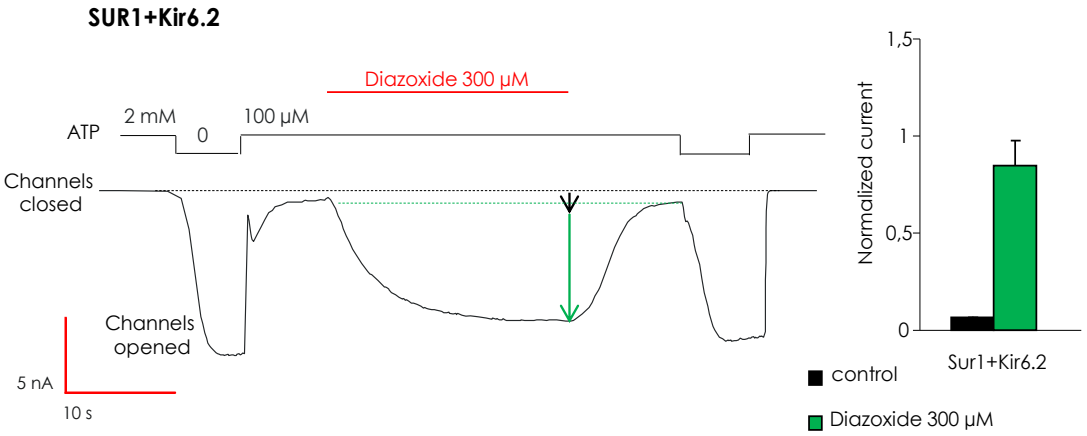

Figure 38. Typical patch-clamp recording in excised inside-out configuration of wild type K-ATP channels and their response to the pharmacological opener Diazoxide (300 µM). The recording is obtained holding the membrane potential at -50 mV. The histogram represents the normalized current.

For inhibition by nucleotides and Glibenclamide:

$$f(|X|)=i_0 / [1+(|X| / K½)^h]$$

where |X| is the concentration of inhibitor, i_0 is the control current in absence of inhibitor, K½ the concentration for half-maximal inhibition and h the Hill coefficient. Results are

displayed as mean ± s.e.m.. Error bars in figures represent s.e.m. and are only shown if greater than symbols.

9.2 The Two-Electrode Voltage-Clamp technique (TEVC)

The Voltage-clamp technique has been used to develop another very powerful method to analyse ion channels in large cells, the TEVC technique. In this case, instead of a single electrode, two electrodes are involved in the experiments: one is used to monitor cell voltage (which is held at -50mV) and the other to inject the current necessary to reach the desired voltage (that is equal to the membrane current) (Baumgartner, Islas, and Sigworth 1999).

9.2.1 Experimental procedure

It involves ligand solutions and microelectrodes preparation. Ligands are prepared in TEVC bath (91 mM KCl, 5 mM HEPES, 1.8 mM $CaCl_2$, $MgCl_2$ 1 mM, 0.3 mM niflumic acid, pH 7.4). Micropipettes are pulled from borosilicate capillaries (Kimble product) to obtain a diameter of ~ 10 µM and a resistance of 0.2-0.8 MΩ. Pipettes are filled with 3 M KCl solution and the silver chloride electrodes are then placed inside.

At the IBS, the Channels group possesses an automated robot for TEVC analysis called 'Robot HiClamp' (Multi Channel Systems). The robot, which has been introduced on the market recently, presents several advantages compared to the manual set up. It allows the screening of a large number of cells in a relative shorter time and the volume of ligand required is sensitively reduced (200 µl against 10 ml for the manual set up). This last advantage is particularly convenient for testing of expensive ligands.

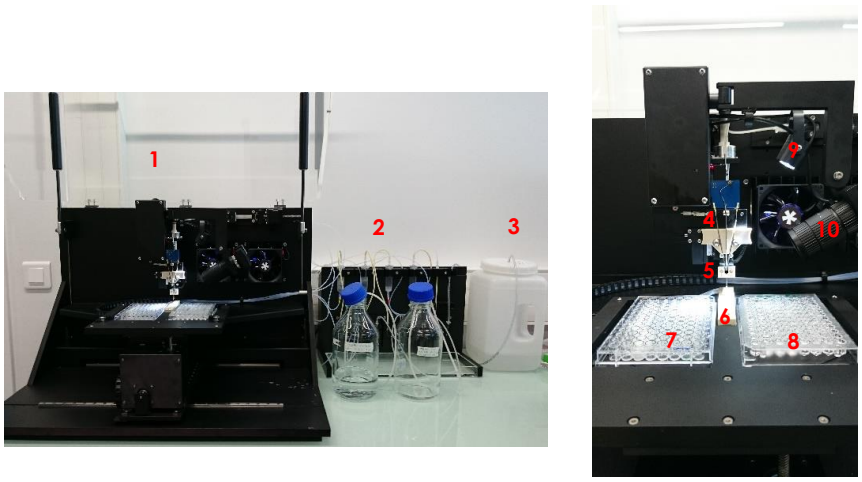

Figure 39. Robot HiClamp (Multi Channel Systems).

As shown in Figure 39, the robot (1) presents a table that contains both oocytes (8) and compound to test (7) in two separate 96-well plates. Oocytes are transferred with the help of a suction pump from the plate into a silver wire basket (5) that serves as a reference electrode. After automatic impalement of the intracellular glass microelectrodes (4), the basket with the oocyte is moved from one compound-containing well to the other. Before testing the ligand, the cell situated inside the basket is placed in the washing station (localized between the plates, 6) and washed with ND96, low-K^+ solution (2) (NaCl 91 mM, KCl 2mM, $CaCl_2$ 1,8 mM, $MgCl_2 \cdot 6H2O$ 1mM, HEPES 5mM, pH 7.4). Application of this solution is essential to test oocyte health: a healthy cell shows a current that is less than 10 μA. After selection in ND96, the oocyte is washed with the TEVC bath solution (high-K^+ solution). At this stage, K^+ ions in the solution are forced to enter the cell following their electrochemical gradient creating an inward current. For cells expressing potassium channels, current value are >0.1 μA. For values of current between 10 and 0.1 μA the oocyte are selected for compound testing and directly moved in the first solution to test. The protocol ends with application of Ba^{2+} (control) to block K^+ channels. All liquids coming from the washing station are trashed into a dedicated bin (3). All steps can be followed with a camera (10) and the relative light source (9).

9.2.2 Data processing and analysis

Data are processed an analysed using the HiClamp software DataMining and then exported to Excel and used to calculate currents values in each applied solution using a software developed by Michel Vivaudou. Currents values are standardized using the '0 current' as the current recorded in Ba^{2+} solution and 1 in the TEVC bath solution (basal current) (Figure 40).

$$I_{normalized} = I - I_{Ba}^{2+} / I_{bath} - I_{Ba}^{2+}$$

where I is the current recorded upon the application of a specific ligand (agonist/antagonist), I_{Ba}^{2+} is the current measured in the presence of barium ions, and I_{bath} in the TEVC bath solution, before ligand application.

The percentage of the change in the current (activation or inhibition) induced by the applied ligand is calculated simply as:

$$\%_{change} = (I_{normalized} - 1) \cdot 100$$

where $I_{normalized}$ is the value obtained upon application of a specific ligand. Subsequently, data is used for fittings according to a standard Hill equation:

$$f(x) = I_{MAX} / 1 + (Ec_{50} / X)^{h}$$

Where I_{MAX} is the asymptotic maximal effect, EC_{50} is the concentration at which half maximal effect of ligand is observed and X is the concentration of the applied ligand.

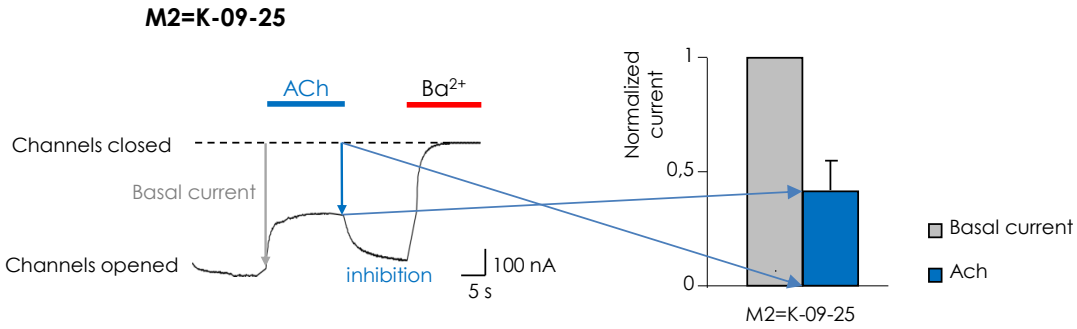

Figure 40. Typical TEVC recording of the Muscarinic-based ICCR and correspondent normalized current histogram. The recording is obtained holding the membrane potential at -50 mV and using ligands prepared in TEVC bath (91 mM K^+). Acetylcholine (5 μM) triggers channel inhibition. This effect is reversible once the oocyte is washed with TEVC bath. Ba^{2+} is used to block all potassium channel. Dashed lines indicate the baseline of Ba^{2+}-sensitive currents.

Results

10. Project 1: 'Structure of the ATP-sensitive potassium channel'

10.1 Relevance of the study

As mentioned before, K-ATP channels are widely expressed in the human body and its activity is essential for insulin secretion. Many mutations in the K-ATP channel have been correlated to severe physiological dysfunctions such as neonatal diabetes, congenital hyperinsulinism, and heart failure. A high-resolution structure of the complex is sorely needed to improve the pharmacology. In fact, drug discovery, in the case of the K-ATP channel, has not been driven by any data based on the atomic structure as these are still missing. Mikhailov and colleagues, who reported a controversial 18 Å structure of the full complex by using cryo-electron microscopy, have published the only data concerning the structure of the complex in 2005 (Mikhailov et al. 2005).

Beside the pharmacological aspect, the K-ATP channel remains a very intriguing protein under an evolutionistic point of view. The SUR protein belongs to a well known family of transporters but it evolved to work as the regulatory subunit of a K^+ channel. Also because of this non-conventional coupling, this channel remains one of the most complex ion channels known so far.

Moreover, even the obtainment of the atomic structure of subunits of the K-ATP such as the SUR or the Kir6, or domains as the TMD0, would sensibly improve our knowledge of this complex protein. There are existing atomic structures of other ABC proteins but none of these contain the TMD0 domain, which remains totally unknown in terms of structure. For this reason, the available SUR models lack the TMD0 domain. For the Kir6 channel it is easier to build models, as other Kir channels have been crystalized, but these structures lack important regions of the N- and C-terminal domains that are essential for Kir6 channels and less important for other Kir channels, as they are not coupled with regulatory proteins.

10.2 Project background and experimental approach

This challenging project was started in the 'Channels' group by Jean Revilloud with the use of insect cells as a system to overexpress the full-length K-ATP channel. Despite encouraging preliminary results for the expression, a considerable amount of protein was lost during the purification steps. The purified protein was further analysed by electron microscopy. Images

showed a very heterogeneous sample, probably scarcely folded and with some aggregates. Hence, the decision to change expression system in order to improve both quality and yield of the sample. The subsequent expression system assayed was the bacteria *E. coli*; a new gene encoding the K-ATP channel optimized for expression in *E. coli* was acquired. The protein did express at the cell membrane but was insoluble in all the tested detergents. The result suggested a possible misfolding, maybe due to a lack of glycosylation, as bacteria do not possess a glycosylation system.

If the high-resolution structure of the full-length complex is very ambitious, solving the structure of small domains of the K-ATP looks less problematic. According to this assumption, we started to work on shorter constructs derived from the K-ATP channel, such as the full-length SUR, the TMD0 domain of SUR and the Kir6.2 subunit. In parallel, we pursued the expression of the full complex. Each domain, or fusion of domains, was tested in several expression systems.

10.3 Results: Expression trials

10.3.1 Expression in *E. coli*

Starting from the evidence that the structures of many ABC proteins and potassium channels have been successfully obtained by over-expressing the proteins in *E.coli*, we decided to test this system as well. An overview of the constructs used and the bacterial strains tested is reported in Table 7.

Table 7. Expression trials in E.coli strains.

Construct	Strain	Expression
SUR2A	BL21, C43, Rosetta	No
TMD0-Kir6.2	BL21, C43, Rosetta	Yes
TMD0-eGFP	BL21, C43	Yes

The trial for the **SUR2A** construct was realized by Charlotte Haas, a technician student, and revealed no expression.

The **TMD0-Kir6.2** fusion construct was expressed only in the BL21 strain. Western blots, used to detect the expression, revealed a considerable degradation of the protein and a weak expression (Figure 41). Bacterial membrane samples, obtained after centrifugation of bacteria

total extract, are loaded into an SDS-PAGE 10% Acrylamide to allow protein separation. Proteins are subsequently transferred on nitrocellulose membrane to allow His-tag recognition by an anti-His tag antibody (Figure 41).

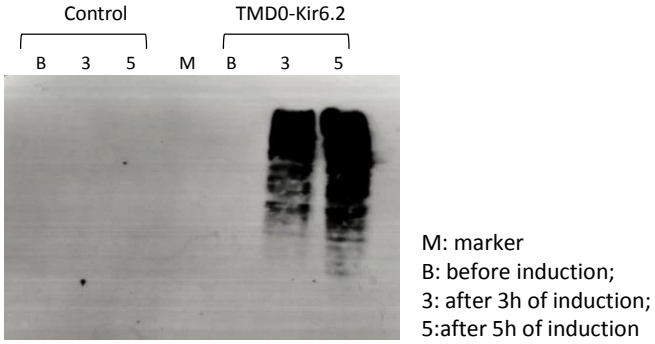

Figure 41. Western blot of the TMD0-Kir6.2 expression trial in E. coli BL21. Control identify the protein samples corresponding to bacteria transformed with a plasmid not carrying the gene (pET 24 a+ vector only). B identifies membrane samples of bacteria collected before induction of protein expression, 3 corresponds to membrane samples collected after three hours of induced expression, 5 identifies membrane samples collected after five hours of induced expression.

Despite the low level of expression, we conducted an experiment to assay the solubility of the protein in presence of detergent in large excess. None of the tested detergents was able to solubilize the protein, which remained trapped in the bacterial membrane.

The construct **TMDO-eGFP**, made by fusing the TMD0 domain with the eGFP protein, was designed to reduce the hydrophobicity of the membrane protein part and for easy detection of expression. The expression trial was realized in both BL21 and C43 strains and we were able to detect very weak levels of proteins only using a very sensitive antibody system targeting the HA tag. No fluorescence was detected.

For both TMD0-Kir6.2 and TMD0-eGFP we tried to improve the expression by supplementing the LB medium with nutrients, avoiding expression leak with the use of glucose before induction and shortening the time of induction. Unfortunately, we did not notice any change in the level of expression or degradation.

10.3.2 Expression in yeasts

As the expression trials in bacteria did not give the expected results, we decided to switch to eukaryotic systems. The result obtained in *E. coli* suggested possible protein misfolding. This problem can be solved by using host cells with a glycosylation machinery. The K-ATP channel presents three glycosylation sites in the SUR subunit only.

Moreover, some Kir channels have been successfully expressed and purified using yeast (D'Avanzo et al. 2010; Tao et al. 2009).

For these reasons, we tested the expression of different constructs in both *S. cerevisiae* and *P. pastoris* in a collaboration with Patrice Catty at CEA Grenoble.

Table 8. Expression trial in S. cerevisiae and P. pastoris.

Construct	Expression
SUR2A-Kir6.2	No
SUR2A	No
Kir6.2	No

Unfortunately, both trials in *S. cerevisiae* and *P. pastoris* were negative. No expression was detected, not even at minimal levels.

The hypothesis of a wrong analysis by Western blot can be excluded as we used positive controls to ensure proper revelation by the antibody. Moreover, the tags present in all constructs have been tested previously in other expression systems, at the same position in the protein, and were found to be accessible by the antibody. A possible explanation for this failure of expression is that, by using a more complex organism as a host cell, we can increase the chance of getting proper folding but we also run the risk that the cell is more efficient at degrading foreign proteins that may be toxic for its metabolism.

10.3.3 *In-vitro* synthesis

Cell-free synthesis of membrane proteins emerged recently as a powerful tool to overcome problems of classical expression systems such as misfolding, protein aggregation and toxicity for the host. The main advantage for membrane proteins production is given by the possibility to supplement the reaction recipe with detergents that help protein folding. The main disadvantage is that cell-free synthesis currently does not work for proteins with a mass > 100 kDa. Because of this limitation, we focused the cell-free experiments on short subunits of the K-ATP channel.

Table 9. Expression trial in cell-free system.

Construct	Expression
TMD0	Yes (in absence of detergent)
TMD0-eGFP	Yes
Kir6.2	Yes

Lionel Imbert (IBS, cell-free facility) performed initial small-scale trials to screen reaction conditions such as temperature, concentration of magnesium and time.

Using this technique, we managed to get expression in presence of detergents only for two constructs: TMD0-eGFP and Kir6.2, while the TMD0 could only be produced in absence of detergents. Membrane proteins produced in absence of detergents do not retain their folding and thus are inactive. For this reason, we decided to focus our attention on TMD0-eGFP and Kir6.2 only, as the refolding of membrane proteins from insoluble fractions is very complex and risky.

The **TMD0-eGFP** was produced using the 'dialysis' mode performing an overnight reaction at 22°C. The size of TMD0-eGFP is 51.9 kDa. The cell-free total extract was recovered after the reaction and used for MAC purification.

The **Kir6.2** construct corresponds to the pore-forming subunit of the K-ATP channel and it has a size of 46 kDa. As for the TMD0 construct, the initial expression trials were positive only in absence of detergent. To solve this problem we collaborated with Yann Huon de Kermadec (PhD student at IBS) who provided nanodiscs to try to solubilize the protein directly during its production. Nanodiscs were added to the reaction mix in the 'batch'

configuration. After 3 hours of reaction, we recovered the sample and performed MAC purification.

10.4 Results: Purification

10.4.1 TMD0-eGFP

After overnight production, the protein is recovered and purified by MAC. Elution fractions were collected and used to run several tests: an acrylamide gel, a Western blot and an N-terminal sequencing to confirm protein identity. The N-terminal sequencing was performed by the dedicated platform at IBS by Jean-Pierre Andrieu.

During MAC, we exchange detergent, as the Brij 35 used during cell-free production is an ionic detergent, not compatible with crystallographic studies. To screen a large number of detergents suitable for TMD0-eGFP, we used the RoBioMol platform at IBS. Several detergents were found compatible. We decided to try DDM since this detergent is widely used in the structural biology field. The concentration of DDM used during the first experiments was 0.0174 % (2 CMC). Both gel analysis and Western blot revealed the presence of several states of oligomerization of the protein (Figure 42).

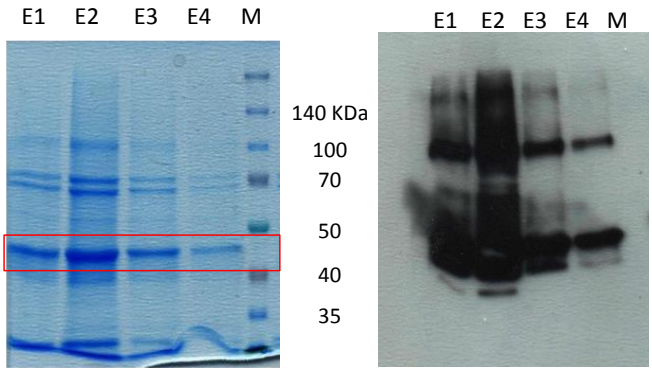

Figure 42. TMD0-eGFP SDS-PAGE and Western blot of the different elutions after MAC in presence of DDM. Protein sample in DDM is loaded into a column containing the high affinity resin for the His-tag present on TMD0-eGFP. The flow-through is discarded while the elution fractions are collected (E1 to E4) and then loaded on a 10 % Acrylamide SDS-PAGE. The monomeric TMD0-eGFP is shown in the red box. The Western blot (right panel) shows other bands corresponding to the TMD0-eGFP above the monomeric specie that may correspond to a dimer (~ 100 kDa) and a possible tetrameric TMD0-eGFP above 140 kDa.

To obtain a homogenous sample for structural studies, it is necessary to separate these different oligomeric states. Following this concept, we performed a Size-Exclusion Chromatography (SEC) that provides separation of molecules according to their mass/shape. Elution fractions collected from the MAC (E1 to E4) were pooled and concentrated to obtain a final volume of 500 µl with a concentration of 0.7 mg/ml (starting from a volume of 2 ml of cell-free reaction). The sample was then injected into column (Superdex 200 10/300 GL, GE Helthcare) to allow proteins separation.

The SEC profile is shown in Figure 43. Because of the principle of the SEC technique, the bigger objects elute from the column first. At the beginning of the chromatogram we expect to visualize big species, such as protein aggregates or tetrameric TMD0-eGFP, followed by the smaller TMD0-eGFP in trimeric, dimeric and monomeric form.

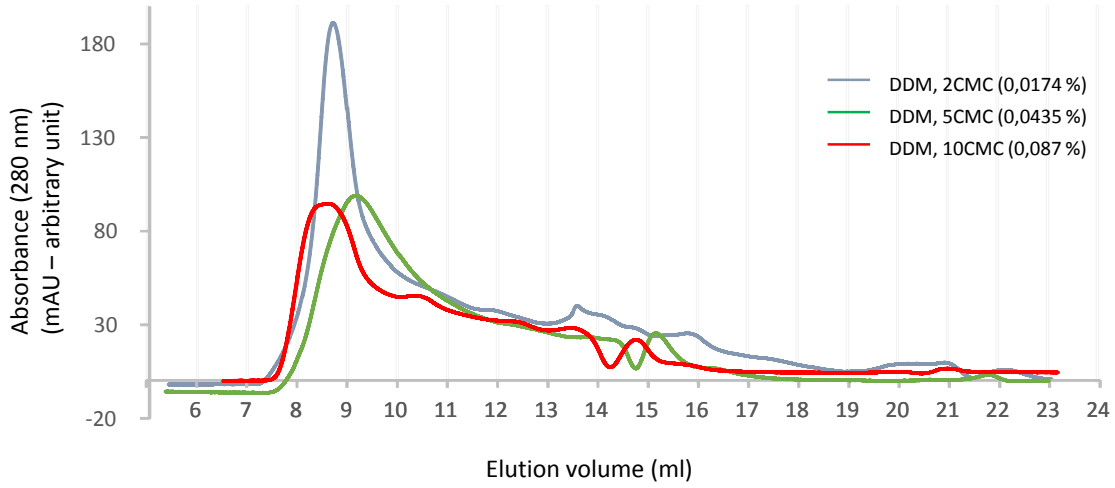

Figure 43. SEC profiles overlap of TMD0-eGFP using increasing concentrations of DDM. The blue curve identifies the purification in presence of 0.0174 % DDM. The green curve corresponds to a purification in presence of 0.043 % DDM. The red curve correspond to a purification in presence of 0.087 % DDM.

As we can see in Figure 43 (blue curve), the first experiment, in which we used a relatively low concentration of detergent, do not provide separated species. We observe a main peak that could correspond to a mixture of aggregates and tetrameric TMD0-eGFP followed by the elution of non-well defined species. To improve the separation, we used increasing concentrations of DDM to solubilize protein aggregates that are present in the first

peak(Figure 43, green and red curves). As the chromatogram illustrates, none of these additional trials provided a reasonable separation of the different states of the protein.

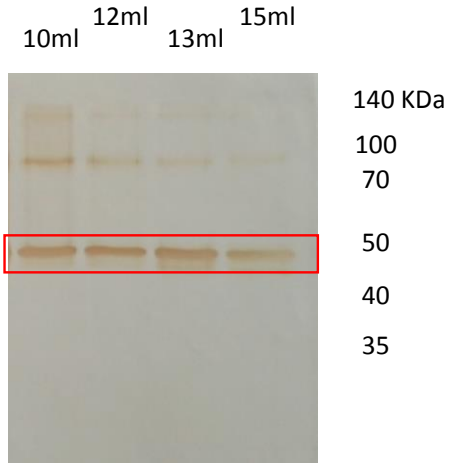

Figure 44. Western blot corresponding to the protein sample in complex with DDM 0.087 % (red curve in Figure 42). Samples eluting at 10, 12, 13 and 15 ml were analysed. The monomeric TMD0-eGFP is highlighted in the red box.

Only by using a very high concentration of DDM (0.087 % or 10 CMC) we were able to visualize a feeble separation of the oligomers. Samples eluting at 10, 12, 13 and 15 ml are analysed by Western blot (Figure 44). With increasing elution volume, the intensity of bands corresponding to multimeric states decreases, in accordance with the decreasing signal of the SEC profile. TMD0-eGFP could be present in different states and DDM might not be the best detergent to solubilize this protein. Other conditions should be explored in order to improve protein separation, for example by analysing the effects of other detergents.

As suggested by the initial detergent screening obtained using the RoBioMol platform at IBS, we successively tested the Cymal-6 and the MNG-3. As for the DDM, we performed detergent exchange during MAC.

High quantity of detergent compromises the success of crystallographic studies. Because of that, for the exchange with **Cymal-6** we started with a concentration of 0.56 %, 20 times the CMC (CMC= 0.028 %), that was reduced to 0.14 % before SEC in order to remove as much detergent as possible. The corresponding SDS-PAGE analysis is shown in Figure 45. Successively, elution fractions 1, 2 and 3 (the most concentrated) were pooled and

concentrated to a final volume of 500 µl for injection into SEC column (concentration= 0.72 mg/ml starting from 1 ml of cell-free reaction).

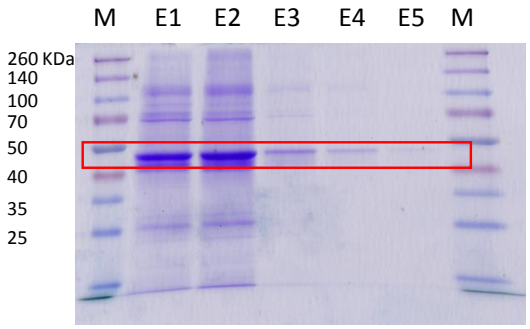

Figure 45.TMD0-eGFP SDS-PAGE of the different elution fractions after MAC in presence of Cymal-6. Protein sample in complex with Cymal-6 is loaded onto a column containing the high affinity resin for the His-tag present on TMD0-eGFP. The flow-through is discarded while the elution fractions are collected (E1 to E5) and then loaded on a 10 % Acrylamide SDS-PAGE. The monomeric TMD0-eGFP (red box) corresponds to the band around 50 kDa.

For the exchange with **MNG-3** we started with a concentration of 40 times CMC (CMC= 0.001 %), so 0.04 %, that was reduced to 0.005 % before SEC. The SDS-PAGE analysis is shown in Figure 46. Successively, elution fractions 1, 2 and 3 were pooled and concentrated to a final volume of 500 µl for injection into SEC column (concentration= 0.48 mg/ml starting from 1 ml of cell-free reaction).

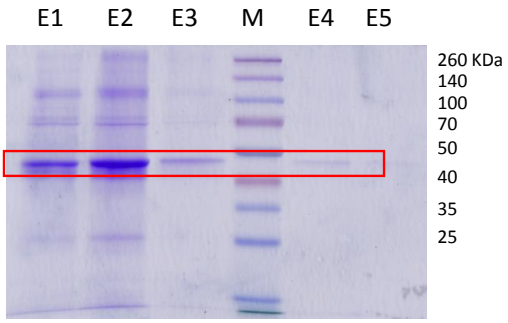

Figure 46. TMD0-eGFP SDS-PAGE of the different elution fractions after MAC in presence of MNG-3. Protein sample in complex with MNG-3 is loaded onto a column containing the high affinity resin for the His-tag present on TMD0-eGFP. The flow-through is discarded while the elution fractions are collected (E1 to E5) and then loaded on a 10 % Acrylamide SDS-PAGE. The monomeric TMD0-eGFP (red box) is shown around 50 kDa.

The SEC chromatogram profiles corresponding to the two purifications are shown below. The fractions highlighted in the black boxes are successively analysed on SDS-PAGE. (Figure 49).

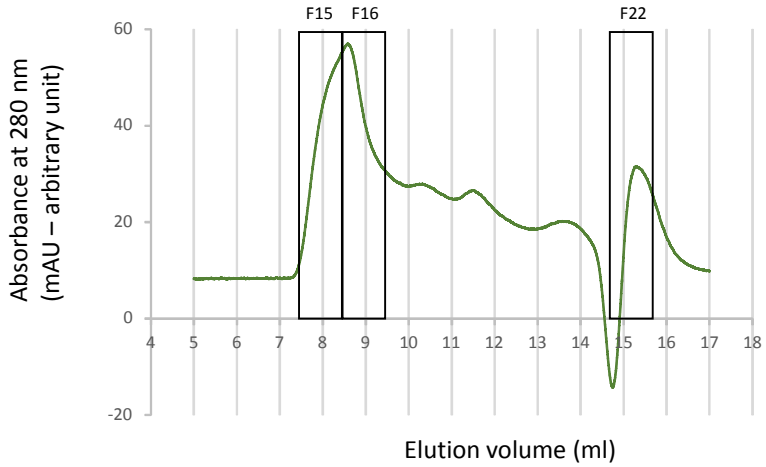

Figure 47. SEC chromatogram corresponding to TMD0-eGFP in Cymal-6. The fractions collected by the machine highlighted in black boxes are subsequently analysed by SDS-PAGE.

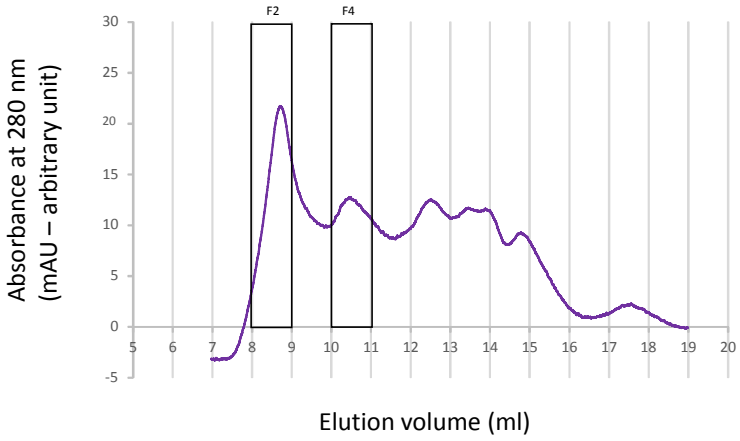

Figure 48. SEC chromatogram corresponding to TMD0-eGFP in MNG-3. The fractions collected by the machine highlighted in black boxes are subsequently analysed by SDS-PAGE.

The exchange of Brj35 with these two new detergents provided an improvement in terms of yield (0.36 mg in Cymal-6 and 0.24 mg in MNG-3 against 0.17 mg in DDM) but protein quality still needs to be determined by further analysis.

The SEC profile of the protein in Cymal-6 shows a main asymmetric peak that evidences the presence of at least two species. The first part of the peak could contain aggregates and the second the tetrameric TMD0-eGFP. Fraction 22 evidences another species, which could correspond to the monomeric TMD0-eGFP, according to its apparent mass. Nevertheless, when this fraction is analysed on an acrylamide gel, we can notice the presence of several bands instead of a single band (Figure 49).

SEC profile of the protein in MNG-3 (Figure 48) shows a main peak eluting at 8 ml, that could correspond to the aggregates and tetrameric TMD0-eGFP, followed by a series of poorly defined peaks.

However, the two chromatograms show that none of the peaks is actually resolved.

These last experiments with Cymal-6 and MNG-3 have been performed during the writing of this manuscript and a deeper biophysical analysis of the SEC profiles will be necessary to fully understand how to improve the separation.

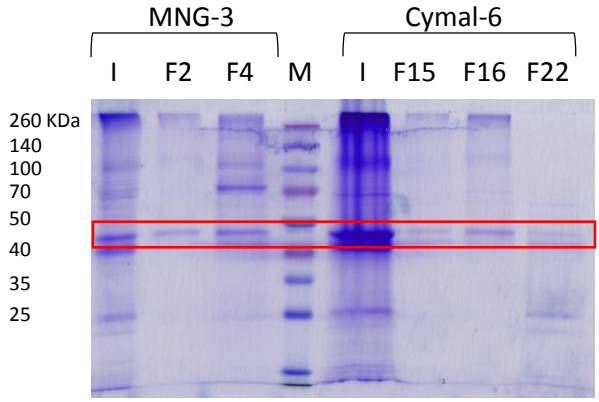

Figure 49. SDS-PAGE to analyse SEC fractions. I corresponds to the highly concentrated sample injected into the SEC column; F2 and F4 correspond to fractions coming from the SEC elutions of the purification with MNG-3; F15, F16 and F22 correspond to fractions coming from the SEC elutions of the purification with Cymal-6.

10.4.2 Kir6.2

The resin used during the MAC did not retain the His-tag present on the Kir6.2 and, during the preliminary experiments, the protein was washed out in the flow-through of the MAC. To solve this problem we used His-tagged Nanodiscs that were efficiently retained by the Ni^{2+} of the resin. The Kir6.2 and the MSP, which forms the belt of the Nanodiscs, were detected after Western blot and the fractions collected after the MAC (Figure 50) were concentrated to a final volume of 500 µl. In this case, the concentration of Kir6.2 is difficult to obtain, as it does not correspond to the measured concentration due to the presence (in large excess) of MSP.

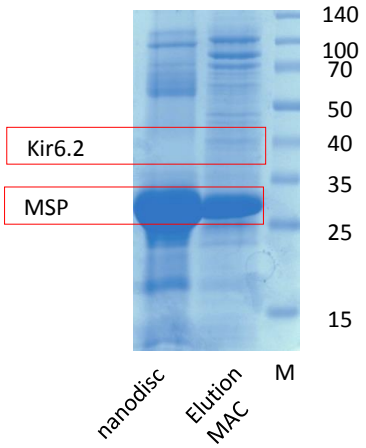

Figure 50. SDS-PAGE after MAC of Kir6.2 in nanodiscs elution fraction and the sample of the empty nanodisc used as control to estimate the amount of MSP compared to Kir6.2. Each visible band was analysed by N-terminal sequencing and only the weak band around 40 kDa (red box) was identified as Kir6.2.

After injection into the SEC column, we obtained the following chromatogram (Figure 51) and the corresponding SDS-PAGE (Figure 52).

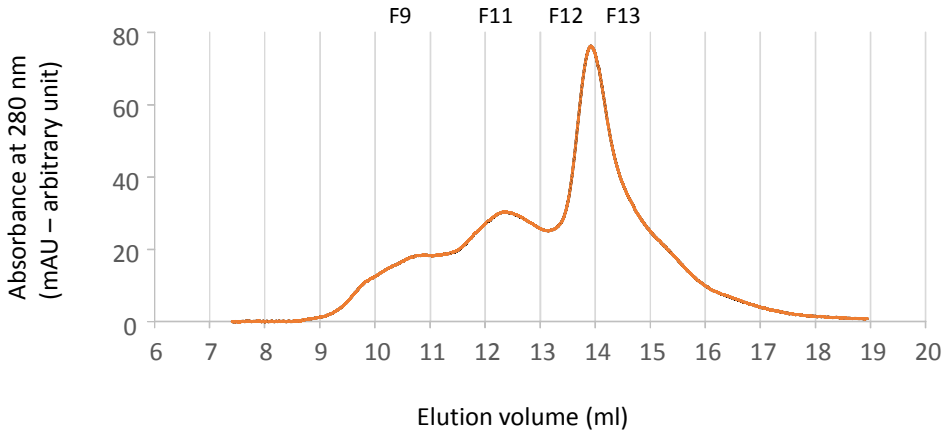

Figure 51. SEC chromatogram corresponding to the Kir6.2 inserted in nanodiscs. Fractions F9, F11 and F13 are further analysed by SDS-PAGE and Western blot.

The chromatogram evidences a main peak (fractions 12-13) plus two shoulders eluting just before the main peak (fractions F9- F11). Western blot analysis revealed the weak presence of Kir6.2 in every fraction plus a large excess of MSP.

Each band present in the SDS-PAGE (both SEC and MAC samples) was further analysed by N-terminal sequencing. Only the weak band around 45 kDa (in the gel after MAC purification, Figure 50) corresponds to Kir6.2. The bands of the SEC gel, initially thought to correspond to oligomers of Kir6.2, were identified as *E. coli* proteins, probably present in the cell-free total extract.

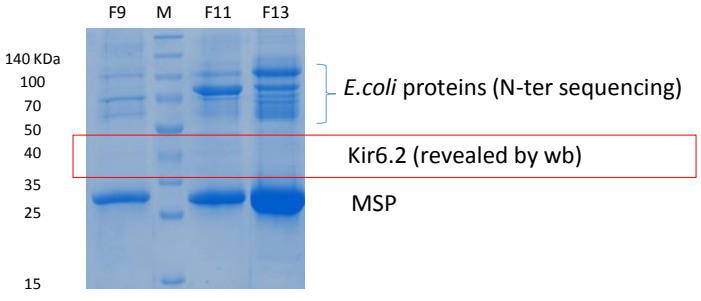

Figure 52. SDS-PAGE of the representative fractions of the SEC. Bands above 70 kDa were initially thought to correspond to Kir6.2 oligomers. The N-terminal sequencing test revealed that these bands actually correspond to contaminant proteins of the E. coli total extract used during the cell-free synthesis.

In conclusion, Kir6.2 is produced and purified using Nanodiscs only in very small amount. Moreover, the fractions eluted from SEC were not pure. There is an evident contamination by proteins of the cell-free mix, which could have an affinity for the lipidic face of the Nanodiscs and therefore remain attached to these during the purification.

10.5 Discussion and perspectives

Despite an effort in trying to screen several constructs in multiple expression systems, we did not manage to get reasonable amounts of proteins of good quality and purity.

A good alternative for expression of the full-length K-ATP is represented by the mammalian cell system such as the Human Embryonic Kidney cells (HEK). These cells emerged recently as an excellent alternative system for membrane protein expression and purification and it is becoming the first choice when starting protein expression trials of highly complex proteins. This system is currently under investigation at the 'Channels' group.

The strategy concerning the screening of separate subunits or domains of the K-ATP did not give the expected outcome, as only the TMD0-eGFP construct looked promising. Indeed, an improvement of the purification step of this last construct is required for future crystallization trials.

11. Project 2: 'Study of the functional coupling between SUR and Kir6.2: focus on the SUR interacting region

11.1 Relevance of the study

ATP-sensitive potassium (K-ATP) channels play a key role in adjusting the membrane potential to the metabolic state of cells. They result from the unique combination of two proteins: the Sulfonylurea Receptor (SUR), an ABC protein, and the inward rectifier K^+ channel Kir6.2. Both subunits associate to form a hetero-octamer (4 SUR/4 Kir6.2). SUR modulates channel gating in response to the binding of nucleotides or drugs and Kir6.2 conducts potassium ions. The mechanism responsible for the conversion of ADP and drugs binding to SUR into a signal of activation is not fully understood. In addition, the activity of the K-ATP channel varies with its composition. In pancreatic β-cells, SUR1/Kir6.2 channels are partly active at rest while in cardiomyocytes SUR2A/Kir6.2 channels are mostly closed. This divergence of function among the different isoforms of the SUR could be related to differences in the interaction of SUR1 and SUR2A with Kir6.2. This project aims at the understanding of the molecular differences between the SUR1- and the SUR2A-evoked activation of Kir6.2.

11.2 Project background and experimental approach

Two main regions of the SUR have been reported to physically interact with Kir6.2: the TMD0 domain and the region linking helix 17 to the NBD2 domain. TMD0 has been shown to play a crucial role in the regulation of Kir6 gating and trafficking (Chan, Zhang, and Logothetis 2003; Fang, Csanády, and Chan 2006). The second region is involved in the physical association of SUR2A with Kir6.2. This fragment (between residues 1295 and 1358) co-precipitates with Kir6.2 and competes with the full-length SUR2A for binding to Kir6.2 (Rainbow et al. 2004). Moreover, this region was also investigated by the 'Channels' group and revealed the essential role of three residues for the transduction of the binding of openers in an activating signal for Kir6.2 (Dupuis et al. 2008).

Alignment of SUR sequences with other ATP-binding cassette family members reveals a high sequence similarity with the multidrug resistance-associated proteins (MRP) which do not physically or functionally interact with Kir6.2. Taking advantage of this similarity, a chimeric strategy has been previously designed to study the role of specific regions of SUR2A

in K-ATP channel function. In order to determine whether a similar mechanism is conserved in other isoforms, we extended our investigations to SUR1-bases channels by using the same chimeric strategy.

11.3 Results: Residues Q1342, I1347 and L1350 of SUR1 are essential in transducing activation by Diazoxide and ADP to Kir6.2

Previously, three residues in the region linking the TMD2 and NBD2 domains of SUR2A were identified as important determinants of the coupling between SUR2A and Kir6.2. Mutating these residues prevented KCO- and ADP-induced activation of the channel without affecting the affinity of SUR2A for both activator families (Dupuis et al. 2008). In the present study, a similar chimeric strategy was applied to the SUR1 isoform in order to identify the key residues involved in the activation of Kir6.2.

Using inside-out patch clamp recordings, MRP1/SUR1 chimeras co-expressed with Kir6.2 in *Xenopus* oocytes were first tested for their response to openers (Diazoxide, 300 μM and MgADP, 100 μM). As described in Figure 53, we were able to measure Kir6.2-generated currents from all constructs except MRP1 co-expressed with Kir6.2, as expected and previously reported (Dupuis et al., 2008).

The SUR1S1M chimera, in which SUR1 residues 1313 to 1394 were replaced by the corresponding amino acids of MRP1, showed no response to Diazoxide although it was still able to traffick to the plasma membrane, suggesting the presence of critical SUR1 residues in this region for Diazoxide-evoked activation of Kir6.2. In order to identify those residues, we progressively replaced shorter regions of SUR1 by the corresponding residues of MRP1.

Chimera SUR1S2M, in which central residues of the region P1336-V1352 were exchanged, displayed also an altered response to Diazoxide, locating the critical residues in this 16 residue-long region.

Further refinements were performed by point mutations as shown in Figure 53 for the chimeras SUR1S3M (4 residues), SUR1S4M (5 residues) and SUR1(QIL/VFY). For SUR1S3M and SUR1S4M, Diazoxide application produced a robust activation equivalent to

that observed with wild-type SUR1. Consequently, the mutated residues are not essential for the Diazoxide-evoked regulation.

In contrast, replacement of the SUR1 QIL residues by the MRP1 VFY residues (SUR1(QIL/VFY)) abolished the activation by the opener indicating that those residues are essential for the Diazoxide-induced activation of Kir6.2.

To verify that the QIL residues are also sufficient to restore the Diazoxide action, the reverse MRP1 chimera was created by reintroducing the SUR1 QIL residues in the MRP1 sequence of the SUR1S2M chimera (SUR1S2M(VFY/QIL)). Application of Diazoxide induced an activation, confirming that the SUR1 QIL residues are not only essential, but also sufficient for activation by Diazoxide.

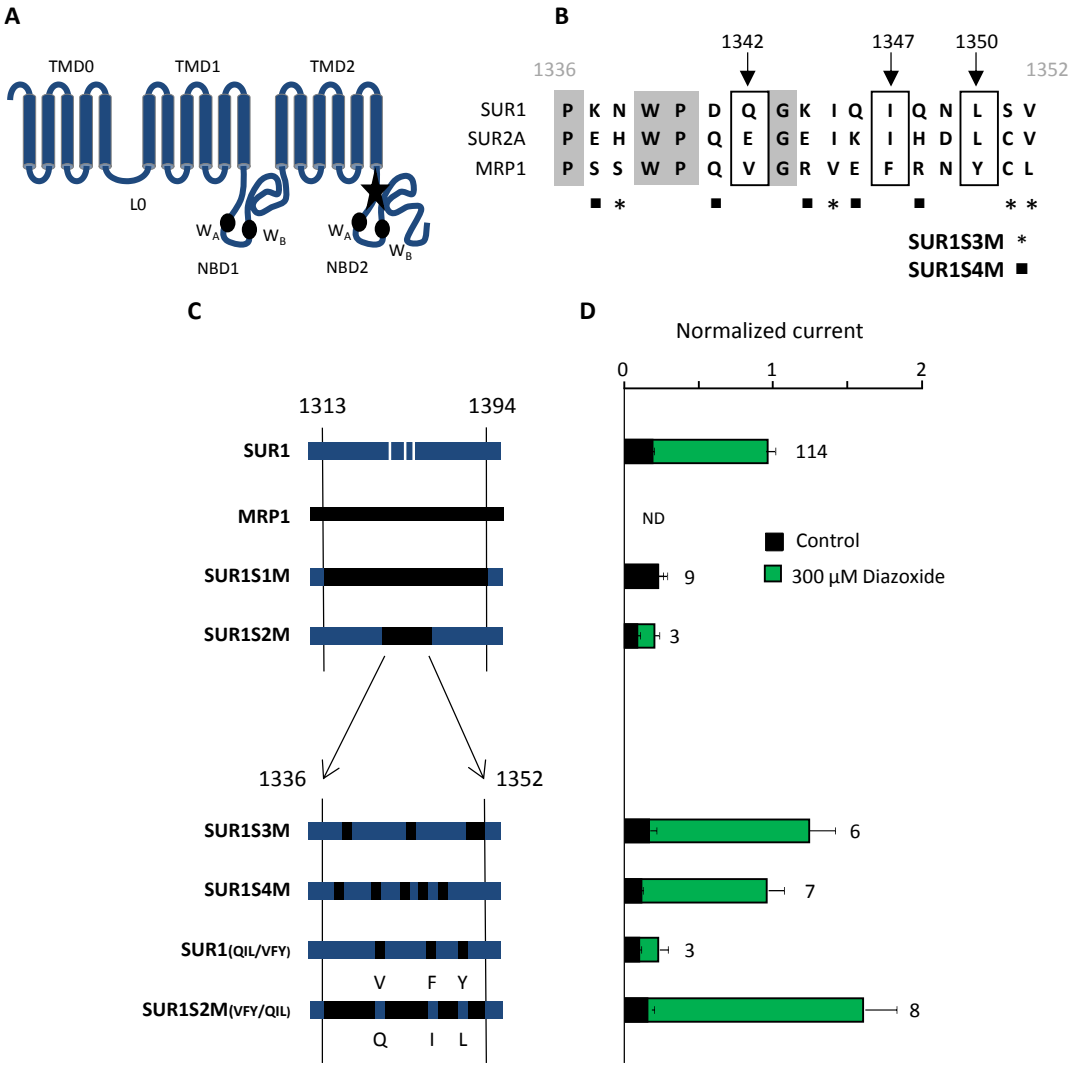

Figure 53. SUR1 residues Q1342, I1347 and L1350 are essential for K-ATP channel activation by Diazoxide. A, putative membrane topology of SUR1 (NBD, nucleotide binding domain; WA, Walker A motif; WB, Walker B motif). The star indicates the region identified by Rainbow et al. (2004) and mutated to obtain the S1M chimera. B, alignment of the amino acid sequences of human SUR1, rat SUR2A and human MRP1. Three residues (boxed) are conserved in SURs and not in MRP1: Q1342, I1347 and L1350. Stars and squares indicate the MRP1 residues introduced in SUR1 to obtain SUR1S3M and SUR1S4M, respectively. C, schematic representation of the chimeras. SUR1 and MRP1 elements are drawn in grey and black, respectively. For clarity, residues Q1342, I1347 and L1350 of SUR1 are indicated by white stripes. D, Diazoxide responses were measured in inside-out patches excised from oocytes co-expressing Kir6.2 and wild-type or chimeric SURs or MRP1 as indicated. Diazoxide (300 µM) was applied in the presence of 100 µM ATP, and currents were normalized to the current measured in the absence of nucleotides immediately before opener application. Application of 100 µM ATP alone (black bars) was used as a control. Numbers at right of bars indicate the number of patches included in each average.

As shown in Figure 55, Diazoxide had negligible effects on SUR1(QIL/VFY), even at a saturating concentration of 1 mM.

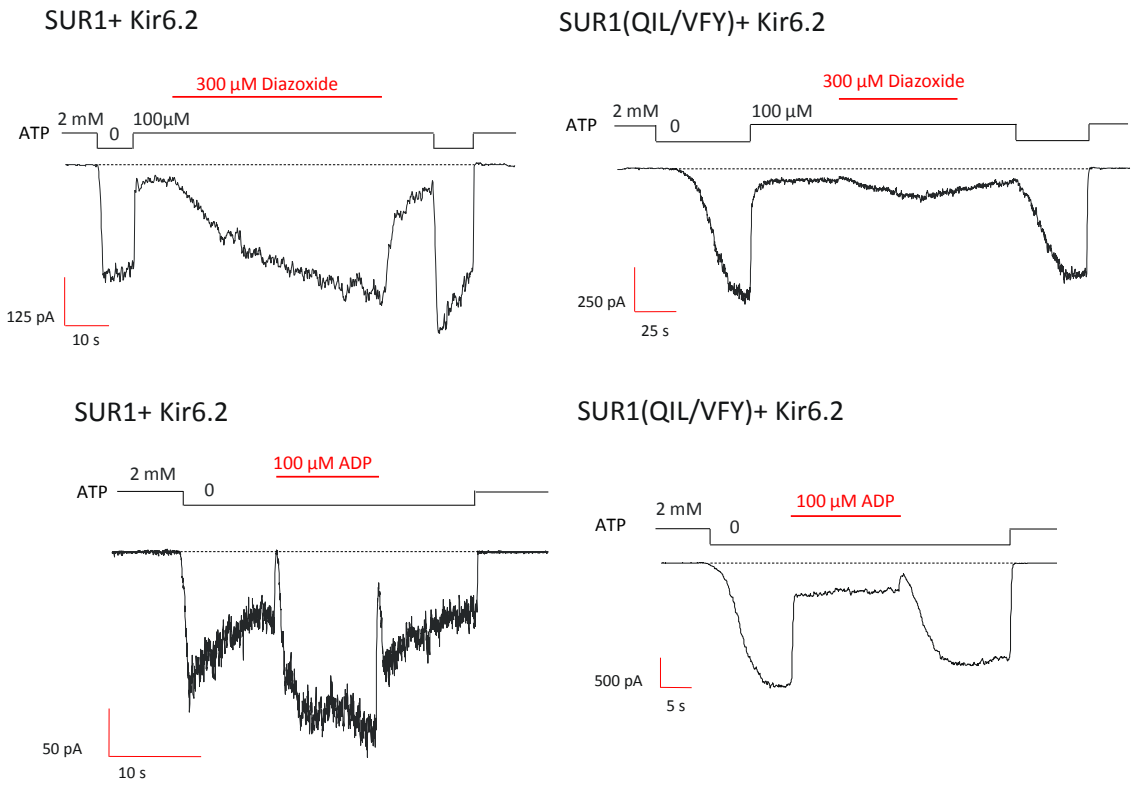

Figure 54. Representative patch-clamp recordings illustrating the responses of wild-type and SUR1(QIL/VFY)-based channels to 300 µM Diazoxide and 100 µM MgADP. Traces were recorded holding the membrane potential at -50 mV. Diazoxide (300 µM) was applied in the presence of 100 µM ATP while MgADP was applied immediately after application of a ligand-free solution.

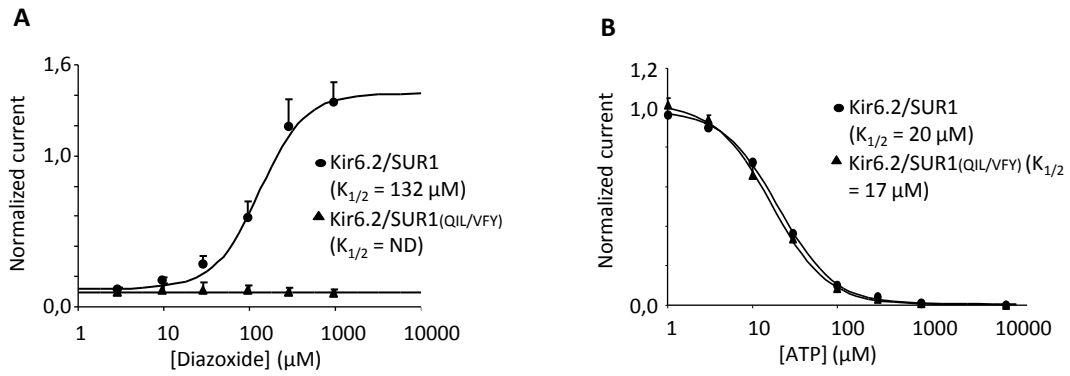

Figure 55. Characterization of the SUR1(QIL/VFY) mutant. A, Diazoxide dose-response relationships for Kir6.2/SUR1 (circles) and Kir6.2/SUR1(QIL/VFY) (triangles). Currents were normalized to the current measured in 0 ATP. Hill equation fitting yielded K1/2 = 132 µM (h = 1.65) for Kir6.2/SUR1. B, ATP dose-response relationships for Kir6.2/SUR1 (circles) and Kir6.2/SUR1(QIL/VFY) (triangles). Currents were normalized to the current measured in 0 ATP. Hill equation fitting yielded K1/2 = 20 µM (h = 1.33) for Kir6.2/SUR1 and K1/2 = 17 µM (h = 1.32) for Kir6.2/SUR1(QIL/VFY).

Involvement of those residues in the activation of Kir6.2 by the physiological opener MgADP was also assessed and the results, shown in Figure 56, were equivalent to the results obtained with Diazoxide.

The SUR1(QIL/VFY)/Kir6.2 channels were strongly inhibited by MgADP (70% inhibition) while the wild-type is activated (53% activation). Such observation is in line with the antagonistic effects of ADP, which causes inhibition by binding to Kir6.2 and activation by binding to SUR (Hosy and Vivaudou 2014). These results suggest that, in SUR1, residues Q1342, I1347 and L1350 are required to transmit activation from SUR1 to Kir6.2. These residues correspond to those previously reported (EIL) for the SUR2A subunit (Figure 53), (Dupuis et al., 2008). However, a difference was observed between SUR2A and SUR1 residues as the basal current of SUR1(QIL/VFY) was 12-fold higher than SUR2A(EIL/VFY) (Figure 56) suggesting that the MRP1 VFY residues disturbed less the SUR1/Kir6.2 interaction than the SUR2A/Kir6.2 and yielded a stronger surface expression. The higher current amplitude for SUR1(QIL/VFY) was not due to a lesser ATP sensitivity

of the channel because dose-dependent inhibition by ATP was unaffected by the mutations, with IC_{50}= 17 μM vs 20 μM for wild-type channels (Figure 55).

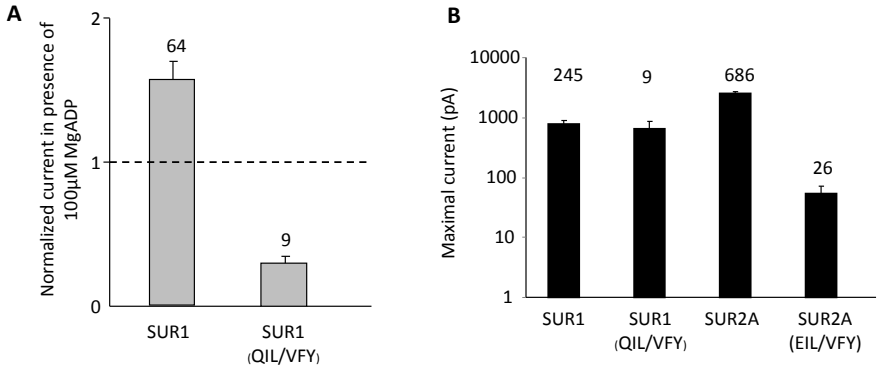

Figure 56. A, Response to 100 μM MgADP of SUR1 wt and SUR1(QIL/VFY). Currents were normalized to the current measured in absence of nucleotides immediately before MgADP application. Numbers indicate the number of patches included in each average. B, Current amplitudes in absence of nucleotides of Kir6.2/SUR1, Kir6.2/SUR1(QIL/VFY), Kir6.2/SUR2A and Kir6.2/SUR2A(EIL/VFY).

11.4 Results: Differences in the coupling of Kir6.2 with SUR1 and SUR2A revealed by alanine mutants

The SUR1 QIL and SUR2A EIL residues appear necessary and sufficient for the activation of Kir6.2 by SUR ligands. To further investigate the role of these residues, we explored their molecular specificity by mutating them to the following amino acids: Ile, Gln, Glu, Ala, Gly. Ile is hydrophobic with a long side chain; Gln is an uncharged polar residue at pH 7 able to create hydrogen bonds; Glu is a negatively charged amino acid, while Ala is hydrophobic with a short side chain and Gly has no side chain. All mutants were tested for their response to MgADP and pharmacological openers. Mutations of the critical residues to Gln or Glu resulted in the loss of MgADP activation for both SUR isoforms, indicating that the hydrophobicity of these residues I and L is essential for MgADP action (Figure 57).

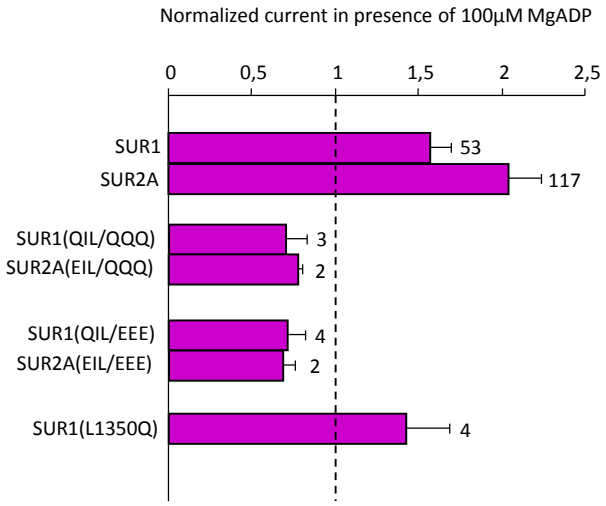

Figure 57. Relative responses to 100µM MgADP of SUR1 and SUR2A wt and mutants. Currents were normalized to the current measured in the absence of nucleotides immediately before MgADP application. Numbers indicate the number of patches included in each average.

The critical role of these residues is emphasized by the mutants SUR1(QIL/III) and SUR2A(EIL/III) which are still activated by MgADP and the pharmacological openers (Figure 58). Mutations to Gly (SUR1(QIL/GGG) and SUR2A(EIL/GGG)) abolished the activation by openers, suggesting that the presence of the lateral chains is required. Unexpectedly, mutations to Ala (SUR1(QIL/AAA) and SUR2A(EIL/AAA)) yielded distinct responses to openers, SUR1(QIL/AAA) is still activated while SUR2A(EIL/AAA) was not (Figure 58). Altogether, these results suggest that similar residues in SUR1 and SUR2A seem to be involved in the regulation of Kir6.2 by SUR, but they also contribute to isoform-specificity of the coupling mechanisms.

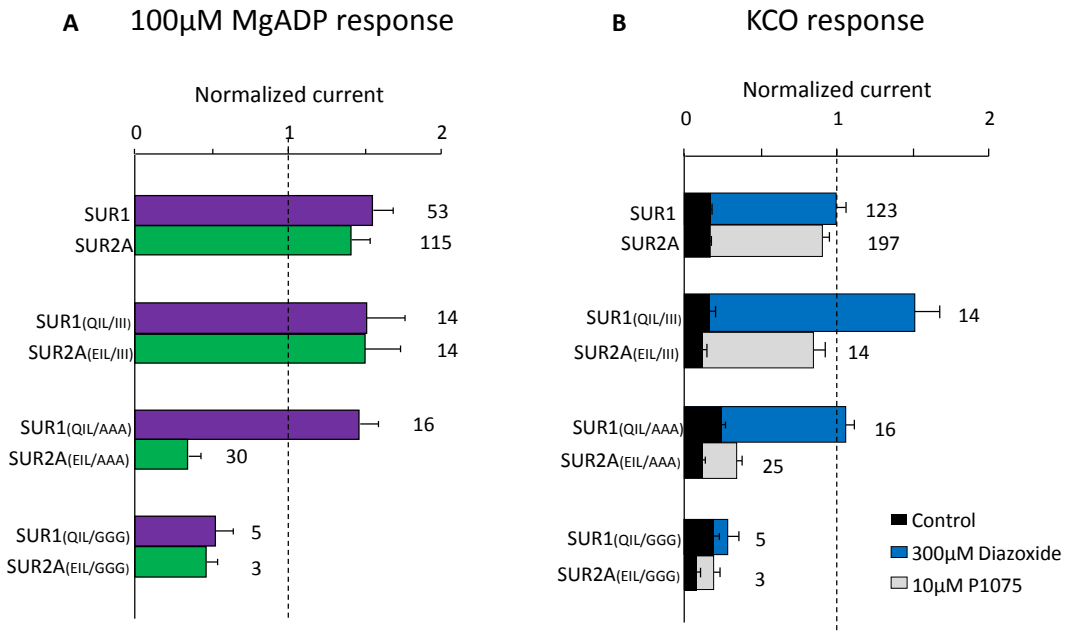

Figure 58. Opener responses by SUR1 and SUR2A wt and relative mutants. Residues Q1341, I1346 and L1349 of SUR1, and the matching residues E1305, I1310 and L1313 of SUR2A were mutated into alanine, glycine and isoleucine. A, The effects of the application of 100 µM MgADP were measured in inside-out patches excised from oocytes co-expressing Kir6.2 and the indicated SUR constructs. Currents were normalized to the current measured in the absence of nucleotides immediately before MgADP application. Numbers at right of bars indicate the number of patches included in each average. B, . The effects of 300 µM Diazoxide or 10 µM P1075 were measured in inside-out patches excised from oocytes. Diazoxide (300 µM) was applied in the presence of 100 µM ATP. P1075 (10 µM) was applied in the presence of 100 µM ATP. Control designates the current measured in 100 µM ATP before application of the tested opener.

11.5 Discussion and perspectives

Using a structure-function approach, we identified crucial residues in the SUR1 subunit responsible for allosteric upregulation of Kir6.2. Indeed, mutations of SUR1 residues Q1342, I1347 and L1350 into the corresponding residues (VFY) of MRP1 prevented K-ATP channel activation by both MgADP and Diazoxide. Mutagenic analysis of these three residues revealed the critical role of the hydrophobic residues for the activation of the channel by openers. Surprisingly, Alanine mutations in the context of SUR1 and SUR2A had opposite impact on the SUR-mediated regulation of Kir6.2, suggesting subtle differences in the molecular mechanisms occurring in the two isoforms (Figure 58). Because the three

identified residues are predicted to be part of the NBD2 domain (Figure 59), their mutation could affect the binding of the openers, leading to an absence of activation by MgADP and KCOs. While this hypothesis cannot be excluded, it is not supported by the unchanged ATP sensitivity of the mutants. Indeed, ATP dose-response experiments performed in absence of MgADP demonstrated that nucleotide inhibition of Kir6.2 was similar in the presence of wild-type SUR1 and in that of the mutant SUR1(QIL-VFY) (Figure 55). Because the binding site for Diazoxide has not been precisely identified, we cannot exclude the hypothesis that it is affected by the triple mutations. However, it is notorious that Diazoxide-activation is dependent on MgADP binding to NBD2 (Gribble, Tucker, and Ashcroft 1997). Moreover since both Diazoxide and ADP responses are similarly impaired, it is unlikely that the effect observed results from a disruption of the binding sites for both molecules. Thus, the likely interpretation of our results is that mutating Q1342V, I1347F and L1350Y affects the communication pathway from SUR1 to Kir6.2 rather than the binding of the effectors to SUR1.

Moreover, residue L1350 has been previously correlated to a mutation (L1350Q) that causes congenital hyperinsulinism by preventing surface expression of K-ATP channels in pancreatic β-cells (Yan et al. 2007). While we tested the functionality of this mutant, we did not observe any difference when comparing its activation ability with the wild-type (Figure 57). Interestingly, comparison of the mutant SUR1(QIL/QQQ) with the mutant SUR1(L1350Q) which is equivalent to SUR1(QIL/QIQ) reveals that mutation of a single residue is not sufficient to disturb the activation as observed with SUR2A (Dupuis et al., 2008).

Mutations in other residues such as Glu and Gly also affect the MgADP activation, but unexpectedly, mutations to Ala preserve the wild-type phenotype. Altogether these results indicate the critical role of these residues which can be replaced by a residue with short and hydrophobic side-chain (Ala) but not by hydrophilic (Q and E), nor side-chain-free residue (Gly), nor large hydrophobic residue (Phe). Similar mutations in SUR2A residues caused equivalent phenotype, except for mutations to Alanine that abolished the activation by MgADP. This unexpected SUR isoform difference suggests that the nature of the side chain is more critical for SUR2A activity than for SUR1. This observation could be explained by at least two hypotheses. In a first scenario, the interaction between SUR subunits and Kir6.2 could occur in different position depending on the global flexibility of the studied region

proximal to NBD2. A second hypothesis would be a difference in the NBD2 activity of SUR1 and SUR2A that has been observed in structure-function studies of the C-terminal domain of SUR isoforms (de Wet et al. 2012).

In absence of high-resolution structure of the K-ATP channel, we used a model of SUR1 published by Bessadok et al. (Bessadok et al. 2011) to spatially locate the residues QIL of SUR1 (Figure 59). Residue Q1342 is predicted to stand in a loop just before a β-sheet of the NBD2, which includes I1347 and L1350. Interestingly, a novel interaction between the NBD2 proximal C-terminus of SUR2A and the cytoplasmic C-terminal domain of Kir6.2 was recently identified (Lodwick et al. 2014). According to their model, SUR2A-Glu1318 is located within the NBD2 domain, just few residues away from those identified by Dupuis et al. (2008). SUR2A-Glu1318 and Kir6.2-Lys338 form a salt bridge responsible for the transmission of allosteric changes to Kir6.2. According to Lodwick and colleagues model, residues Q1342, I1347 and L1350 of SUR1 (and the corresponding residues in SUR2A) could stand at the interface between SURs and Kir6.2 and thereby be part of a mechanism of allosteric regulation of the pore-forming subunit.

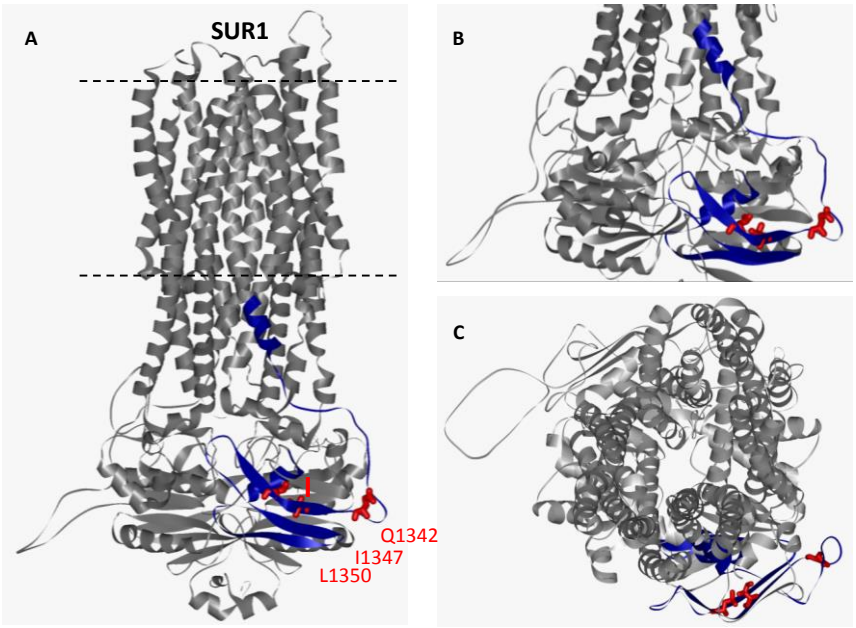

Figure 59. SUR1 homology model based on MDR1 (Bessadok et al., 2011). A, lateral view. The region identified by Rainbow et al. (2004) is highlighted in dark blue (SUR1S1M fragment). Residues Q1342, I1347 and L1350 are represented in ball-and-stick format and coloured in red. B, Close-up lateral view of the cytoplasmic domain. C, axial view from the extracellular side.

To confirm a differential coupling between SUR2A and SUR1-based channels a high-resolution structure of the two complexes is required.

This work has been published (Principalli et al. 'Kir6.2 activation by sulfonylurea receptors: a different mechanism of action for SUR1 and SUR2A subunits via the same residues', Physiological Reports, 2015).

12. Project 3: 'Role of a cluster of arginines in the N-terminal region of Kir6.2 in its regulation by natural and unnatural partners'

12.1 Relevance of the study

The identification of the domains of the Kir6.2 channel involved in the functional coupling with SUR cannot be easily achieved using a mutagenic strategy. SUR regulates Kir6.2 activity through ligand induced conformational changes, but also through the solely physical interaction that affects both gating and ATP sensitivity of the channel. Therefore, it is difficult to discriminate between mutated residues that have an impact on the transmission of conformational changes or on the physical interaction. Moreover, it is known that the region spanning from Kir6.2 N-terminal to its first helix is in tight physical association with SUR (Schwappach et al. 2000; Babenko and Bryan 2002). Mutations at this level could compromise both physical association and communications between SUR and Kir6, resulting in misinterpretation of the data. To overcome this problem we used the ICCR technology developed in the 'Channels' group.

Ion channel-coupled-receptors (ICCRs) are artificial biosensors created by physical and functional link of a GPCR C-terminus to the Kir6.2 N-terminus (Moreau et al. 2008). The ICCR provides a unique method to study the function of the Kir6.2 channel N-terminal, as the fusion between GPCR and channel ensures both physical and functional coupling between these two unnatural partners. Mutations affecting the gating can only influence the transmission of the conformational changes, as the covalent link between the two proteins is unaltered.

For this third project, we performed structure-function studies of the domain linking the GPCR to the ion channel. The project has a dual purpose: It will provide a deeper

understanding of the nature of the biosensors, improving their development, and it will help to understand the activation mechanism of Kir6.2 used by both GPCR and SUR.

12.2 Project background and experimental approach

The domain linking the GPCR to the Kir6.2 is crucial for ICCR function and its length and sequence affect channel regulation in terms of signal amplitude and sign (activation or inhibition).

This observation emerged during the development of the ICCR technique. The fusion of the GPCR required the optimisation of the linker region to obtain functional coupling. Experiments performed using both Muscarinic and Dopaminergic receptor-based ICCRs revealed the crucial role of deletions in the Kir6.2 N-terminus for efficient coupling and the importance of the GPCR C-terminus length for the sign of the channel regulation (article in preparation). While the linker length is clearly a functional parameter in the ICCR function, the peptidic sequence could also be critical. Truncation of nine residues in the M2 C-terminus (M2=K-9-25) or in the channel N-terminus (M2=K0-34) does not induce the same phenotype. In the first case, ACh induces inhibition of the channel and no response for the second case. These two ICCRs possess a linker of the same length but with a different sequence (Figure 61). Here we investigate the impact of the sequence of the linker in channel regulation.

The inactive ICCR (M2=K0-34) is characterized by the lack of residues 26 to 34 in the channel N-terminus that are substituted by their counterparts in the M2 sequence. This string in the Kir6.2 N-terminal contains five arginine residues out of nine amino acids.

Thus, the project focus is the investigation of the role of this arginine cluster.

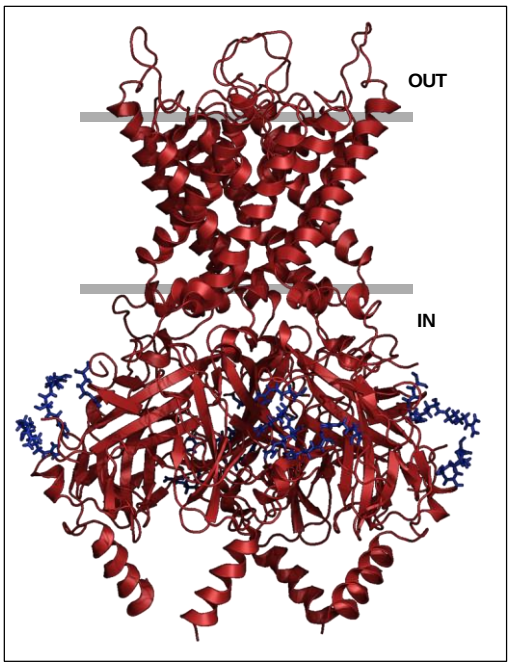

Figure 60. Kir6.2 model based on the structure of Kir3.2 with extended N- and C-termini (N. Sapay, L. Darre Castel). The arginine cluster in the N-terminal region is highlighted in blue and in stick format.

In order to understand if the differences between the inhibited M2=K-9-25 and the non-responsive M2=K0-34 are related to the arginines cluster, C. Moreau designed an approach in which arginines are progressively reintroduced in the non-regulated construct M2=K0-34 to try to restore the function.

A. C. Godet, K. Langer and A. Rongier realized the experiments for this first part of the project. Their results are shown in Figure 61.

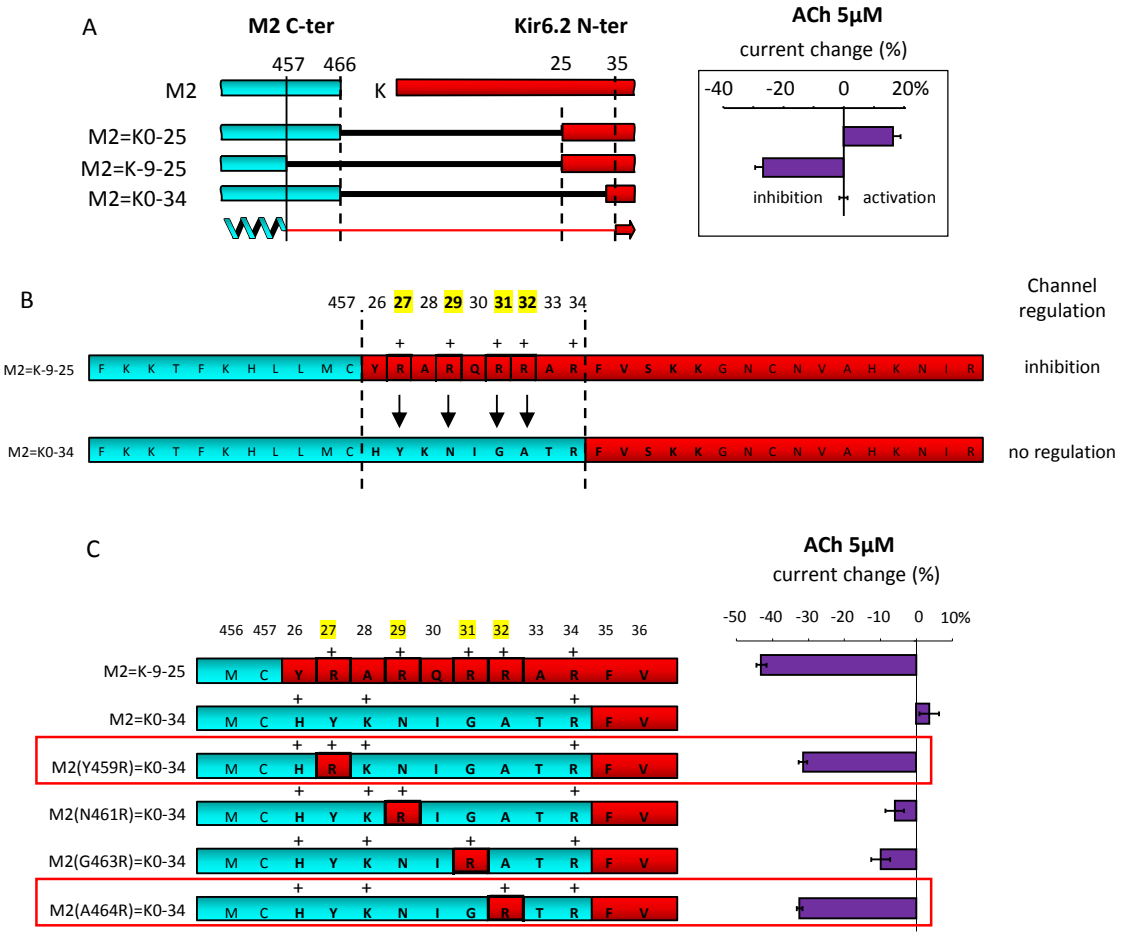

Figure 61. A, ICCR linker region illustrating the ligand (ACh 5 µM) response obtained per each construct after modification of the linker length. Responses were measured on oocytes in TEVC, holding the membrane potential at -50 mV with solutions prepared in TEVC bath. A minimum of seven recordings per each construct was used to calculate an average of current change (%). B, overlap between the linker region of the inhibited M2=K-9-25 and the non-responsive M2=K0-34. Residues Y459, N461, G463 and A464 in the M2=K0-34 are progressively substitute by the corresponding arginines in the M2=K-9-25 to try to restore inhibition. C, panel showing the ACh response of each M2=K0-34 mutant. Responses were measured on oocytes in TEVC, holding the membrane potential at -50 mV with solutions prepared in TEVC bath. A minimum of seven recordings per each construct was used to calculate an average of current change (%).

Substitution of Y459 or A464 with arginine 27 (Y459R) and 32 (A464R) respectively is sufficient to restore the channel regulation by ACh (inhibition). On the contrary, substitution with arginine 29 (N461R) or 31 (G461R) is not sufficient to recover the communication

between receptor and channel. Surprisingly, substitution with one between arginines 27 and 32 is sufficient to restore the inhibition.

Having identified two distinct arginines able to restore the ICCR function, the second part of the project aims at confirming their implication by the characterization of the M2=K-9-25 constructs in which the arginines are progressively substituted by the corresponding residues of the M2=K0-34 construct.

12.3 Results: Substitution of the arginines to confirm their role in ICCR function

To confirm that arginines in position 27 and 32 of the Kir6.2 N-terminus are not only sufficient but also essential for channel gating regulation by the fused GPCR, we created a series of mutants in which we progressively substituted the arginines from the functional M2=K-9-25. Indeed, these arginines were replaced by their counterparts of the M2=K0-34 (Figure 62).

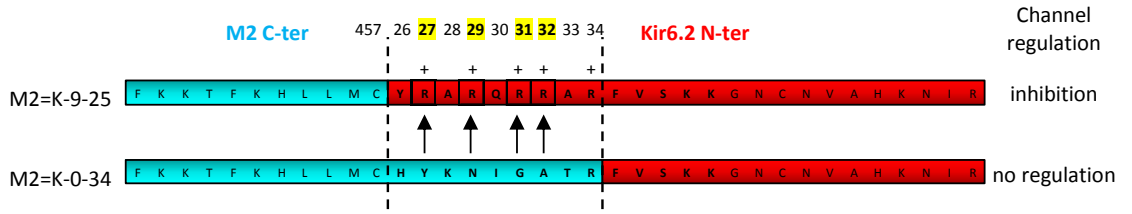

Figure 62. ICCR linker region. Arginines in the M2=K-9-25 are progressively substituted by the corresponding residues from the M2=K0-34 construct.

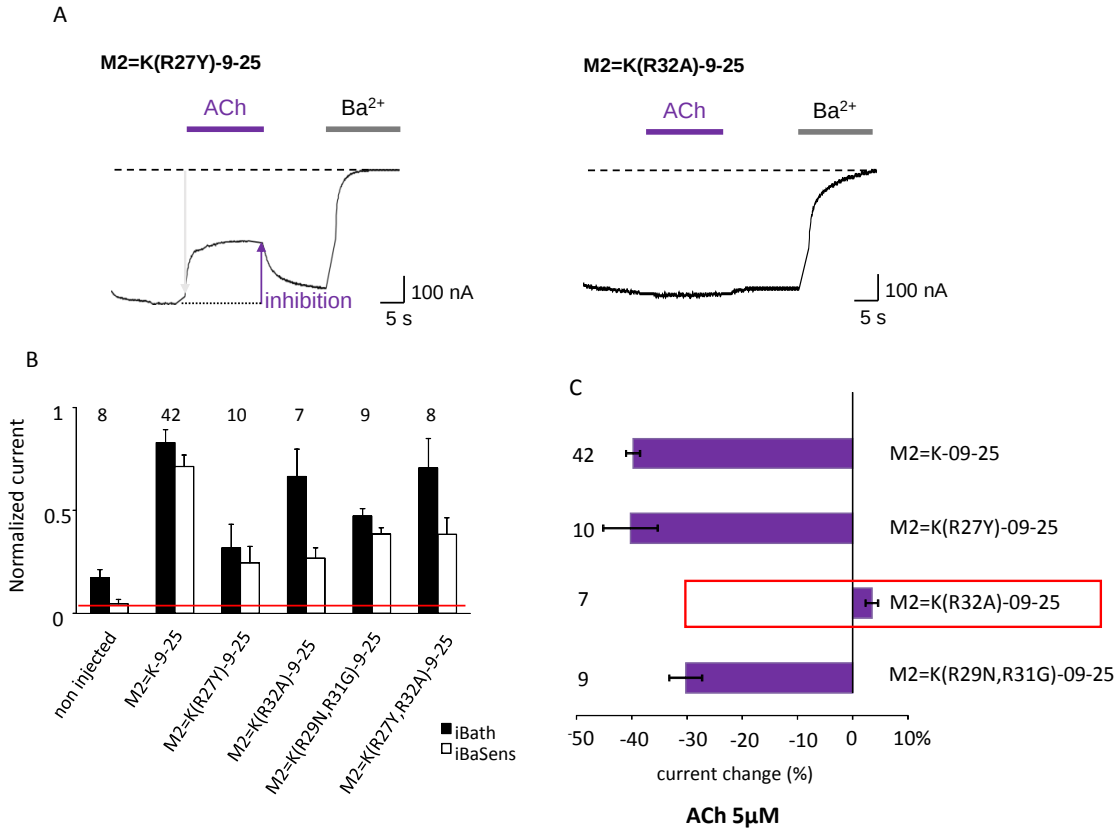

Figure 63. A, representative TEVC traces from Xenopus oocytes expressing M2=K(R27Y)-9-25 and M2=K(R32A)-9-25. Current amplitude was recorded at −50 mV. Dashed line indicates the Ba^{2+}-sensitive current baseline. Blue and grey bars represent the application of ACh and Ba^{2+} respectively. B, expression levels of non-injected oocytes (control), M2=K-9-25 and M2=K-9-25 mutants. Black bars represent the average current measured in TEVC bath while white bars represent the average Ba^{2+}-sensitive current. The red line indicates the Ba^{2+}-sensitive current level of non-injected oocytes. C, percent change in current induced by application of 5 µM ACh. The significative mutant M2=K(R32A)-9-25 is highlighted in the red box.

The R27 was previously identified as sufficient to restore ICCR function. Surprisingly, its substitution in the construct M2=K(R27Y)-9-25 does not affect the capacity of the channel to be regulated by ACh (Figure 63). This can be explained with the presence of the essential arginine at position 32.

In the case of the R32, replacement of the arginine with an alanine [M2=K(R32A)-9-25)] originates a non-responsive channel, despite the presence of the arginine at position 27. This result confirms the essential role of residue 32 in M2-Kir6.2 functional coupling but is in

contrast with the expected role of the arginine 27, thought to be sufficient to maintain the functional communication between M2 and Kir6.2.

As expected, substitution of R29 and R31 [M2=K(R29N,R31G)-9-25] does not alter ICCR function, confirming that these arginines are not essential for the regulation of Kir6.2 by the GPCR.

12.4 Role of arginine R32 in ICCR function

Why is arginine 32 sufficient and necessary for Kir6.2 gating regulation by the GPCR? To understand its role, our collaborators Nicolas Sapay and Leonardo Darre-Castell have built a model of Kir6.2 that we used to locate possible acidic residues interacting with R32. The model (reported in Figure 60 and Figure 64), in which N-terminus and C-terminus have been extended as they are missing in the crystal structure of Kir3.2, suggested that the arginine 32 could interact with negatively charged residues located in the C-terminus of the same chain (D307 and/or E308). While a small β-sheet connecting the N- and C-terminal domains has been observed in crystal structures, the lack of resolution of the surrounding regions in the N-terminal domain suggest an incomplete view of the real N-ter/C-ter interface.

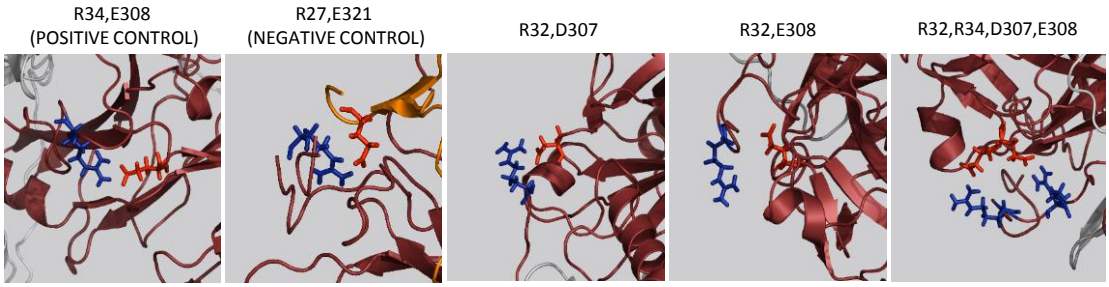

Figure 64. Predicted interactions between arginines in the N-terminus and negatively charged residues in the C-terminus of the same subunit (dark red) or of a neighbour chain (orange). Residues involved in the interaction are shown in sticks. Arginines are shown in blue, negatively charged residues in brilliant red.

The interaction between R34 and E308 is observed in the crystal structure of Kir3.2 and both residues are highly conserved among the members of the Kir family. Therefore, we use them as positive control in our approach to identify arginines/acidic residues pairs. In our strategy to identify the negatively charged residues possibly interacting with the R32, N-terminal residues R32 and R34 were first mutated into aspartate and glutamate respectively.

Successively, C-terminal candidates D307 and E308 were mutated into arginine. The predicted negatively charged partners are mutated into arginines to invert their charge and create a repulsion that should abolish the ICCR function if the interaction with the N-terminal region is critical. Thus, mutants of the negatively charged residues that will no longer respond to ACh have high probability to be involved in an interaction with critical arginines.

To confirm their implication, the interaction will be confirmed using a 'swapping charge' method: the arginines in the N-terminus are mutated in glutamate or aspartate while the negative residues in the C-terminus are mutated into arginines. Theoretically, the double mutants able to restore the ionic bond should restore the inhibition as well.

The arginine R27, which appeared non-essential for Kir6.2 regulation, is predicted to interact with E321 (a residue in the C-terminal domain of a neighbour chain), according to our model. We therefore used this interaction as a negative control as it is not essential for the ICCR function (Figure 64).

This part of the project has been experimentally realized together with Laura Lemel, master student under my technical supervision from January to June 2015.

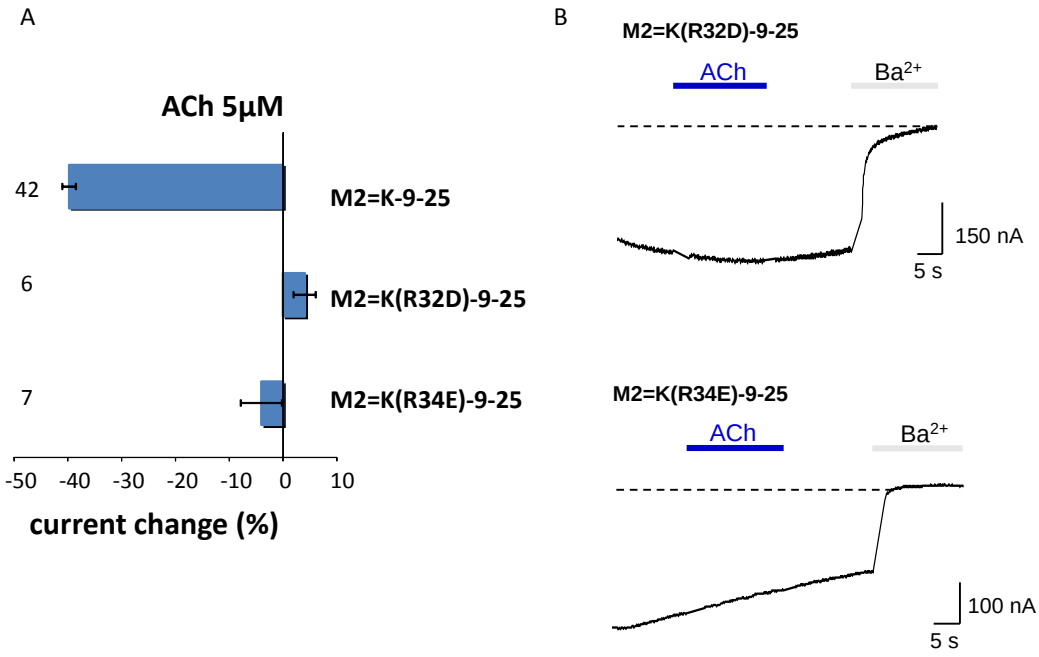

Figure 65. A, percent change in current induced by application of 5 µM ACh of M2=K-9-25 and M2=K-9-25 mutants. Responses were measured in TEVC. B, representative TEVC traces from Xenopus oocytes expressing M2=K(R32D)-9-25 and M2=K(R34E)-9-25. Current amplitude was recorded at −50 mV. Dashed line indicates the Ba^{2+}-sensitive current baseline. Blue and grey bars represent the application of ACh and Ba^{2+} respectively.

As expected, mutation of residues R32 and R34 in D and E respectively, results in non-responsive channels (Figure 65), confirming their essential role in the ICCR function. Interestingly, using this strategy we were able to test the role of the arginine at position 34, as with the previous approach this residue was conserved between constructs M2=K-9-25 and M2=K0-34. However, this arginine alone is not sufficient for channel gating regulation as despite its presence, the M2=K0-34 does not respond to ACh. Consequently R34 is necessary but not sufficient for ICCR function.

Subsequently, we mutated negatively charged residues in the C-terminal region into arginines (Figure 66).

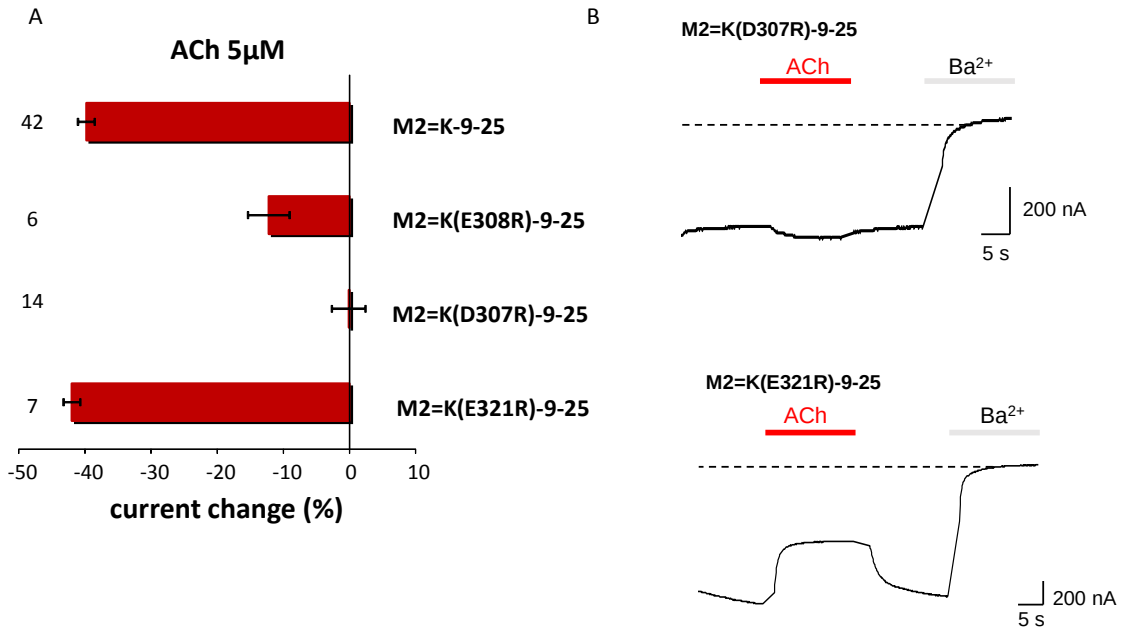

Figure 66. A, change in current in % induced by application of 5 µM ACh of M2=K-9-25 and M2=K-9-25 mutants. Responses were measured in TEVC. B, representative TEVC traces from Xenopus oocytes expressing M2=K(D307R)-9-25 and M2=K(E321R)-9-25. Current amplitude was recorded at −50 mV. Dashed line indicates the Ba^{2+}-sensitive current baseline. Blue and grey bars represent the application of ACh and Ba^{2+} respectively.

C-terminal residues D307, E308 and E321, predicted to interact with R32, R34 and R27 respectively, were mutated in arginines to invert their charge. Figure 65Figure 66 reveals loss of ACh-induced inhibition for D307R and E308R while E321R is still functional. These results indicate that D307 and E308 are involved in ICCR function, while E321 is not. This last result confirm the non-essential role of the arginine R27, predicted to interact with E321.

Subsequently, we tested the double mutations to try to restore the inhibition and confirm the pairs. Negatively charged C-terminal residues are swapped with the positively charged N-terminal arginines and reciprocally, the arginines are mutated in negatively charged residues (D or E).

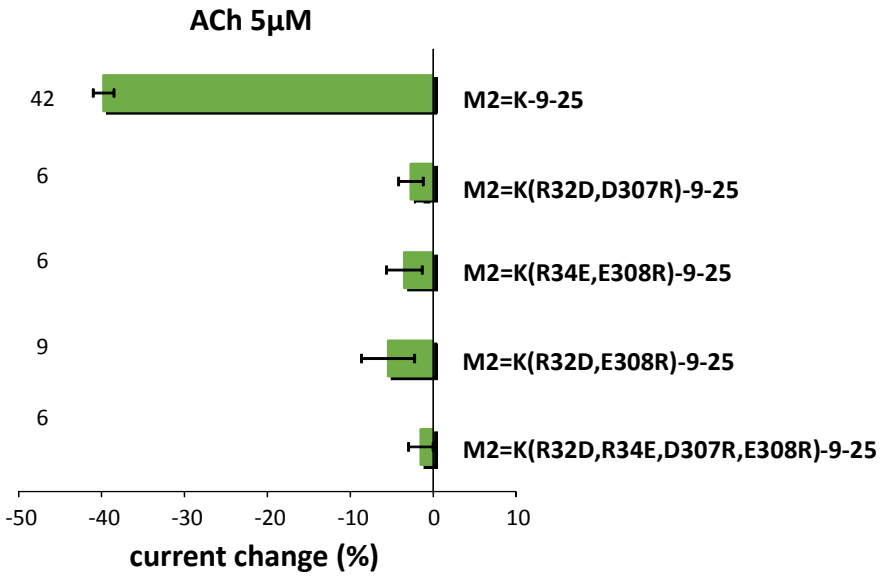

Figure 67. Change in current in % induced by application of 5 µM ACh on wild type and mutated M2=K-9-25. Current amplitude was recorded at −50 mV in TEVC.

The pairs R32-D307, R34-E308 (positive control) and R32-E308 were tested. This last one has been chosen to test the two possibilities as D307 and E308 are in close proximity in the model. Statistics in Figure 67 show non-significant effect on constructs M2=K(R32D,D307R)-9-25 and M2=K(R32D,E308R)-9-25 when ACh is applied. Neither, the positive control pair M2=K(R34E,E308R)-9-25, present in the crystal structure of Kir3.2, is able to respond to ACh, suggesting that either the approach does not suite to this channel or the crystal structure shows an erroneous interaction due to crystal packing. Postulating that the first hypothesis has a higher rate of probability, we envisioned a more complex network of charges, involving all critical and spatially closed residues (R32, R34, D307 and E308). Therefore, we designed the construct M2=K(R32D,R34E,D307R,E308R)-9-25 to test the possibility that a double substitution could help reactivate channel regulation. However, this channel does not respond to ACh suggesting that the network is more complex, or that the strategy is not adapted to this ion channel, or that the crystal structure is inaccurate to display the real interaction between N-ter and C-ter domains of Kir6.2.

12.5 Results: role of the Kir6.2 N-terminal arginines in the natural K-ATP channel

The arginines critical for Kir6.2 gating regulation by GPCR, pinpointed using the ICCR technology, were identified in the Kir6.2 N-terminal domain and not in the GPCR C-terminal domain. In K-ATP channels, Kir6.2 N-terminal physically and functionally interacts with the SUR subunit, especially for the action of the sulfonylurea glibenclamide. Therefore, it is tempting to assume that the arginines identified as critical for Kir6.2 gating in ICCR could also have a role in the regulation of Kir6.2 in K-ATP channels. To investigate this hypothesis in the context of the K-ATP channel, we mutated Kir6.2 at positions R27 and R32. The corresponding RNA was co-injected with SUR1 or SUR2A RNA in *Xenopus* oocytes. The resulting K-ATP complexes were characterized by the patch-clamp technique in the excised inside-out configuration to test the regulation of this mutated Kir6.2 by SUR. Several SUR ligands were tested as the role of Kir6.2 N-terminus in their action is not well known and could be different for different classes of ligands (physiological or pharmaceutical, openers or blockers).

12.5.1 Response to the physiological opener MgADP

As shown in Figure 68, the tested mutations did not affect ADP response mediated by SUR1 or by SUR2A, as responses are comparable with those of the wild type K-ATP. Residues R27 and R32 appear not involved in the activation pathway that links ADP binding to SUR to Kir6.2 opening.

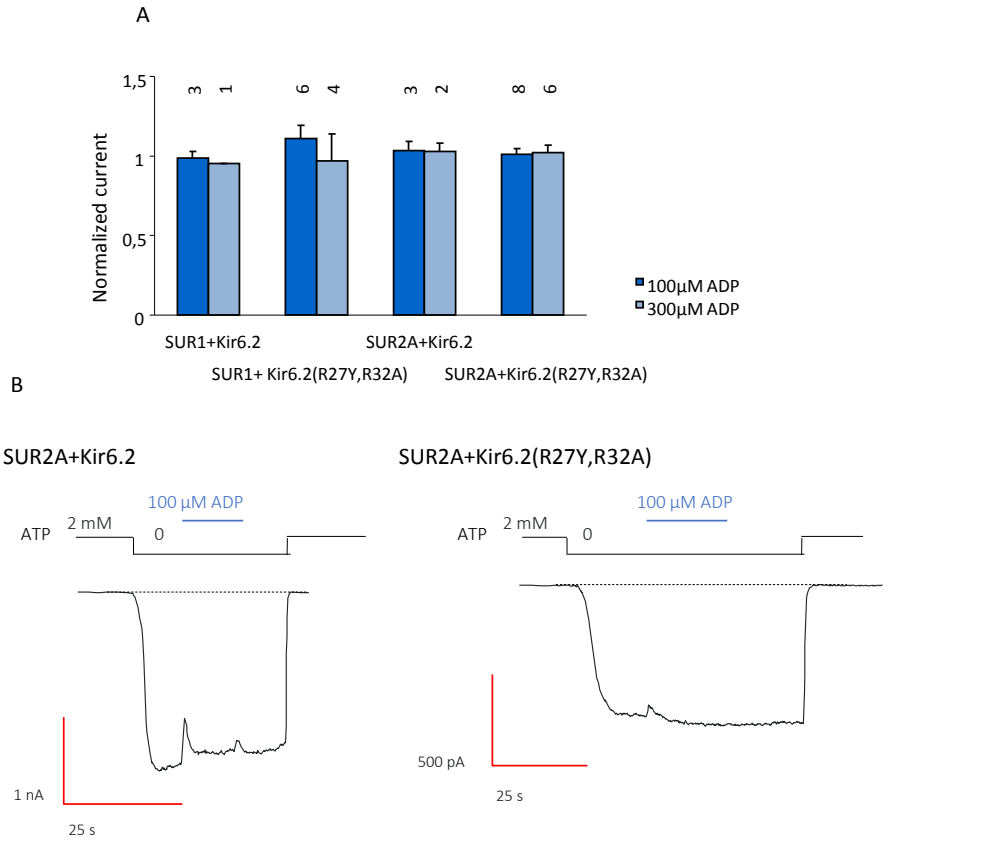

Figure 68. A, response to 100 µM and 300 µM MgADP of SUR1 and SUR2A co-injected with Kir6.2 wild type and mutants. Responses were measured in inside-out patches excised from oocytes. Currents were normalized to the current measured in absence of nucleotides immediately before MgADP application. Numbers indicate the number of patches included in each average. B, representative patch clamp traces obtained from oocytes expressing wild type and mutated channels. Traces were recorded clamping the voltage at -50 mV.

12.5.2 Response to pharmacological openers

Mutant channels were also tested for the response to pharmacological openers, specific for SUR1- (Diazoxide, Figure 69) and for SUR2A-based channels (P1075, Figure 70). As observed for the ADP, there are no evident changes between mutants and wild type channels responses, suggesting that R27 and R32 are not critical for the action of pharmaceutical openers on K-ATP channels.

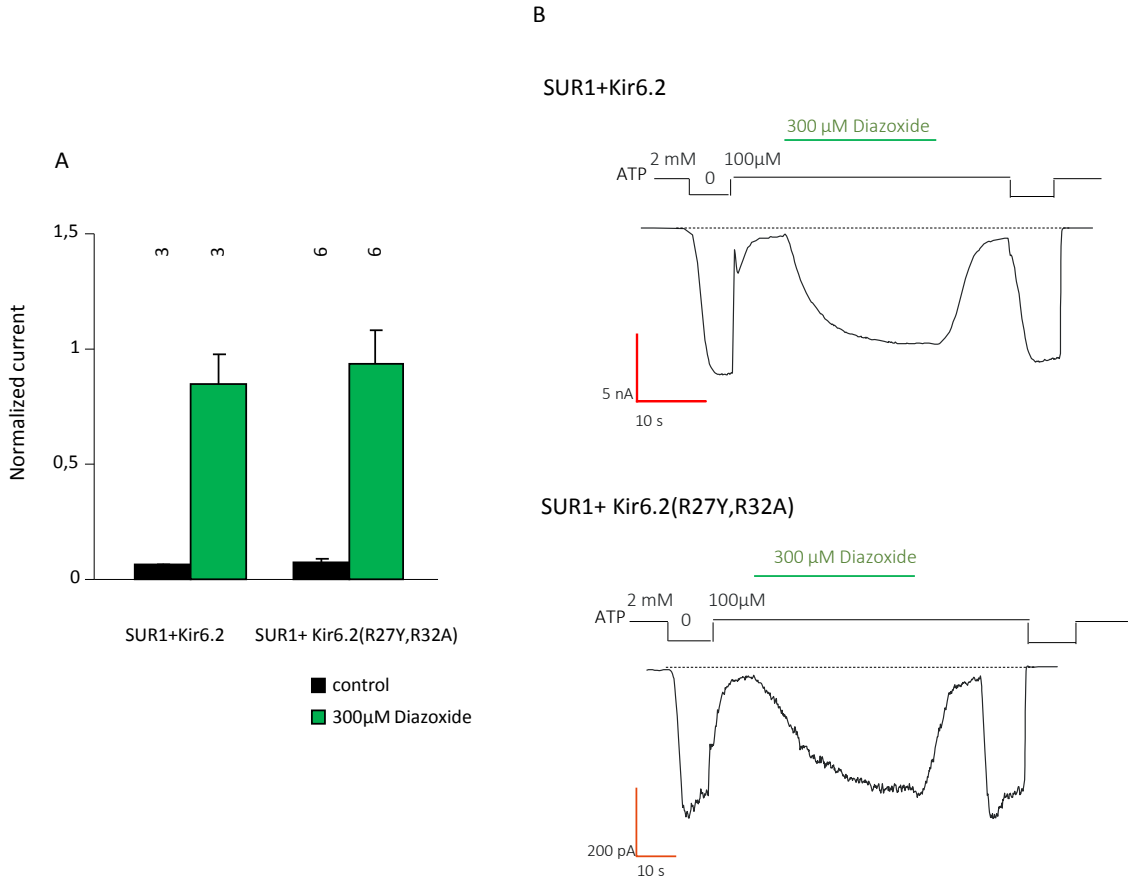

Figure 69. A, Diazoxide responses of wild type and mutated K-ATP channels. Responses were measured in inside-out patches excised from oocytes co-expressing SUR1 and Kir6.2 wild type or mutant. Diazoxide (300 µM) was applied in the presence of 100 µM ATP, and currents were normalized to the current measured in the absence of nucleotides immediately before opener application. Application of 100 µM ATP alone (black bars) was used as a control. Numbers indicate the number of patches included in each average. B, representative patch clamp traces obtained from oocytes expressing wild type and mutated channels. Traces were recorded clamping the voltage at -50 mV.

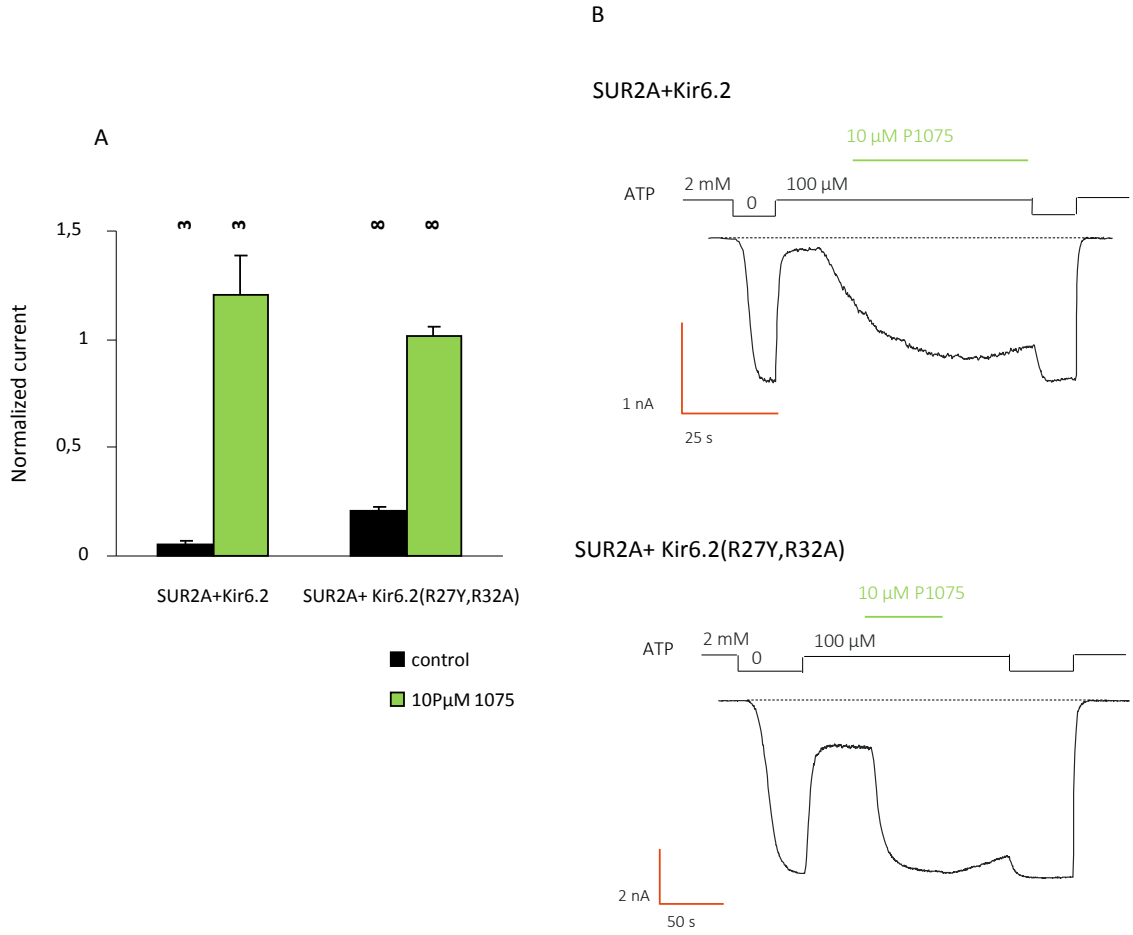

Figure 70. P1075 responses of wild type and mutated K-ATP channels. Responses were measured in inside-out patches excised from oocytes co-expressing SUR2A and Kir6.2 wild type or mutant. P1075 (10 µM) was applied in the presence of 100 µM ATP, and currents were normalized to the current measured in the absence of nucleotides immediately before opener application. Application of 100 µM ATP alone (black bars) was used as a control. Numbers indicate the number of patches included in each average.

12.5.3 Response to the K-ATP channel blocker Glibenclamide

It is generally accepted that in the K-ATP channel there are at least two different pathways using two different interfaces between SUR and Kir6.2 for the regulation of the gating: an 'activator' pathway used by openers and an 'inhibitory' pathway used by blockers. In order to assess if mutations at position 27 and 32 affect the ability of the blocker to close channel gate, we performed patch-clamp experiment using the blocker Glibenclamide.

Figure 71 reports no change in the response of mutated and wild type K-ATP channels, suggesting that the inhibitory pathway remains intact in mutated Kir6.2 channels.

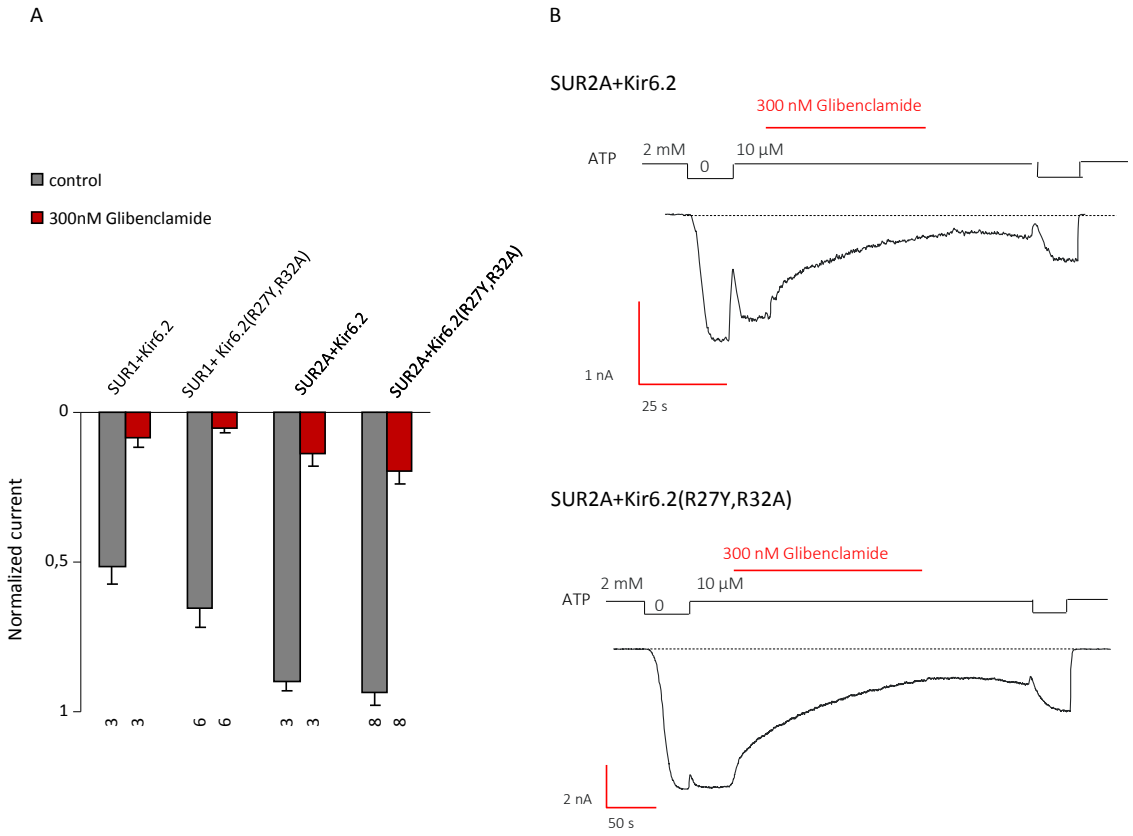

Figure 71. A, Glibenclamide responses of wild type and mutated K-ATP channels. Responses were measured in inside-out patches excised from oocytes co-expressing SUR1or SUR2A and Kir6.2 wild type or mutant. Glibenclamide (300 nM) was applied in the presence of 10 µM ATP, and currents were normalized to the current measured in 10 µM ATP before blocker application. Application of 10 µM ATP alone (gray bars) was used as a control. Numbers indicate the number of patches included in each average. B, representative patch clamp recordings obtained in the excised inside-out configuration. Voltage was clamped at -50 mV.

12.5.4 Whole-cell experiments with TEVC

As differences in ligand sensitivity are observed between excised and whole-cell conditions, openers and glibenclamide were also tested using TEVC technique, to confirm in intact cells the results obtained in the 'excised' configuration used in patch clamp experiments. Results are reported below (Figure 72).

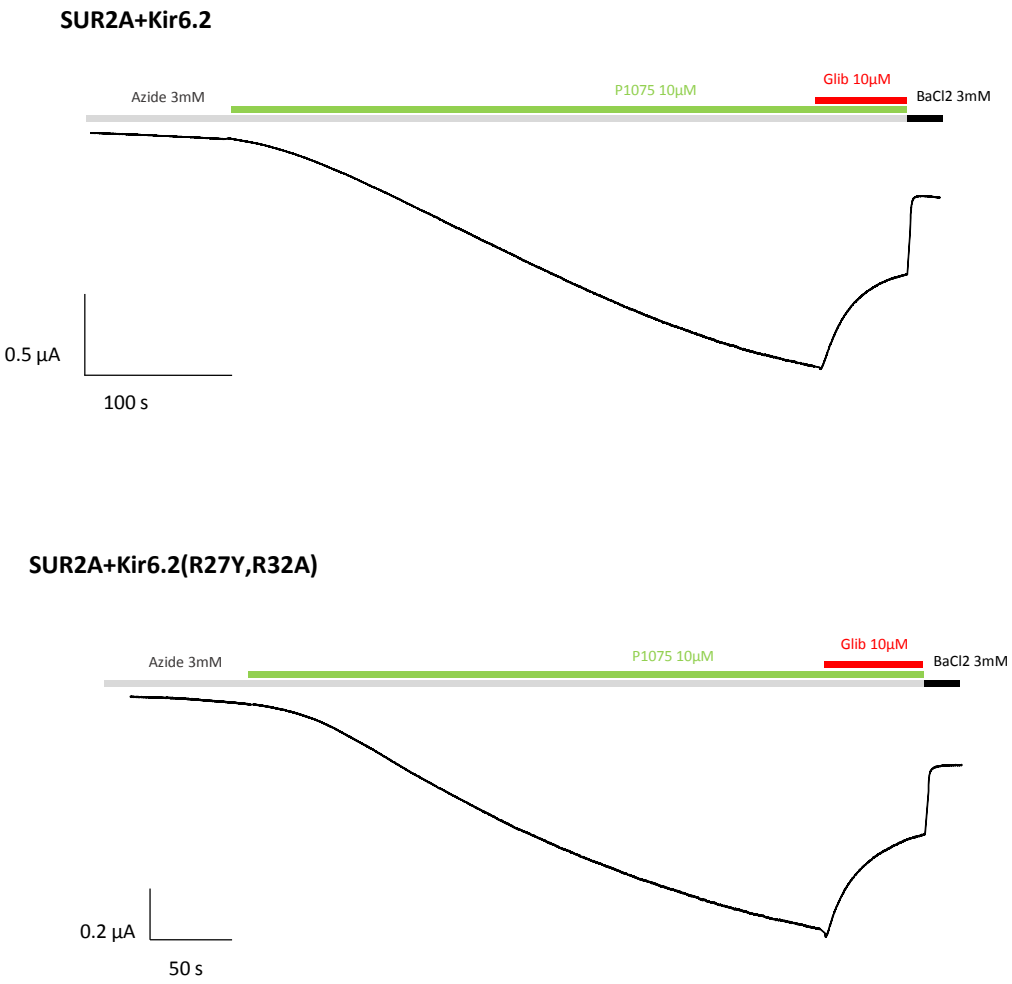

Figure 72. TEVC representative traces of wild type and mutant K-ATP channels. Recordings were obtained at -50 mV. Azide (inhibitor of the respiratory chain used to decrease the intracellular level of ATP) (3 mM) was applied at the beginning of the protocol to reduce the intracellular concentration of ATP and favour channel opening. Azide was maintained in both opener and blocker solutions as control. Glibenclamide 10 µM was applied in presence of the opener P1075 to measure the amplitude of the blocking. Ba^{2+} was used to define the Ba^{2+}-sensitive current (potassium channel current).

Representative traces in Figure 72 show no evident differences between wild type and mutated K-ATP channels. These results confirm what has been observed in patch clamp: Both activation and inhibition pathways seems unaffected by mutation of arginines R27 and R32.

12.6 Discussion and perspectives

12.6.1 ICCR regulation

The arginine cluster present in Kir6.2 N-terminus has been functionally mapped by using the ICCR technology. This approach provided insights in the functional role of the Kir6.2 N-terminal that could not be discovered otherwise. In particular, the regulation of the channel gating proceeds from the GPCR through the arginine 32 present at the fusion point. The R32 represent an essential hub for the communication between the two partners.

Arginine in position **32** has been confirmed as essential and sufficient to both abolish (in the M2=K(R32A)-9-25) or restore (in the M2(A464R)=K0-34) the communication between GPCR and channel. This residue is highly conserved among Kir channels and interestingly is replaced in the Kir6.1 by a lysine, so that a positive charge is maintained (Figure 73).

The results obtained for the arginine in position **27** suggested initially a primary role in the function of ICCR in the construct M2(Y459R)=K0-34 which was not confirmed later in M2=K(R27Y)-9-25. In the case of the M2=K0-34 mutant, by restoring the arginine in position 27 we were able to restore channel inhibition by ACh as well. To confirm the result we successively substitute this arginine with a tyrosine in the M2=K(R27Y)-9-25 but we did not abolish the regulation. This result could mean that in this last case the arginine at this position is less critical compared to R32. This behaviour can be explained by comparing the sequence of the two linkers. As shown in Figure 61, the linker of the M2=K0-34 presents other positive charges that surround the residue in position 27, a histidine and a lysine. The insertion of another positive charge between these two could be sufficient to restore the regulation. In the M2=K-9-25 these surrounding charges are missing but the R32 is present so that even if the arginine 27 is missing the positive charge provided by R32 is enough to maintain the regulation.

The arginine at position **34** could not be studied using the same approach as the arginine is conserved in both M2=K0-34 and M2=K-9-25. Nevertheless, we had the opportunity to

assess the importance of this arginine while searching for its partner in the C-terminal region of the channel. When this residue was exchanged with a negatively charged aminoacid, the regulation by ACh was lost, highlighting the importance of a positive charge at this position. In the alignment, this residue is conserved in all Kir channels with no exception, confirming its importance. However, its presence in the M2=K0-34 it is not sufficient to preserve the communication between GPCR and channel. These results suggest that the fares we move along the linker region, the closest we get to a predicted network of interaction between N- and C-termini. Charges reversion of both R32 and R34 is probably responsible for disruption of this network.

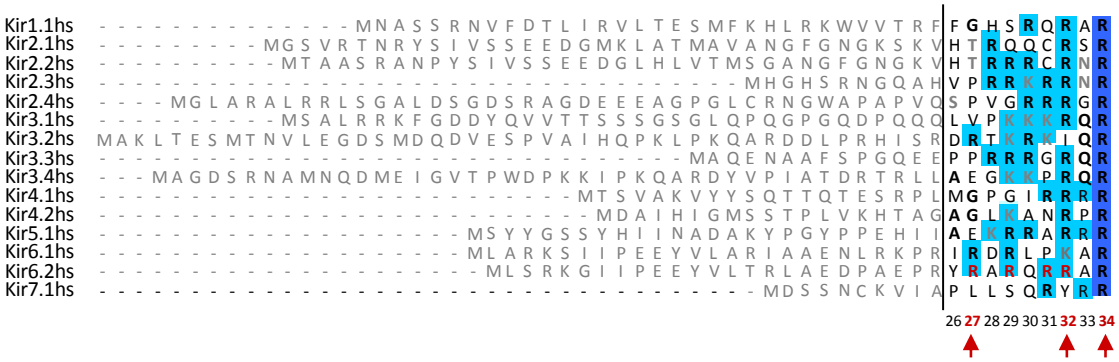

Figure 73. Alignment of Kir channel family members. Arginine residues are highlighted black in boxes in shades of blue depending on the degree of conservation. Other positive residues are reported in dark grey and in blue boxes.

12.6.2 Finding arginine partners in Kir6.2 C-terminal

The results showed in Figure 65 underline the importance of residues D307 and E308 in the gating modulation of Kir6.2 in ICCRs, as mutation of these residues result in loss of regulation. Unfortunately, the 'swapping charge' approach, which consisted in inverting the charge between N- and C-termini, did not work as expected. While this approach has been successful with some other ion channels (Ng et al. 2014), it was not the best in the case of Kir6.2 as the interaction of charged residues could be more complex than expected in the region of interest. Moreover, these amino acids are part of the same chain as residues R32 and R34, but in the 3D model of the complex, the N-terminus could also interact with the C-terminus of a neighbour chain. Investigation of possible partners in the neighbour chain could provide new insights in the interaction network. Residue **E321**, located in the C-terminus of a neighbour chain, was used to confirm the non-essential role of residue R27.

Indeed, this mutant retains the regulation mechanism, meaning that it is probably located outside of the network of interaction within the essential arginine R32. The next step of the project will be to focus the attention on possible partners in the C-terminal of the other chain, always using the model as starting point.

In a second scenario, the approach used could have failed because of the possible interaction between the arginines and a negatively charged lipid, PIP_2. This phospholipid is essential to stabilize Kir6.2 open state (Fan and Makielski 1997). Crystal structures of Kir channels show that arginines of the channel N-terminal could interact with the phosphate groups of the lipid. On the other hands, molecular dynamic studies of the Kir6.2 realized by our collaborators show that these lipids are located too far from the critical arginines to be able to interact with them (unpublished data), emphasizing the hypothesis of an interactions within the C-terminal domain of the channel rather than with PIP_2.

12.6.3 Impact of mutation R27Y and R32A on K-ATP channel regulation

Important arginines, identified in the primary screening using M2=K0-34 constructs, were also tested for their role in the communication between Kir6.2 and SUR.

Data in figures do not show any significant variation between wild type and mutated channels, suggesting that arginines 27 and 32 are not involved in the communication that proceeds from SUR ligand binding sites to Kir6.2 gates. This result shows a discrepancy between what we see using the ICCR and what we observe in the K-ATP channel. In the original hypothesis, we thought that the SUR, like the GPCR, would have acted on Kir6.2 activation through the same region. These unexpected findings bring new light on an interesting hypothesis, which consider the possibility that there are at least two different ways to modulate channel opening. One way is through what has been found thanks to the ICCR, by acting on a cluster of positive charges in the Kir6.2 N-terminal, and the other, used by the SUR, still unknown.

As a matter of fact, we are comparing two different systems. The K-ATP channel is a natural protein in which SUR and Kir6.2 are separately expressed and spontaneously interact, certainly through several interfaces in both the lipid bilayer and the cytoplasmic domains. The ICCR is an artificial protein that we engineered to obtain a fusion between a receptor and a channel, probably interacting through a minimal interface. Interestingly, we identified critical residues for the ICCR function progressing in the understanding of the molecular

mechanism of ICCR which is required to elaborate a general protocol of GPCR-Kir6.2 functional coupling.

The atomic structure of the proteins would greatly facilitate the deciphering of the mechanisms involved in the natural and the artificial channels.

BIBLIOGRAPHY

Aguilar-Bryan, L., and J. Bryan. 1999. "Molecular Biology of Adenosine Triphosphate-Sensitive Potassium Channels." *Endocrine Reviews* 20 (2): 101–35. doi:10.1210/edrv.20.2.0361.

Aguilar-Bryan, L., C. G. Nichols, S. W. Wechsler, J. P. Clement, A. E. Boyd, G. González, H. Herrera-Sosa, K. Nguy, J. Bryan, and D. A. Nelson. 1995. "Cloning of the Beta Cell High-Affinity Sulfonylurea Receptor: A Regulator of Insulin Secretion." *Science (New York, N.Y.)* 268 (5209): 423–26.

Aller, Stephen G., Jodie Yu, Andrew Ward, Yue Weng, Srinivas Chittaboina, Rupeng Zhuo, Patina M. Harrell, et al. 2009. "Structure of P-Glycoprotein Reveals a Molecular Basis for Poly-Specific Drug Binding." *Science (New York, N.Y.)* 323 (5922): 1718–22. doi:10.1126/science.1168750.

Antcliff, Jennifer F, Shozeb Haider, Peter Proks, Mark S P Sansom, and Frances M Ashcroft. 2005. "Functional Analysis of a Structural Model of the ATP-Binding Site of the KATP Channel Kir6.2 Subunit." *The EMBO Journal* 24 (2): 229–39. doi:10.1038/sj.emboj.7600487.

Apponyi, Margit A., Kiyoshi Ozawa, Nicholas E. Dixon, and Gottfried Otting. 2008. "Cell-Free Protein Synthesis for Analysis by NMR Spectroscopy." *Methods in Molecular Biology (Clifton, N.J.)* 426: 257–68. doi:10.1007/978-1-60327-058-8_16.

Ashcroft, F. M., and F. M. Gribble. 1999. "ATP-Sensitive K+ Channels and Insulin Secretion: Their Role in Health and Disease." *Diabetologia* 42 (8): 903–19. doi:10.1007/s001250051247.

Ashcroft, F. M., D. E. Harrison, and S. J. Ashcroft. 1984. "Glucose Induces Closure of Single Potassium Channels in Isolated Rat Pancreatic Beta-Cells." *Nature* 312 (5993): 446–48.

Ashcroft, Frances M. 2005. "ATP-Sensitive Potassium Channelopathies: Focus on Insulin Secretion." *Journal of Clinical Investigation* 115 (8): 2047–58. doi:10.1172/JCI25495.

Ashfield, R., F. M. Gribble, S. J. Ashcroft, and F. M. Ashcroft. 1999. "Identification of the High-Affinity Tolbutamide Site on the SUR1 Subunit of the K(ATP) Channel." *Diabetes* 48 (6): 1341–47.

Babenko, Andrey P., and Joseph Bryan. 2002. "SUR-Dependent Modulation of KATP Channels by an N-Terminal KIR6.2 Peptide DEFINING INTERSUBUNIT GATING INTERACTIONS." *Journal of Biological Chemistry* 277 (46): 43997–4. doi:10.1074/jbc.M208085200.

———. 2003. "SUR Domains That Associate with and Gate KATP Pores Define a Novel Gatekeeper." *Journal of Biological Chemistry* 278 (43): 41577–80. doi:10.1074/jbc.C300363200.

Babenko, A. P., G. Gonzalez, and J. Bryan. 2000. "Pharmaco-Topology of Sulfonylurea Receptors. Separate Domains of the Regulatory Subunits of K(ATP) Channel Isoforms Are Required for Selective Interaction with K(+) Channel Openers." *The Journal of Biological Chemistry* 275 (2): 717–20.

Bakos, Éva, Raymond Evers, Gergely Szakács, Gábor E. Tusnády, Ervin Welker, Katalin Szabó, Marcel de Haas, et al. 1998. "Functional Multidrug Resistance Protein (MRP1) Lacking the N-Terminal Transmembrane Domain." *Journal of Biological Chemistry* 273 (48): 32167–75. doi:10.1074/jbc.273.48.32167.

Bancila, Victor, Thierry Cens, Dominique Monnier, Frédéric Chanson, Cécile Faure, Yves Dunant, and Alain Bloc. 2005. "Two SUR1-Specific Histidine Residues Mandatory

for Zinc-Induced Activation of the Rat KATP Channel." *The Journal of Biological Chemistry* 280 (10): 8793–99. doi:10.1074/jbc.M413426200.

Baumgartner, W., L. Islas, and F. J. Sigworth. 1999. "Two-Microelectrode Voltage Clamp of Xenopus Oocytes: Voltage Errors and Compensation for Local Current Flow." *Biophysical Journal* 77 (4): 1980–91. doi:10.1016/S0006-3495(99)77039-6.

Beek, Josy ter, Albert Guskov, and Dirk Jan Slotboom. 2014. "Structural Diversity of ABC Transporters." *The Journal of General Physiology* 143 (4): 419–35. doi:10.1085/jgp.201411164.

Bessadok, Anis, Elisabeth Garcia, Hélène Jacquet, Solenne Martin, Alexia Garrigues, Nicolas Loiseau, François André, Stéphane Orlowski, and Michel Vivaudou. 2011. "Recognition of Sulfonylurea Receptor (ABCC8/9) Ligands by the Multidrug Resistance Transporter P-Glycoprotein (ABCB1)." *The Journal of Biological Chemistry* 286 (5): 3552–69. doi:10.1074/jbc.M110.155200.

Bichet, Delphine, Friederike A. Haass, and Lily Yeh Jan. 2003. "Merging Functional Studies with Structures of Inward-Rectifier K(+) Channels." *Nature Reviews. Neuroscience* 4 (12): 957–67. doi:10.1038/nrn1244.

Bienengraeber, Martin, Alexey E. Alekseev, M. Roselle Abraham, Antonio J. Carrasco, Christophe Moreau, Michel Vivaudou, Petras P. Dzeja, and Andre Terzic. 2000. "ATPase Activity of the Sulfonylurea Receptor: A Catalytic Function for the KATP Channel Complex." *The FASEB Journal* 14 (13): 1943–52. doi:10.1096/fj.00-0027com.

Caro, Lydia N., Christophe J. Moreau, Argel Estrada-Mondragón, Oliver P. Ernst, and Michel Vivaudou. 2012. "Engineering of an Artificial Light-Modulated Potassium Channel." *PloS One* 7 (8): e43766. doi:10.1371/journal.pone.0043766.

Caro, Lydia N., Christophe J. Moreau, Jean Revilloud, and Michel Vivaudou. 2011. "β2-Adrenergic Ion-Channel Coupled Receptors as Conformational Motion Detectors." *PloS One* 6 (3): e18226. doi:10.1371/journal.pone.0018226.

Chan, Kim W., Hailin Zhang, and Diomedes E. Logothetis. 2003. "N-Terminal Transmembrane Domain of the SUR Controls Trafficking and Gating of Kir6 Channel Subunits." *The EMBO Journal* 22 (15): 3833–43. doi:10.1093/emboj/cdg376.

Choudhury, Hassanul G., Zhen Tong, Indran Mathavan, Yanyan Li, So Iwata, Séverine Zirah, Sylvie Rebuffat, Hendrik W. van Veen, and Konstantinos Beis. 2014. "Structure of an Antibacterial Peptide ATP-Binding Cassette Transporter in a Novel Outward Occluded State." *Proceedings of the National Academy of Sciences of the United States of America* 111 (25): 9145–50. doi:10.1073/pnas.1320506111.

Clement IV, John P., Kumud Kunjilwar, Gabriela Gonzalez, Mathias Schwanstecher, Uwe Panten, Lydia Aguilar-Bryan, and Joseph Bryan. 1997. "Association and Stoichiometry of KATP Channel Subunits." *Neuron* 18 (5): 827–38. doi:10.1016/S0896-6273(00)80321-9.

Cole, Susan P. C. 2014. "Multidrug Resistance Protein 1 (MRP1, ABCC1), a 'Multitasking' ATP-Binding Cassette (ABC) Transporter." *Journal of Biological Chemistry* 289 (45): 30880–88. doi:10.1074/jbc.R114.609248.

Craig, Tim J., Kenju Shimomura, Reinhard W. Holl, Sarah E. Flanagan, Sian Ellard, and Frances M. Ashcroft. 2009. "An in-Frame Deletion in Kir6.2 (KCNJ11) Causing Neonatal Diabetes Reveals a Site of Interaction between Kir6.2 and SUR1." *The*

Journal of Clinical Endocrinology and Metabolism 94 (7): 2551–57. doi:10.1210/jc.2009-0159.

Dabrowski, Michael, Andrei Tarasov, and Frances M Ashcroft. 2004. "Mapping the Architecture of the ATP-Binding Site of the KATP Channel Subunit Kir6.2." *The Journal of Physiology* 557 (Pt 2): 347–54. doi:10.1113/jphysiol.2003.059105.

D'Avanzo, Nazzareno, Wayland W.L. Cheng, Xiaobing Xia, Liang Dong, Pavel Savitsky, Colin G. Nichols, and Declan A. Doyle. 2010. "Expression and Purification of Recombinant Human Inward Rectifier K+ (KCNJ) Channels in Saccharomyces Cerevisiae." *Protein Expression and Purification* 71 (1): 115–21. doi:10.1016/j.pep.2010.01.010.

Dawson, Roger J. P., and Kaspar P. Locher. 2006. "Structure of a Bacterial Multidrug ABC Transporter." *Nature* 443 (7108): 180–85. doi:10.1038/nature05155.

De Wet, Heidi, Kenju Shimomura, Jussi Aittoniemi, Nawaz Ahmad, Mathilde Lafond, Mark SP Sansom, and Frances M Ashcroft. 2012. "A Universally Conserved Residue in the SUR1 Subunit of the KATP Channel Is Essential for Translating Nucleotide Binding at SUR1 into Channel Opening." *The Journal of Physiology* 590 (Pt 20): 5025–36. doi:10.1113/jphysiol.2012.236075.

D'hahan, N., C. Moreau, A. L. Prost, H. Jacquet, A. E. Alekseev, A. Terzic, and M. Vivaudou. 1999. "Pharmacological Plasticity of Cardiac ATP-Sensitive Potassium Channels toward Diazoxide Revealed by ADP." *Proceedings of the National Academy of Sciences of the United States of America* 96 (21): 12162–67.

Dorsam, Robert T., and J. Silvio Gutkind. 2007. "G-Protein-Coupled Receptors and Cancer." *Nature Reviews Cancer* 7 (2): 79–94. doi:10.1038/nrc2069.

Doyle, Declan A., João Morais Cabral, Richard A. Pfuetzner, Anling Kuo, Jacqueline M. Gulbis, Steven L. Cohen, Brian T. Chait, and Roderick MacKinnon. 1998. "The Structure of the Potassium Channel: Molecular Basis of K+ Conduction and Selectivity." *Science* 280 (5360): 69–77. doi:10.1126/science.280.5360.69.

Dupuis, Julien P, Jean Revilloud, Christophe J Moreau, and Michel Vivaudou. 2008. "Three C-Terminal Residues from the Sulphonylurea Receptor Contribute to the Functional Coupling between the KATP Channel Subunits SUR2A and Kir6.2." *The Journal of Physiology* 586 (Pt 13): 3075–85. doi:10.1113/jphysiol.2008.152744.

Enkvetchakul, D., G. Loussouarn, E. Makhina, S. L. Shyng, and C. G. Nichols. 2000. "The Kinetic and Physical Basis of K(ATP) Channel Gating: Toward a Unified Molecular Understanding." *Biophysical Journal* 78 (5): 2334–48. doi:10.1016/S0006-3495(00)76779-8.

Fang, Kun, László Csanády, and Kim W Chan. 2006. "The N-Terminal Transmembrane Domain (TMD0) and a Cytosolic Linker (L0) of Sulphonylurea Receptor Define the Unique Intrinsic Gating of KATP Channels." *The Journal of Physiology* 576 (Pt 2): 379–89. doi:10.1113/jphysiol.2006.112748.

Fan, Zheng, and Jonathan C. Makielski. 1997. "Anionic Phospholipids Activate ATP-Sensitive Potassium Channels." *Journal of Biological Chemistry* 272 (9): 5388–95. doi:10.1074/jbc.272.9.5388.

Fernández, Sara B. Mateus, Zsolt Holló, Andras Kern, Éva Bakos, Paul A. Fischer, Piet Borst, and Raymond Evers. 2002. "Role of the N-Terminal Transmembrane Region of the Multidrug Resistance Protein MRP2 in Routing to the Apical Membrane in MDCKII Cells." *Journal of Biological Chemistry* 277 (34): 31048–55. doi:10.1074/jbc.M204267200.

Fredriksson, Robert, Malin C. Lagerström, Lars-Gustav Lundin, and Helgi B. Schiöth. 2003. "The G-Protein-Coupled Receptors in the Human Genome Form Five Main

Families. Phylogenetic Analysis, Paralogon Groups, and Fingerprints." *Molecular Pharmacology* 63 (6): 1256–72. doi:10.1124/mol.63.6.1256.

Gloyn, Anna L., Juveria Siddiqui, and Sian Ellard. 2006. "Mutations in the Genes Encoding the Pancreatic Beta-Cell KATP Channel Subunits Kir6.2 (KCNJ11) and SUR1 (ABCC8) in Diabetes Mellitus and Hyperinsulinism." *Human Mutation* 27 (3): 220–31. doi:10.1002/humu.20292.

Gribble, Fiona M., Peter Proks, Barbara E. Corkey, and Frances M. Ashcroft. 1998. "Mechanism of Cloned ATP-Sensitive Potassium Channel Activation by Oleoyl-CoA." *Journal of Biological Chemistry* 273 (41): 26383–87. doi:10.1074/jbc.273.41.26383.

Gribble, F. M., R. Ashfield, C. Ammälä, and F. M. Ashcroft. 1997. "Properties of Cloned ATP-Sensitive K+ Currents Expressed in Xenopus Oocytes." *The Journal of Physiology* 498 (Pt 1) (January): 87–98.

Gribble, F M, S J Tucker, and F M Ashcroft. 1997. "The Essential Role of the Walker A Motifs of SUR1 in K-ATP Channel Activation by Mg-ADP and Diazoxide." *The EMBO Journal* 16 (6): 1145–52. doi:10.1093/emboj/16.6.1145.

Gumina, Richard J., D. Fearghas O'Cochlain, Christopher E. Kurtz, Peter Bast, Darko Pucar, Prasanna Mishra, Takashi Miki, Susumu Seino, Slobodan Macura, and Andre Terzic. 2007. "KATP Channel Knockout Worsens Myocardial Calcium Stress Load in Vivo and Impairs Recovery in Stunned Heart." *American Journal of Physiology. Heart and Circulatory Physiology* 292 (4): H1706–13. doi:10.1152/ajpheart.01305.2006.

Haga, Kazuko, Andrew C. Kruse, Hidetsugu Asada, Takami Yurugi-Kobayashi, Mitsunori Shiroishi, Cheng Zhang, William I. Weis, et al. 2012. "Structure of the Human M2 Muscarinic Acetylcholine Receptor Bound to an Antagonist." *Nature* 482 (7386): 547–51. doi:10.1038/nature10753.

Hamill, O. P., A. Marty, E. Neher, B. Sakmann, and F. J. Sigworth. 1981. "Improved Patch-Clamp Techniques for High-Resolution Current Recording from Cells and Cell-Free Membrane Patches." *Pflügers Archiv: European Journal of Physiology* 391 (2): 85–100.

Hernández-Sánchez, C., A. S. Basile, I. Fedorova, H. Arima, B. Stannard, A. M. Fernandez, Y. Ito, and D. LeRoith. 2001. "Mice Transgenically Overexpressing Sulfonylurea Receptor 1 in Forebrain Resist Seizure Induction and Excitotoxic Neuron Death." *Proceedings of the National Academy of Sciences of the United States of America* 98 (6): 3549–54. doi:10.1073/pnas.051012898.

Heusser, Katja, Hebao Yuan, Ioana Neagoe, Andrei I. Tarasov, Frances M. Ashcroft, and Blanche Schwappach. 2006. "Scavenging of 14-3-3 Proteins Reveals Their Involvement in the Cell-Surface Transport of ATP-Sensitive K+ Channels." *Journal of Cell Science* 119 (20): 4353–63. doi:10.1242/jcs.03196.

Hibino, Hiroshi, Atsushi Inanobe, Kazuharu Furutani, Shingo Murakami, Ian Findlay, and Yoshihisa Kurachi. 2010. "Inwardly Rectifying Potassium Channels: Their Structure,

Function, and Physiological Roles." *Physiological Reviews* 90 (1): 291–366. doi:10.1152/physrev.00021.2009.

Hilgemann, D. W., and R. Ball. 1996. "Regulation of Cardiac Na+,Ca2+ Exchange and KATP Potassium Channels by PIP2." *Science (New York, N.Y.)* 273 (5277): 956–59.

Hohl, Michael, Christophe Briand, Markus G. Grütter, and Markus A. Seeger. 2012. "Crystal Structure of a Heterodimeric ABC Transporter in Its Inward-Facing Conformation." *Nature Structural & Molecular Biology* 19 (4): 395–402. doi:10.1038/nsmb.2267.

Hollenstein, Kaspar, Dominik C. Frei, and Kaspar P. Locher. 2007. "Structure of an ABC Transporter in Complex with Its Binding Protein." *Nature* 446 (7132): 213–16. doi:10.1038/nature05626.

Hosey, M. M., J. L. Benovic, S. K. DebBurman, and R. M. Richardson. 1995. "Multiple Mechanisms Involving Protein Phosphorylation Are Linked to Desensitization of Muscarinic Receptors." *Life Sciences* 56 (11-12): 951–55.

Hosy, Eric, and Michel Vivaudou. 2014. "The Unusual Stoichiometry of ADP Activation of the KATP Channel." *Frontiers in Physiology* 5 (January). doi:10.3389/fphys.2014.00011.

Inagaki, N., J. Inazawa, and S. Seino. 1995. "cDNA Sequence, Gene Structure, and Chromosomal Localization of the Human ATP-Sensitive Potassium Channel, uKATP-1, Gene (KCNJ8)." *Genomics* 30 (1): 102–4. doi:10.1006/geno.1995.0018.

Inagaki, Nobuya, Tohru Gonoi, and Susumu Seino. 1997. "Subunit Stoichiometry of the Pancreatic B-Cell ATP-Sensitive K+ Channel." *FEBS Letters* 409 (2): 232–36. doi:10.1016/S0014-5793(97)00488-2.

Kadaba, Neena S., Jens T. Kaiser, Eric Johnson, Allen Lee, and Douglas C. Rees. 2008. "The High-Affinity E. Coli Methionine ABC Transporter: Structure and Allosteric Regulation." *Science (New York, N.Y.)* 321 (5886): 250–53. doi:10.1126/science.1157987.

Karger, Amy B., Sungjo Park, Santiago Reyes, Martin Bienengraeber, Roy B. Dyer, Andre Terzic, and Alexey E. Alekseev. 2008. "Role for SUR2A ED Domain in Allosteric Coupling within the K(ATP) Channel Complex." *The Journal of General Physiology* 131 (3): 185–96. doi:10.1085/jgp.200709852.

Katritch, Vsevolod, Vadim Cherezov, and Raymond C. Stevens. 2012. "Diversity and Modularity of G Protein-Coupled Receptor Structures." *Trends in Pharmacological Sciences* 33 (1): 17–27. doi:10.1016/j.tips.2011.09.003.

Kodan, Atsushi, Tomohiro Yamaguchi, Toru Nakatsu, Keita Sakiyama, Christopher J. Hipolito, Akane Fujioka, Ryo Hirokane, et al. 2014. "Structural Basis for Gating Mechanisms of a Eukaryotic P-Glycoprotein Homolog." *Proceedings of the National Academy of Sciences of the United States of America* 111 (11): 4049–54. doi:10.1073/pnas.1321562111.

Kolakowski, L. F. 1994. "GCRDb: A G-Protein-Coupled Receptor Database." *Receptors & Channels* 2 (1): 1–7.

Krasnoperov, Valery, Yun Lu, Leonid Buryanovsky, Thomas A. Neubert, Konstantin Ichtchenko, and Alexander G. Petrenko. 2002. "Post-Translational Proteolytic Processing of the Calcium-Independent Receptor of Alpha-Latrotoxin (CIRL), a Natural Chimera of the Cell Adhesion Protein and the G Protein-Coupled Receptor.

Role of the G Protein-Coupled Receptor Proteolysis Site (GPS) Motif." *The Journal of Biological Chemistry* 277 (48): 46518–26. doi:10.1074/jbc.M206415200.

Kruse, Andrew C., Aaron M. Ring, Aashish Manglik, Jianxin Hu, Kelly Hu, Katrin Eitel, Harald Hübner, et al. 2013. "Activation and Allosteric Modulation of a Muscarinic Acetylcholine Receptor." *Nature* 504 (7478): 101–6. doi:10.1038/nature12735.

Kubo, Yoshihiro, and Yoshimichi Murata. 2001. "Control of Rectification and Permeation by Two Distinct Sites after the Second Transmembrane Region in Kir2.1 K+ Channel." *The Journal of Physiology* 531 (Pt 3): 645–60. doi:10.1111/j.1469-7793.2001.0645h.x.

Kuo, Anling, Jacqueline M. Gulbis, Jennifer F. Antcliff, Tahmina Rahman, Edward D. Lowe, Jochen Zimmer, Jonathan Cuthbertson, Frances M. Ashcroft, Takayuki Ezaki, and Declan A. Doyle. 2003. "Crystal Structure of the Potassium Channel KirBac1.1 in the Closed State." *Science (New York, N.Y.)* 300 (5627): 1922–26. doi:10.1126/science.1085028.

Lagerström, Malin C., and Helgi B. Schiöth. 2008. "Structural Diversity of G Protein-Coupled Receptors and Significance for Drug Discovery." *Nature Reviews. Drug Discovery* 7 (4): 339–57. doi:10.1038/nrd2518.

Lee, Jonas Y., Janet G. Yang, Daniel Zhitnitsky, Oded Lewinson, and Douglas C. Rees. 2014. "Structural Basis for Heavy Metal Detoxification by an Atm1-Type ABC Exporter." *Science (New York, N.Y.)* 343 (6175): 1133–36. doi:10.1126/science.1246489.

Lim, Jong Hyun, Eun Hae Oh, Juhun Park, Seunghun Hong, and Tai Hyun Park. 2015. "Ion-Channel-Coupled Receptor-Based Platform for a Real-Time Measurement of G-Protein-Coupled Receptor Activities." *ACS Nano* 9 (2): 1699–1706. doi:10.1021/nn506494e.

Linton, Kenneth J. 2007. "Structure and Function of ABC Transporters." *Physiology* 22 (2): 122–30. doi:10.1152/physiol.00046.2006.

Liss, B., R. Bruns, and J. Roeper. 1999. "Alternative Sulfonylurea Receptor Expression Defines Metabolic Sensitivity of K-ATP Channels in Dopaminergic Midbrain Neurons." *The EMBO Journal* 18 (4): 833–46. doi:10.1093/emboj/18.4.833.

Locher, Kaspar P. 2009. "Structure and Mechanism of ATP-Binding Cassette Transporters." *Philosophical Transactions of the Royal Society B: Biological Sciences* 364 (1514): 239–45. doi:10.1098/rstb.2008.0125.

Locher, Kaspar P., Allen T. Lee, and Douglas C. Rees. 2002. "The E. Coli BtuCD Structure: A Framework for ABC Transporter Architecture and Mechanism." *Science* 296 (5570): 1091–98. doi:10.1126/science.1071142.

Lodwick, David, Richard D. Rainbow, Hussein N. Rubaiy, Mohammed Al Johi, Geerten W. Vuister, and Robert I. Norman. 2014. "Sulfonylurea Receptors Regulate the Channel Pore in ATP-Sensitive Potassium Channels via an Intersubunit Salt Bridge." *The Biochemical Journal* 464 (3): 343–54. doi:10.1042/BJ20140273.

Lorenz, Eva, and Andre Terzic. 1999. "Physical Association Between Recombinant Cardiac ATP-Sensitive K+Channel Subunits Kir6.2 and SUR2A." *Journal of Molecular and Cellular Cardiology* 31 (2): 425–34. doi:10.1006/jmcc.1998.0876.

Lu, Zhe, and Roderick MacKinnon. 1994. "Electrostatic Tuning of Mg2+ Affinity in an Inward-Rectifier K+ Channel." *Nature* 371 (6494): 243–46. doi:10.1038/371243a0.

Maeda, Akiko, Kiichiro Okano, Paul S.-H. Park, Janis Lem, Rosalie K. Crouch, Tadao Maeda, and Krzysztof Palczewski. 2010. "Palmitoylation Stabilizes Unliganded Rod

Opsin." *Proceedings of the National Academy of Sciences of the United States of America* 107 (18): 8428–33. doi:10.1073/pnas.1000640107.

Markworth, E., C. Schwanstecher, and M. Schwanstecher. 2000. "ATP4- Mediates Closure of Pancreatic Beta-Cell ATP-Sensitive Potassium Channels by Interaction with 1 of 4 Identical Sites." *Diabetes* 49 (9): 1413–18.

Matsuoka, T., K. Matsushita, Y. Katayama, A. Fujita, K. Inageda, M. Tanemoto, A. Inanobe, S. Yamashita, Y. Matsuzawa, and Y. Kurachi. 2000. "C-Terminal Tails of Sulfonylurea Receptors Control ADP-Induced Activation and Diazoxide Modulation of ATP-Sensitive K(+) Channels." *Circulation Research* 87 (10): 873–80.

Mikhailov, Michael V, Jeff D Campbell, Heidi de Wet, Kenju Shimomura, Brittany Zadek, Richard F Collins, Mark S P Sansom, Robert C Ford, and Frances M Ashcroft. 2005. "3-D Structural and Functional Characterization of the Purified KATP Channel Complex Kir6.2–SUR1." *The EMBO Journal* 24 (23): 4166–75. doi:10.1038/sj.emboj.7600877.

Mikhailov, M. V., E. A. Mikhailova, and S. J. Ashcroft. 2001. "Molecular Structure of the Glibenclamide Binding Site of the Beta-Cell K(ATP) Channel." *FEBS Letters* 499 (1-2): 154–60.

Miki, T., K. Nagashima, and S. Seino. 1999. "The Structure and Function of the ATP-Sensitive K+ Channel in Insulin-Secreting Pancreatic Beta-Cells." *Journal of Molecular Endocrinology* 22 (2): 113–23. doi:10.1677/jme.0.0220113.

Miledi, R., I. Parker, and K. Sumikawa. 1983. "Recording of Single Gamma-Aminobutyrate- and Acetylcholine-Activated Receptor Channels Translated by Exogenous mRNA in Xenopus Oocytes." *Proceedings of the Royal Society of London. Series B, Biological Sciences* 218 (1213): 481–84.

Miller, Christopher. 2001. "See Potassium Run." *Nature* 414 (6859): 23–24. doi:10.1038/35102126.

Moreau, Christophe, Fabienne Gally, Hélène Jacquet-Bouix, and Michel Vivaudou. 2005. "The Size of a Single Residue of the Sulfonylurea Receptor Dictates the Effectiveness of K ATP Channel Openers." *Molecular Pharmacology* 67 (4): 1026–33. doi:10.1124/mol.104.008698.

Moreau, Christophe J., Julien P. Dupuis, Jean Revilloud, Karthik Arumugam, and Michel Vivaudou. 2008. "Coupling Ion Channels to Receptors for Biomolecule Sensing." *Nature Nanotechnology* 3 (10): 620–25. doi:10.1038/nnano.2008.242.

Moreau, Christophe, Anne-Lise Prost, Renaud Dérand, and Michel Vivaudou. 2005. "SUR, ABC Proteins Targeted by KATP Channel Openers." *Journal of Molecular and Cellular Cardiology* 38 (6): 951–63. doi:10.1016/j.yjmcc.2004.11.030.

Mukai, E., H. Ishida, M. Horie, A. Noma, Y. Seino, and M. Takano. 1998. "The Antiarrhythmic Agent Cibenzoline Inhibits KATP Channels by Binding to Kir6.2." *Biochemical and Biophysical Research Communications* 251 (2): 477–81. doi:10.1006/bbrc.1998.9492.

Ng, Chai Ann, Kevin Phan, Adam P. Hill, Jamie I. Vandenberg, and Matthew D. Perry. 2014. "Multiple Interactions between Cytoplasmic Domains Regulate Slow Deactivation

of Kv11.1 Channels." *The Journal of Biological Chemistry* 289 (37): 25822–32. doi:10.1074/jbc.M114.558379.

Nichols, C. G., and A. N. Lopatin. 1997. "Inward Rectifier Potassium Channels." *Annual Review of Physiology* 59: 171–91. doi:10.1146/annurev.physiol.59.1.171.

Nichols, Colin G., Gautam K. Singh, and Dorothy K. Grange. 2013. "KATP Channels and Cardiovascular Disease: Suddenly a Syndrome." *Circulation Research* 112 (7): 1059–72. doi:10.1161/CIRCRESAHA.112.300514.

Niescierowicz, Katarzyna. 2013. "Développement de la technologie des récepteurs couplés à un canal ionique pour des études structure-fonction des récepteurs couplés aux protéines G et du canal Kir6.2." Phdthesis, Université de Grenoble. https://tel.archives-ouvertes.fr/tel-01067669/document.

Niescierowicz, Katarzyna, Lydia Caro, Vadim Cherezov, Michel Vivaudou, and Christophe J. Moreau. 2014. "Functional Assay for T4 Lysozyme-Engineered G Protein-Coupled Receptors with an Ion Channel Reporter." *Structure (London, England: 1993)* 22 (1): 149–55. doi:10.1016/j.str.2013.10.002.

Ockenga, Wymke, Sina Kühne, Simone Bocksberger, Antje Banning, and Ritva Tikkanen. 2013. "Non-Neuronal Functions of the M2 Muscarinic Acetylcholine Receptor." *Genes* 4 (2): 171–97. doi:10.3390/genes4020171.

Oh, Eun Hae, Seung Hwan Lee, Hwi Jin Ko, Jong Hyun Lim, and Tai Hyun Park. 2015. "Coupling of Olfactory Receptor and Ion Channel for Rapid and Sensitive Visualization of Odorant Response." *Acta Biomaterialia* 22 (August): 1–7. doi:10.1016/j.actbio.2015.04.034.

Oldham, Michael L., Dheeraj Khare, Florante A. Quiocho, Amy L. Davidson, and Jue Chen. 2007. "Crystal Structure of a Catalytic Intermediate of the Maltose Transporter." *Nature* 450 (7169): 515–21. doi:10.1038/nature06264.

Pinkett, H. W., A. T. Lee, P. Lum, K. P. Locher, and D. C. Rees. 2007. "An Inward-Facing Conformation of a Putative Metal-Chelate-Type ABC Transporter." *Science (New York, N.Y.)* 315 (5810): 373–77. doi:10.1126/science.1133488.

Proks, Peter, Frank Reimann, Nick Green, Fiona Gribble, and Frances Ashcroft. 2002. "Sulfonylurea Stimulation of Insulin Secretion." *Diabetes* 51 Suppl 3 (December): S368–76.

Proks, P., F. M. Gribble, R. Adhikari, S. J. Tucker, and F. M. Ashcroft. 1999. "Involvement of the N-Terminus of Kir6.2 in the Inhibition of the KATP Channel by ATP." *The Journal of Physiology* 514 (Pt 1) (January): 19–25.

Prost, Anne-Lise, Alain Bloc, Nicolas Hussy, Renaud Derand, and Michel Vivaudou. 2004. "Zinc Is Both an Intracellular and Extracellular Regulator of KATP Channel Function." *The Journal of Physiology* 559 (Pt 1): 157–67. doi:10.1113/jphysiol.2004.065094.

Rainbow, Richard D, Marian James, Diane Hudman, Mohammed Al Johi, Harprit Singh, Peter J Watson, Ian Ashmole, Noel W Davies, David Lodwick, and Robert I Norman. 2004. "Proximal C-Terminal Domain of Sulphonylurea Receptor 2A Interacts with Pore-Forming Kir6 Subunits in KATP Channels." *Biochemical Journal* 379 (Pt 1): 173–81. doi:10.1042/BJ20031087.

Raman, Malathi, and Karen Martin. 2014. "One Solution for Cloning and Mutagenesis: In-Fusion® HD Cloning Plus." *Nature Methods* 11 (9). doi:10.1038/nmeth.f.373.

Reimann, Frank, and Frances M Ashcroft. 1999. "Inwardly Rectifying Potassium Channels." *Current Opinion in Cell Biology* 11 (4): 503–8. doi:10.1016/S0955-0674(99)80073-8.

Russ, U., U. Lange, C. Löffler-Walz, A. Hambrock, and U. Quast. 2001. "Interaction of the Sulfonylthiourea HMR 1833 with Sulfonylurea Receptors and Recombinant ATP-

Sensitive K(+) Channels: Comparison with Glibenclamide." *The Journal of Pharmacology and Experimental Therapeutics* 299 (3): 1049–55.

Schwanstecher, M., C. Sieverding, H. Dörschner, I. Gross, L. Aguilar-Bryan, C. Schwanstecher, and J. Bryan. 1998. "Potassium Channel Openers Require ATP to Bind to and Act through Sulfonylurea Receptors." *The EMBO Journal* 17 (19): 5529–35. doi:10.1093/emboj/17.19.5529.

Schwappach, Blanche, Noa Zerangue, Yuh Nung Jan, and Lily Yeh Jan. 2000. "Molecular Basis for KATP Assembly: Transmembrane Interactions Mediate Association of a K+ Channel with an ABC Transporter." *Neuron* 26 (1): 155–67. doi:10.1016/S0896-6273(00)81146-0.

Shintre, Chitra A., Ashley C. W. Pike, Qiuhong Li, Jung-In Kim, Alastair J. Barr, Solenne Goubin, Leela Shrestha, et al. 2013. "Structures of ABCB10, a Human ATP-Binding Cassette Transporter in Apo- and Nucleotide-Bound States." *Proceedings of the National Academy of Sciences of the United States of America* 110 (24): 9710–15. doi:10.1073/pnas.1217042110.

Srinivasan, Vasundara, Antonio J. Pierik, and Roland Lill. 2014. "Crystal Structures of Nucleotide-Free and Glutathione-Bound Mitochondrial ABC Transporter Atm1." *Science (New York, N.Y.)* 343 (6175): 1137–40. doi:10.1126/science.1246729.

Sturgess, N. C., M. L. Ashford, D. L. Cook, and C. N. Hales. 1985. "The Sulphonylurea Receptor May Be an ATP-Sensitive Potassium Channel." *Lancet (London, England)* 2 (8453): 474–75.

Suzuki, M., K. Fujikura, N. Inagaki, S. Seino, and K. Takata. 1997. "Localization of the ATP-Sensitive K+ Channel Subunit Kir6.2 in Mouse Pancreas." *Diabetes* 46 (9): 1440–44.

Szewczyk, Paul, Houchao Tao, Aaron P. McGrath, Mark Villaluz, Steven D. Rees, Sung Chang Lee, Rupak Doshi, Ina L. Urbatsch, Qinghai Zhang, and Geoffrey Chang. 2015. "Snapshots of Ligand Entry, Malleable Binding and Induced Helical Movement in P-Glycoprotein." *Acta Crystallographica Section D: Biological Crystallography* 71 (Pt 3): 732–41. doi:10.1107/S1399004715000978.

Tammaro, Paolo, and Frances M. Ashcroft. 2007. "A Mutation in the ATP-Binding Site of the Kir6.2 Subunit of the KATP Channel Alters Coupling with the SUR2A Subunit." *The Journal of Physiology* 584 (Pt 3): 743–53. doi:10.1113/jphysiol.2007.143149.

Tao, Xiao, Jose L. Avalos, Jiayun Chen, and Roderick MacKinnon. 2009. "Crystal Structure of the Eukaryotic Strong Inward-Rectifier K+ Channel Kir2.2 at 3.1 Å Resolution." *Science (New York, N.Y.)* 326 (5960): 1668. doi:10.1126/science.1180310.

Tate, Christopher G. 2012. "A Crystal Clear Solution for Determining G-Protein-Coupled Receptor Structures." *Trends in Biochemical Sciences* 37 (9): 343–52. doi:10.1016/j.tibs.2012.06.003.

Teramoto, Noriyoshi. 2006. "Pharmacological Profile of U-37883A, a Channel Blocker of Smooth Muscle-Type ATP-Sensitive K Channels." *Cardiovascular Drug Reviews* 24 (1): 25–32. doi:10.1111/j.1527-3466.2006.00025.x.

Teramoto, Noriyoshi, Hai-Lei Zhu, Atsushi Shibata, Manami Aishima, Emma J. Walsh, Masaya Nagao, and William C. Cole. 2009. "ATP-Sensitive K+ Channels in Pig Urethral Smooth Muscle Cells Are Heteromultimers of Kir6.1 and Kir6.2." *American Journal of Physiology - Renal Physiology* 296 (1): F107–17. doi:10.1152/ajprenal.90440.2008.

Trapp, S., S. J. Tucker, and F. M. Ashcroft. 1997. "Activation and Inhibition of K-ATP Currents by Guanine Nucleotides Is Mediated by Different Channel Subunits."

Proceedings of the National Academy of Sciences of the United States of America 94 (16): 8872–77.

Tucker, S. J., F. M. Gribble, P. Proks, S. Trapp, T. J. Ryder, T. Haug, F. Reimann, and F. M. Ashcroft. 1998. "Molecular Determinants of KATP Channel Inhibition by ATP." *The EMBO Journal* 17 (12): 3290–96. doi:10.1093/emboj/17.12.3290.

Tucker, S. J., F. M. Gribble, C. Zhao, S. Trapp, and F. M. Ashcroft. 1997. "Truncation of Kir6.2 Produces ATP-Sensitive K+ Channels in the Absence of the Sulphonylurea Receptor." *Nature* 387 (6629): 179–83. doi:10.1038/387179a0.

Ueda, K., N. Inagaki, and S. Seino. 1997. "MgADP Antagonism to Mg2+-Independent ATP Binding of the Sulfonylurea Receptor SUR1." *The Journal of Biological Chemistry* 272 (37): 22983–86.

Uhde, I., A. Toman, I. Gross, C. Schwanstecher, and M. Schwanstecher. 1999. "Identification of the Potassium Channel Opener Site on Sulfonylurea Receptors." *The Journal of Biological Chemistry* 274 (40): 28079–82.

Van Bon, Bregje W.M., Christian Gilissen, Dorothy K. Grange, Raoul C.M. Hennekam, Hülya Kayserili, Hartmut Engels, Heiko Reutter, et al. 2012. "Cantú Syndrome Is Caused by Mutations in ABCC9." *American Journal of Human Genetics* 90 (6): 1094–1101. doi:10.1016/j.ajhg.2012.04.014.

Vergani, Paola, Steve W. Lockless, Angus C. Nairn, and David C. Gadsby. 2005. "CFTR Channel Opening by ATP-Driven Tight Dimerization of Its Nucleotide-Binding Domains." *Nature* 433 (7028): 876–80. doi:10.1038/nature03313.

Wada, Y., T. Yamashita, K. Imai, R. Miura, K. Takao, M. Nishi, H. Takeshima, et al. 2000. "A Region of the Sulfonylurea Receptor Critical for a Modulation of ATP-Sensitive K(+) Channels by G-Protein Betagamma-Subunits." *The EMBO Journal* 19 (18): 4915–25. doi:10.1093/emboj/19.18.4915.

Ward, Andrew, Christopher L. Reyes, Jodie Yu, Christopher B. Roth, and Geoffrey Chang. 2007. "Flexibility in the ABC Transporter MsbA: Alternating Access with a Twist." *Proceedings of the National Academy of Sciences of the United States of America* 104 (48): 19005–10. doi:10.1073/pnas.0709388104.

Whorton, Matthew R., and Roderick MacKinnon. 2011. "Crystal Structure of the Mammalian GIRK2 K+ Channel and Gating Regulation by G Proteins, PIP2, and Sodium." *Cell* 147 (1): 199–208. doi:10.1016/j.cell.2011.07.046.

Wilkens, Stephan. 2015. "Structure and Mechanism of ABC Transporters." *F1000Prime Reports* 7 (February). doi:10.12703/P7-14.

Wise, Alan, Katy Gearing, and Stephen Rees. 2002. "Target Validation of G-Protein Coupled Receptors." *Drug Discovery Today* 7 (4): 235–46. doi:10.1016/S1359-6446(01)02131-6.

Woo, Jae-Sung, Antra Zeltina, Birke A. Goetz, and Kaspar P. Locher. 2012. "X-Ray Structure of the Yersinia Pestis Heme Transporter HmuUV." *Nature Structural & Molecular Biology* 19 (12): 1310–15. doi:10.1038/nsmb.2417.

Yamada, K., J. J. Ji, H. Yuan, T. Miki, S. Sato, N. Horimoto, T. Shimizu, S. Seino, and N. Inagaki. 2001. "Protective Role of ATP-Sensitive Potassium Channels in Hypoxia-Induced Generalized Seizure." *Science (New York, N.Y.)* 292 (5521): 1543–46. doi:10.1126/science.1059829.

Yan, Fei-Fei, Yu-Wen Lin, Courtney MacMullen, Arupa Ganguly, Charles A. Stanley, and Show-Ling Shyng. 2007. "Congenital Hyperinsulinism–Associated ABCC8

Mutations That Cause Defective Trafficking of ATP-Sensitive K+ Channels." *Diabetes* 56 (9): 2339–48. doi:10.2337/db07-0150.

Yang, Jian, Yuh Nung Jan, and Lily Y Jan. 1995. "Control of Rectification and Permeation by Residues in Two Distinct Domains in an Inward Rectifier K+ Channel." *Neuron* 14 (5): 1047–54. doi:10.1016/0896-6273(95)90343-7.

Zerangue, Noa, Blanche Schwappach, Yuh Nung Jan, and Lily Yeh Jan. 1999. "A New ER Trafficking Signal Regulates the Subunit Stoichiometry of Plasma Membrane KATP Channels." *Neuron* 22 (3): 537–48. doi:10.1016/S0896-6273(00)80708-4.

Zhou, Y., J. H. Morais-Cabral, A. Kaufman, and R. MacKinnon. 2001. "Chemistry of Ion Coordination and Hydration Revealed by a K+ Channel-Fab Complex at 2.0 A Resolution." *Nature* 414 (6859): 43–48. doi:10.1038/35102009.

Title: 'Structure-function studies of the Kir6.2 channel and of its coupling with natural and artificial partners'.

Abstract: K-ATP channels play a key role in adjusting the membrane potential to the metabolic state of cells. They result from the combination of the SulfonylUrea Receptor, SUR, and the inward rectifier K+ channel Kir6. Both associate to form a heterooctamer of ~ 1MDa. This PhD project aimed at obtaining structural and functional information on the coupling between Kir6 and SUR. We identified three residues in the SUR1 isoform essential to mediate activation of the Kir6.2 isoform upon binding of activators. We also investigated the role of the Kir6.2 N-terminal in gating modulation using Ion channel-coupled receptors (ICCRs), artificial GPCR-Kir6.2 channels formed by fusing the GPCR C-terminus to the Kir6.2 N-terminus. We identified arginine R32 as an essential hub to allow Kir6.2 modulation by the GPCR. This residue is not involved in the regulation of natural SUR-Kir6 channels, suggesting that SUR uses a differential mechanism to regulate Kir6.2 gating.

Titre: 'Étude structure-fonction du canal Kir6.2 et de son couplage avec des partenaires naturels et artificiels'.

Résumé: Les Canaux K-ATP jouent un rôle clé dans l'ajustement du potentiel de membrane à l'état métabolique des cellules. Ils résultent de la combinaison du récepteur des sulfonylurées, SUR, et du canal K + rectifiant entrant, Kir6. Cette thèse vise à obtenir des informations structurales et fonctionnelles sur le couplage SUR-Kir6. Nous avons identifié trois résidus dans l'isoforme SUR1 essentiels pour médier l'activation de l'isoforme Kir6.2 lors de la liaison d'activateurs. Nous avons également étudié le rôle de l'extrémité N-terminale de Kir6.2 dans la régulation des *Ion channel-coupled receptors* (ICCRs), canaux artificiels GPCR-Kir6.2 formés par la fusion de la partie C-terminale du GPCR à l'extrémité N-terminale de Kir6.2. Nous avons identifié le résidu R32 comme un élément essentiel pour la modulation de Kir6.2 par le GPCR. Ce résidu n'est pas impliquée dans la régulation de canaux SUR-Kir6 naturels, ce qui suggère que SUR utilise un mécanisme différent pour réguler Kir6.2.

Discipline: Biologie Structurale et Nanobiologie.

Mots clef: canal K-ATP, récepteur des sulfonylurées, couplage fonctionnel, canal Kir6.2.

Keywords: K-ATP channel, sulfonylurea receptor, functional coupling, Kir6.2 channel.

Laboratoire d'accueil: Institut de Biologie Structurale, Channels group, 71 Avenue des Martyrs, 38044 Grenoble Cedex 9.